Nano Today 25 (2019) 38–67

Contents lists available at ScienceDirect

Nano Today

journal homepage: www.elsevier.com/locate/nanotoday

Review

Stimuli-responsive nanotheranostics based on lanthanide-doped upconversion nanoparticles for cancer imaging and therapy: current advances and future challenges

Yinghui Wang[a], Shuyan Song[a], Songtao Zhang[a,b], Hongjie Zhang[a,b,*]

[a] State Key Laboratory of Rare Earth Resource Utilization, Changchun Institute of Applied Chemistry (CIAC), Chinese Academy of Sciences (CAS), Changchun, 130022 PR China
[b] University of Chinese Academy of Sciences, Beijing 100049, PR China

ARTICLE INFO

Article history:
Received 2 November 2018
Received in revised form 29 January 2019
Accepted 26 February 2019
Available online 26 March 2019

Keywords:
upconversion nanoparticles
stimuli-responsive
theranostics
cancer
imaging and therapy

ABSTRACT

Theranostic nanoplatform integrated with concurrent diagnostic and therapeutic capabilities has attracted increasing attentions recently in the field of nanomedicine since it offers great opportunities in the fight against various major diseases, such as cancer. In recent years, lanthanide-doped upconvertion nanoparticles (UCNPs), have been explored for potential applications in cancer diagnostics and treatment owing to their unique merits such as enhancing penetration depths and minimizing background auto-fluorescence, photo-bleaching as well as photodamage to biological specimens, and reducing adverse side effects of NIR triggered treatments. Of particular interest is to construct stimuli-responsive nanotheranostic platforms based on UCNPs that imaging and anticancer activities in response to various internal/external stimuli. In this review article, we would like to focus on the recent progress of UCNPs in their applications of stimuli-responsive theranostics that trigger the diagnostic and therapeutic functions in response to various stimuli, including near infrared (NIR) light, pH, glutathione (GSH), reactive oxygen species (ROS), enzyme, and temperature. Furthermore, the future directions and challenges in the development of UCNPs for stimuli-responsive theranostics are discussed.

Contents

* Corresponding author.
E-mail address: hongjie@ciac.ac.cn (H. Zhang).

https://doi.org/10.1016/j.nantod.2019.02.007
1748-0132/

Introduction

Cancer is one of the main diseases that seriously threaten people's health and life [1]. Despite enormous efforts have been made to seek a cure for cancer, each patient gave different responses to the same treatment owing to the heterogeneity and complexity of cancer [2–4]. Therefore, it is urgent to develop a patient-focused approach to cancer treatment, i.e. personalized medicine. Theranostics, the integration of diagnostic and therapy, have been proposed as a promising strategy to fight against various fatal diseases, such as cancer in next-generation personalized medicine [5–10]. Co-delivery contrast agent and drug possess the same biodistribution, and therefore imaging functionality can not only identify the location and size of tumor but also give an accurate assessment of therapeutic effect. Thanks to the rapid development of nanoscience and nanotechnology in the world, various nanomaterials have been explored for potential applications in cancer diagnostics and treatment in the last few decades, such as magnetic nanoparticles, [11–14] quantum dots, [15–17] metal nanoparticles, [18–22] silica, [23–26] carbon-based nanomaterials, [17,27–30] polymeric nanoparticles, [31–37] lipid-based nanoparticles, [38–41] transition metal dichalcogenides [42–46] and so on. These nanomaterials are beneficial to serve as theranostics agents due to their unique property and versatility embraces multiple inherent imaging functions, anticancer therapeutic abilities or delivery multiple types of drugs to achieve concurrent diagnostic and therapy. However, drug molecules can only be released by the simple diffusion effect in conventional theranostics platform, resulting in irregular distribution of drugs in the body and serious side effect to normal tissue. Ideal theranostics platforms require "zero-release" before reaching the cancer cells, while the drug release can be controlled in temporally and spatially, i.e. delivering the drugs to the right place and releasing at the right time. With this end in view, great efforts have been devoted to design "smart" stimuli-responsive theranostics that can respond to specific stimuli to control drug release on demand, which brings new chances and space for theranostics. Many endogenous or exogenous stimuli have been exploited to achieve sustained drug release in a controlled manner, including endogenous stimuli pH, H_2O_2, glutathione (GSH), adenosine triphosphate (ATP), enzymes, exogenous stimuli light, temperature, and electric or magnetic fields.

Imaging probes, as the diagnostic tool to delineate tumors, monitor physiological responses to therapy, and evaluate the therapeutic efficacy, are one of the most important parts of the theranostic nanoplatform. Various noninvasive imaging techniques have been applied in clinical applications, such as magnetic resonance imaging (MRI), computed tomography (CT), photoacoustic imaging (PAI), optical imaging, positron emission tomography (PET), and single-photon emission tomography (SPECT). As an important molecular imaging technology, optical imaging, especially fluorescence imaging can be used to visualize morphological details with subcellular resolution, and elucidate important signaling pathways and fundamental biological processes at the cellular level. More importantly, its application range is extensive from sub micrometer level viruses and bacteria, to micrometer level cells, and to macroscopic animals. Therefore, it is a powerful imaging mode that can provide comprehensive anatomical and physiological details for diagnostic work. Nonetheless, the currently used fluorescent probes, including organic dyes, [47,48] semiconductor quantum dots (QDs), [49–52] metal complexes, [53–55] and fluorescent proteins, [56–59] usually require ultraviolet (UV) or visible radiation as excitation source, which results in a series of insurmountable defects and severely limited their applications in theranostics. For example, (i) low tissue penetration inherent to the UV or visible excitation; (ii) low signal-to-noise ratio caused by the serious autofluorescence interference from biological tissues, (iii) possible severe DNA photodamage and even the cell death due to the long-term irradiation, and (iv) potential biosafety concerns of the toxicity of heavy metals that will be release with photooxidation. In contrast, near infrared (NIR) light within the "optical transmission window" of biological tissues as excitation exhibits several significant advantages, such as deeper penetration, weaker background autofluorescence, none photobleaching as well as minimizing photodamage to biological specimens [51,60–62].

Over the past decades, lanthanide-doped upconversion nanoparticles (UCNPs) that convert lower-energy radiation (usually NIR light) to higher-energy emission (e.g., visible, UV, and NIR) have been proposed as new generation of fluorescent probes with great potential in biomedical imaging [63–74]. The upconversion luminescence featured with large anti-Stokes shift is a process by which two or more photons combine in a medium to produce a higher-energy photon [70,73,75]. This is a rather unusual process that can be driven by an economic and continuous wave (CW) diode laser, which is different from nonlinear multiphoton absorption. As theranostic agents, UCNPs have a series of attractive features: (i) the excitation wavelength, usually 980 nm or 808 nm, located in the "optical transmission window" of biological tissues (700-1000 nm), thereby significantly enhancing penetration depths; (ii) there is no background autofluorescence when UCNPs served as UCL imaging probes, because endogenous and exogenous fluorophores in the organisms can't be excited by NIR light, resulting in high signal-to-noise ratio; (iii) UCNPs could be applied as multi-modality contrasts through doping with different rare-earth ions without additional modification of other functionalities owing to the similar ionic radii and chemical properties of Ln ions, such as MRI, CT, and so on; [61,63,76–79] (iv) UCNPs possess large versatile

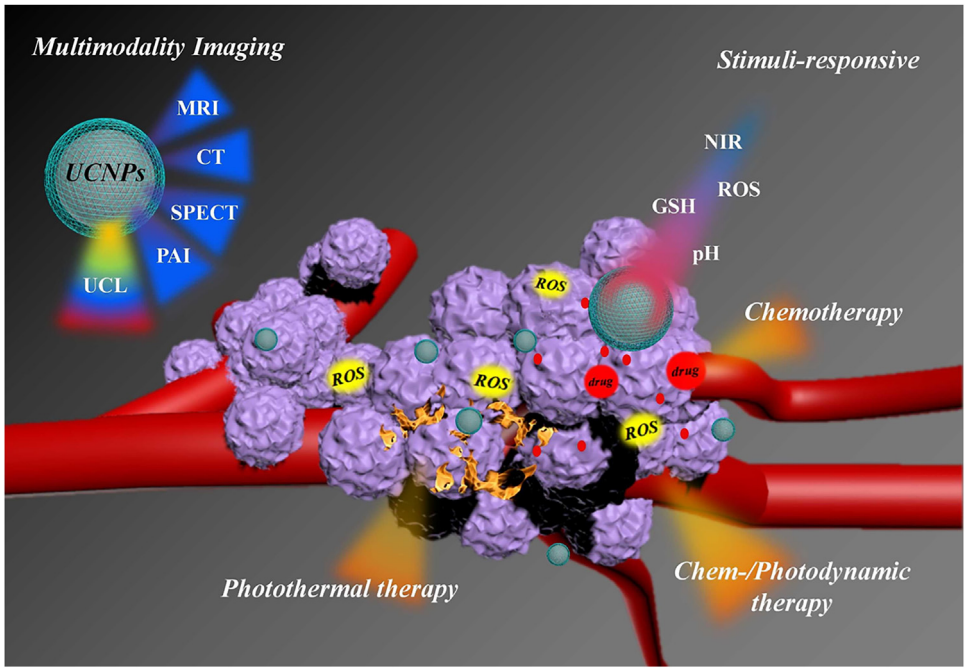

Scheme 1. Schematic illustration of the structure of this Review.

surface that can be easily modified to conjugate with hydrophilic ligands, biomolecules, and various therapeutic agents, making them well-suited for use in theranostics and stimuli-responsive theranostics; (v) the high photostability enable UCNPs to monitor the therapeutics both in vitro and in vivo; (vi) most importantly, there is no toxic elements in the composition of UCNPs, thus endowing them with great potentials for biomedical application. These unique merits have greatly accelerated research of UCNPs in theranostic, and significant advances have been made in recent year. In spite of many outstanding reviews have surveyed to different aspects of UCNPs, [55,65,70,80–94] such as synthesis methods, surface modification, upconversion multicolor tuning, size and morphology controlling, and biological applications, rarely focusing on their theranostics applications, especially stimuli-driven theranostics [95,96]. Therefore, it is necessary and significant to introduce the latest progress concerning the application of UCNPs in stimuli-responsive theranostics, which would promote the development of this field and arouse more extensive interests of researchers.

In this review, we aim to summarize the recent progress and future prospects of UCNPs in their stimuli-responsive theranostices applications rather than attempting to exhaustively cover the whole field (Scheme 1). Section 2 describes the principal synthesis strategies of typical structured UCNP-based theranostic agents. The current progress that has been made in UCNPs for high sensitivity, high resolution as well as deep tissue imaging is discussed in section 3. In sections 4, we highlight recent research progress on UCNPs in their applications of stimuli-responsive theranostics that trigger the therapeutic functions in response to various stimuli, including NIR, pH, GSH, ROS, enzyme, and temperature. Finally, we discuss the current challenges and future prospects of using UCNPs for cancer theranostics (Scheme 2).

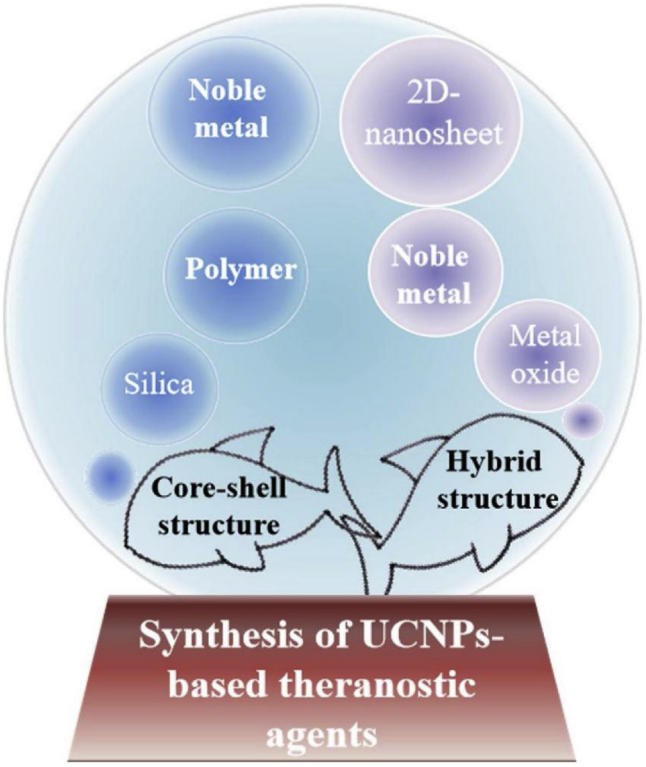

Scheme 2. General strategies to synthesis of UCNPs-based theranostic agents.

Synthesis of UCNPs-based theranostic agents

The principal design concept of UCNPs-based theranostic nanoagents is integrating multiple types of functional nanomaterials with UCNPs into a single nanoplatform through well-established chemistry process and nanotechnology, resulting in that the scaffold can perform multiple functions, such as diagnosis, therapy, tracking of the biodistribution and monitoring of therapeutic progression. In general, a theranostic agent consists of at least four components, i.e., imaging agents (UCNPs), therapeutic agents (anticancer drugs, photothermal agents, photosensitizers (PS), small interfering ribonucleic acid [siRNA], etc.), carrier (polymer, silica, graphene, etc.), and surface modifier (PEG, target molecule, stimuli-responsive molecular valve, etc.). The structure of ther-

anostic agents, i.e. the position of UCNPs and other functional components, is a vital factor in determining their performance for specific applications. Therefore, this section will elaborate the design and constructing of typical structured UCNPs-based theranostic nanoagents.

Synthesis of core-shell structured UCNPs-based theranostic nanoagents

Core-shell structure is the most respective structure of UCNPs-based theranostic nanoagents. Coating the shell on the surface of UCNPs (UCNPs@shell) not only endows UCNPs with a hydrophilic surface for good dispersity in physiological environment, but also introduces the other functional units into theranostic platform. So in this section, we focus on the design and synthesis of core-shell structured UCNPs theranostic nanoagents with different kinds of materials as shell, such as polymer, silica, and noble metal (Au or Ag), etc.

UCNPs@SiO_2 theranostic nanoagents

Interests in coating of silica shell on UCNPs through silanization technique have been grown in the field of nanomedicine since silica exhibit good biocompatible and their surface are easily functionalized with various groups (e.g., −COOH, $-NH_2$, −SH, etc.), which make them feasible to combine with different kinds of biological molecules, functional nanoparticles and responsive molecules for imaging, drug delivery, gene delivery, photothermal therapy (PTT), photodynamic therapy (PDT), and stimuli-responsive therapy. Depending on the different forms of silica shells, UCNPs@SiO_2 structure includes three categories, i.e., dense silica shell ($dSiO_2$), mesoporous silica shell ($mSiO_2$), and hollow mesoporous silica shell ($hmSiO_2$).

Typically, two routes are applied to $dSiO_2$ shell according to the polarity of the capping ligands on the surface of UCNPs. When UCNPs capped with hydrophilic ligands, the Stöber method is used to coat the $dSiO_2$ shell through the hydrolysis and condensation of TEOS around the UCNPs [97]. Otherwise, the reverse micelle method is exploited for growth a uniform $dSiO_2$ shell onto UCNPs with hydrophobic capping ligands [98]. Zhang and co-workers coated a $dSiO_2$ shell onto UCNPs surface and further modified with amine groups. The obtained UCNPs@SiO_2-NH_2 nanoparticles were first demonstrated the potential of UCNPs for gene delivery [99]. However, the capability of delivery therapeutic agents of $dSiO_2$ shell is limited owing to the absence of porous structures. Alternatively, coating $mSiO_2$ shell has prevailed in surface modification of UCNPs due to the unique merits of $mSiO_2$, such as large surface area, tunable pore size, and ease of surface functionalization, which makes UCNPs@$mSiO_2$ not only serve as excellent drug carriers but also realize stimuli-responsive release via attaching responsive molecules on $mSiO_2$ [100–102]. Shi's group reported the growth of a uniform $mSiO_2$ shell on the hydrophobic surface of UCNPs using cetyltrimethylammonium bromide (CTAB) as both surfactant for transforming hydrophobic UCNPs to hydrophilic ones and organic template for the formation of the mesoporous shell, [100] as shown in Fig. 1a. The ultrasonication treatments during the coating process can effectively avoid agglomeration of UCNPs cores, thereby achieving monodisperse UCNPs@$mSiO_2$ core-shell nanostructures. Apart from directly coating the $mSiO_2$ layer on the surface of UCNPs, $mSiO_2$ shell also could be growth on the surface of UCNP@$dSiO_2$ by using octadecyltrimethoxysilane (C18TMS) [103,104] or CTAB [105] as a mesopore template, as shown in Fig. 1b. Inserting of a $dSiO_2$ interlayer endows UCNP@$dSiO_2$@$mSiO_2$ with improved the chemical stability as well as tunable separation between the UCNPs core and channel/surface tethered components, which is important for fluorescence resonance energy transfer (FRET)-based applications, such as biosensors and PDT.

Rattle-structure (i.e. yolk-shell structure) with $hmSiO_2$ shell has aroused significant interests because their attractive properties, such as unique hollow structure, high surface to volume ratio and large pore volume, which are highly desirable for many potential bioapplications [106,107]. Etching strategy was widely applied to synthesize $hmSiO_2$ nanomaterials. However, traditional acidic etchant cannot be used for fabricating UCNPs@$hmSiO_2$ because UCNPs cores were liable to dissolved in the acidic environment. Thereby, mild etchant "hot water" has been successfully employed to synthesize UCNPs@$hmSiO_2$ through surface-protected etching strategy [78,108,109]. Su et al. prepared PEI-protected UCNPs@$mSiO_2$ through the reverse micelle method, and then etched with hot water to obtain yolk-shell structures [108]. Bu and co-workers developed a rattle-structured nanotheranostic composed of a movable UCNP core, $mSiO_2$ shell and large cavity in between them through growth two layers of SiO_2 shells [78,109]. Firstly, a $dSiO_2$ shell was coating on the surface of oleic acid capped UCNPs via the reverse micelle method, subsequently the second $mSiO_2$ shell was achieved. Then, a surface-protected hot water etching process was conducted to selectively etch the inner $dSiO_2$ shell using PVP as protector and product pores in the second silica shell, as shown in Fig. 1c. Comparing to $dSiO_2$ as the second shell, the obtained yolk-shell structure possesses ordered and regular porous structure, which is feasible to the release of drug. Importantly, the large hollow cavity of rattle structures endows UCNPs@$hmSiO_2$ with many intriguing properties: i) larger loading capacity; ii) higher FRET efficiency; and iii) higher sensing sensitivity.

UCNPs@polymer theranostic nanoagents

For theranostic application, the necessary requirements of theranostic nanoagents based on UCNPs are stable in water, biocompatiblity, and the feasibility for further functionalization. Unfortunately, UCNPs with high monodispersity, controllable sizes, regular shapes, high crystallinity and upconversion emission efficiency are mainly synthesized via wet-chemical techniques so far, which are hydrophobic in nature owing to their capping ligands. Organic polymers have been regarded as another kind of potential surface modifier for rendering hydrophobic UCNPs to water-dispersible and providing active chemical groups for further functionalization [110]. More importantly, polymer shell could improve the circulation time of nanoparticles in the bloodstream and reduce the nonspecific uptake by cells in the reticuloendothelial system [111]. Various polymers have been used to modify UCNPs, such as poly(acrylic acid) (PAA), [112–115] polyethylenimine (PEI), [116,117] poly(allylamine) (PAAm), [118] polyethylene glycol (PEG)-grafted amphiphilic polymer (C18PMH-PEG), [72,119] PEG-phospholipid, [120–122] polydopamine (PDA), [123] TWEEN, [124,125] and so on. Depending on the properties of the polymer, different strategies were explored to construct UCNPs@polymer theranostic nanoagents. For example, ligand exchange method is often employed to wrap the hydrophilic polymers with polydentate ligands on the surface of hydrophobic UCNPs. Lin's group reported a UCNPs theranostic nanoagent using PEI as surface modifier to not only transfer UCNPs into water phase and provide free functional amine groups for further functionalization with transplatinum(IV) pro-drug. Such UCNPs theranostic nanoagent could be a promising candidate for UCL/CT/MRI trimodality imaging guided NIR-initiated platinum prodrug release of cancer therapy [117]. The amphiphilic polymer attachment strategy is another widely used method for converting hydrophobic UCNPs to hydrophilic ones through the van der Waals interactions between the hydrophobic segment of the amphiphilic polymer and the hydrophobic ligands capped on UCNPs. Thereby, the exposed hydrophilic segments make the UCNPs well disperse in water. Liu's group synthesized an amphiphilic polymer C18PMH-PEG, and coated it on the sur-

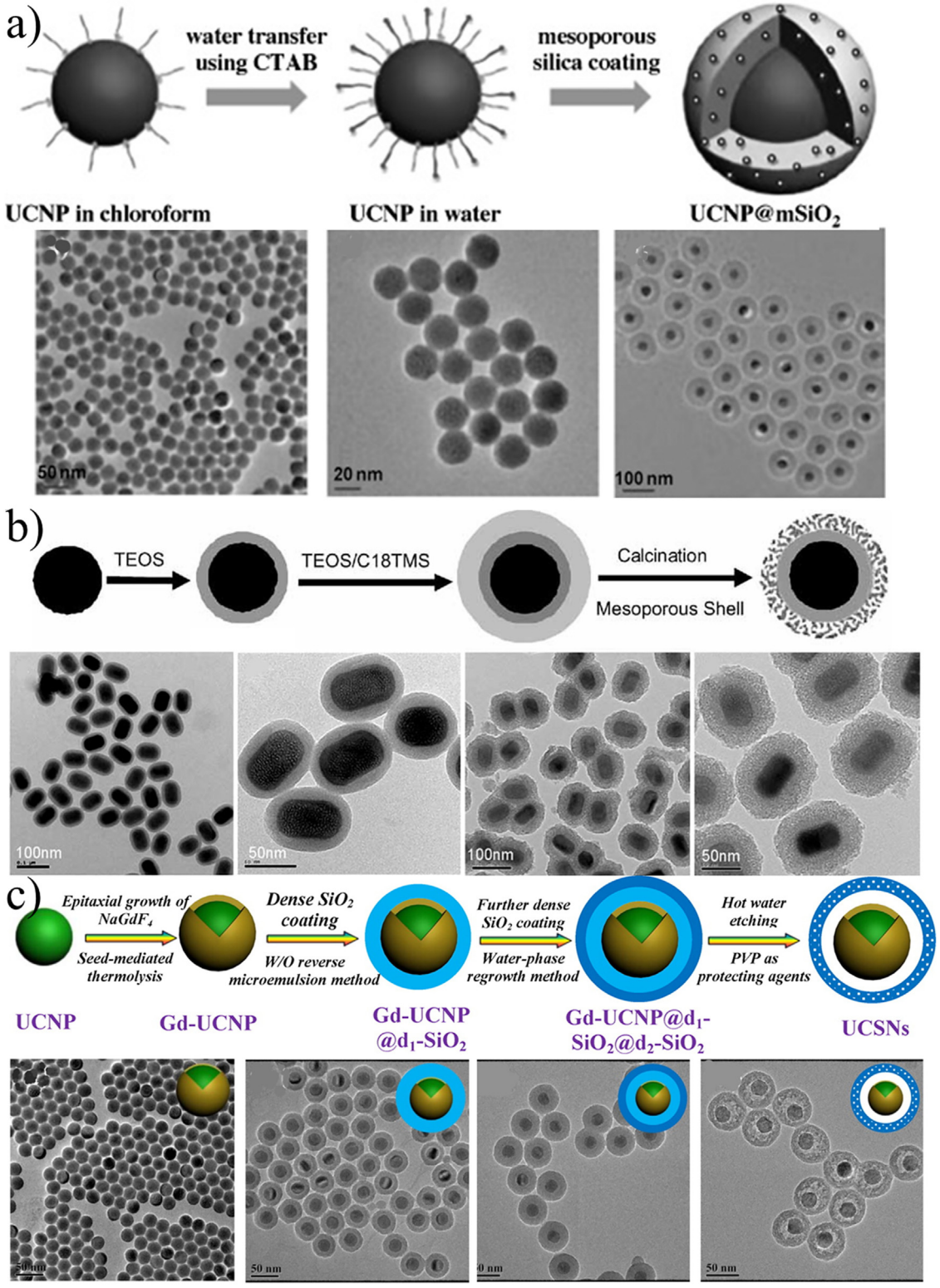

Fig. 1. Schematic illustration of the synthesis of UCNPs@mSiO$_2$ using CTAB a) or C18TMS b) as structure-directing agents, and c) the synthesis procedure of UCSNs and the corresponding TEM images. [Reference 101] printed with permission from Wiley.

face of OA-capped UCNPs (Fig. 2a). The obtained PEGylated UCNPs with excellent water solubility possessed "hydrophobic pockets" for loading the anticancer drug DOX by absorbed physical absorption, and the release of DOX could be controlled by pH [72]. Such strategy is facile and flexible, and can be expanded to loading other therapeutic agents [119]. It is meaningful that the amphiphilic polymer attachment strategy is in favor of keeping the UC efficacy compared to ligand exchange method due to the fact that water molecules were prevented from entering the Ln luminescence centers by hydrophobic layer on the surface of UCNPs. Layer by layer (LBL) technology based on electrostatic attraction is another important method to make UCNPs hydrophilic with controllable coating

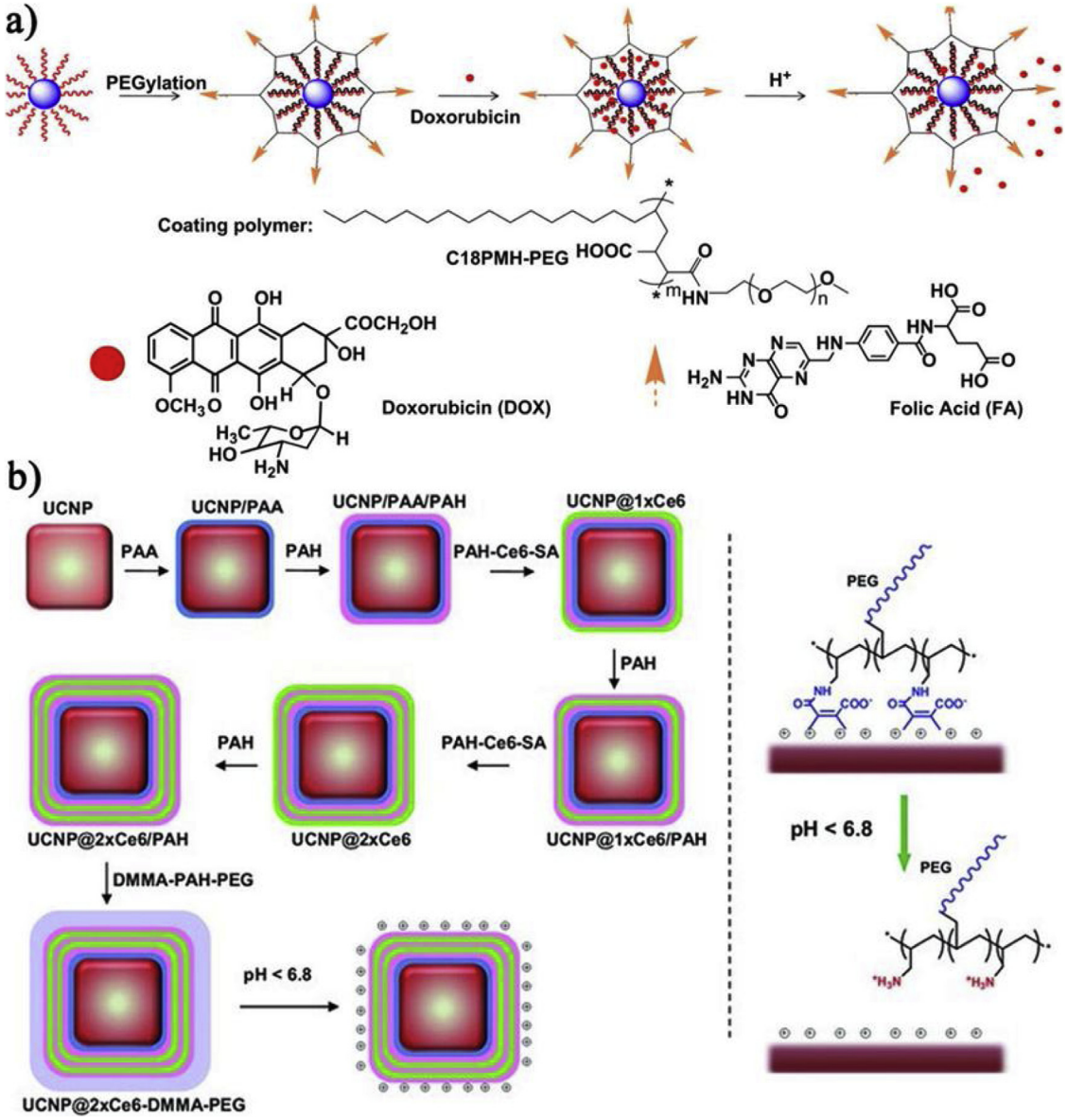

Fig. 2. Schematic diagrams of synthesis procedures for UCNPs@polymer theranostic nanoagents: a) by amphiphilic polymer C18PMH-PEG capped on UCNPs, Printed with permission from Elsevier [72]. b) via LBL strategy. Printed with permission from Wiley [127].

thickness, surface charge and active groups. Liu and coworkers constructed a theranostic nanoagent based on UCNPs for imaging-guided pH-sensitive photodynamic therapy via LBL (Fig. 2b) [126]. The Mn^{2+} -doped UCNPs core gave a strong red emission, which could not only be used as UCL imaging but also activate PS Ce6 to realize PDT for cancer. The Ce6 was conjugated with polyanion (PAH-Ce6-SA), and deposited on the surface of UCNPs functionalized with poly (allylamine hydrochloride) (PAH) polycation. The loading amounts of PS could be controlled by adjusting the number of PAH/PAH-Ce6-SA layers. The outermost layer was deposited by pH-sensitive polymer, realizing pH-sensitive photodynamic therapy. Such rationally design and facile preparation approach stimulate interest in developing new theranostic nanoplatform.

UCNPs@noble metal (Au or Ag) theranostic nanoagents

Localized surface plasmon resonance (LSPR) has been used to enhance the UC efficiency of UCNPs [127–130]. Thanks to the strong NIR absorption of Au/Ag nanostructures, UCNPs@noble metal (Au or Ag) nanocomposites have been designed and constructed for cancer theranostic [131–133]. For assembling the metallic nanoparticles onto the surface of UCNPs, the surface of UCNPs have to modified to render UCNPs well disperse in water and carry positive charges or ligand for attracting negatively charged metal nanoparticles. Song and coworkers reported a core-shell structured $NaYF_4$:Yb,Er@Ag nanocomposite for UCL imaging and PTT [131]. Thioglycolic acid (TGA) not only transferred UCNPs into water phase, but also attracted Ag^+ ions through its thiol group. The wavelength of LSPR can be tuned to 980 nm by adjusting the thickness of the silver layer. Thereby, the generated Ag shell converting light to heat and UCL imaging could be performed simultaneously under single NIR irradiation, which enables $NaYF_4$:Yb,Er@Ag nanocomposite potential application in theranostic. Comparing with Ag shell, Au shell has better NIR absorption. Liu et al. coated Au shell onto the surface of UCNPs with the assistance of an intermediate iron oxide layer [132]. With the assistance of the magnet, the resulting nanocomposites show high tumor accumulation and outstanding photothermal therapeutic efficacy with 100% of tumor elimination.

Core-shell structured UCNPs nanotheranostics modified by different shells exhibit good performances in imaging and therapy, but each of these different kinds of shells have their strengths and limitations in theranostics. The porous structure of silica shell endows UCNPs@SiO_2 with large drug loading capacity, which is beneficial to chemotherapy. However, the PS molecules encapsulated inside the silica network suffered from the long distance to UCNPs, making unsatisfactory FRET efficiency for PDT. In contrast, covalent bonding of PS molecules on the surface of UCNPs@polymer is a promising strategy to ameliorate this hurdle. But, the colloidal stability of most of polymer coated UCNPs under physiological conditions are often unsatisfactory, ascribing to the high affinity between salts in buffers and lanthanide ions on the surface of UCNPs. As a consequence, the design and choosing the shell should depend on the treatment of UCNPs nanotheranostics. In addition, developing new materials to constructing core-shell structured UCNPs nanotheranostics will be appealing in the future.

Synthesis of hybrid structured UCNPs-based theranostic nanoagents

With the rapid development of nanotechnology, the combination of UCNPs with other nanomaterials to construct multifunctional hybrid nanocomposites has aroused significant interests for implementing multimodality bioapplications simultaneously. Comparing to core-shell structure, the hybrid structure endows UCNPs-based theranostic with more functions in both imaging and therapy. It is demonstrated that the linker-assisted strategy is suitable to construct hybrid structured UCNPs-based theranostic nanoagents. Such strategy not only introduces the new functional nanomaterials, but also avoids the adverse influence on the luminescence of UCNPs. The recent work on hybrid structured UCNPs-based theranostic nanoagents are summarized in Table 1. In this section, we describe two types of representative linker, and the design and application of the generated hybrid structured UCNPs-based theranostic nanoagents.

SiO_2-assisted method

SiO_2-assisted method is versatile to link UCNPs with other functional components since the silica layer are easily functionalized with various groups (e.g., –COOH, $-NH_2$, –SH, etc.). With the help of the surface functional group, the biological molecules and functional nanoparticles can easily be combined with UCNPs. Targeting agent (e.g., folic acid, urokinase plasminogen activator), as an important part of theranostic agents, can be easily conjugated with the amine functionalized UCNPs@SiO_2 nanocomposites to realize the targeting theranostics [159]. Many inorganic nanoparticles can be grown on the silica layer through coordination, electrostatic interactions or covalent grafting [134–158]. For example, ultrasmall CuS nanoparticles were decorated onto the surface of UCNPs with electrostatic adsorption technique between positively charged UCNP@SiO_2-NH_2 and negatively charged citrate-stabilized CuS NPs for enhanced radiotherapy and PTT synergistic therapy [146]. Au nanoparticles were also integrated with UCNPs with the assistance of SiO_2 shells for CT imaging, PTT, gene therapy or sensing [138–142]. Our group developed a novel ZnO functionalized UCNP@SiO_2 nanocomposite through covalent grafting method [153]. The as-designed nanotheranostic platform has been demonstrated the potentials for multi-modality bioimaging and specific pH-triggered on-demand drug release.

Bio-/Organic molecules -assisted method

Owing to the coordination ability of rare earth with some functional groups, such as –COOH, $-PO_3H$, and $-NH_2$, the organic or bio-molecules with two or more coordination sites are usually used as the linker to connect UCNPs and other nanoparticles. Our

Table 1
A summary of recent work on hybrid structured UCNPs-based theranostic nanoagents.

Nanomaterials	Type of UCNPs	Type of linker	Application	Ref.
Fe_3O_4 nanoparticle	$NaYF_4$: Yb,Er	SiO_2	Imaging	[134]
	$NaYF_4$:Yb,Er/Tm	SiO_2	Imaging	[135]
	$NaYF_4$:Yb, Er	Organic molecule	Proof of principle	[136]
Au nanoparticle	β-NaY/GdF_4:Yb,Er,Tm	SiO_2	Trimodal imaging (UCL/CT/MRI)	[137]
	$NaYF_4$:Yb/Tm	SiO_2	Deep-tissue imaging guided controlled drug release.	[138]
	$NaYF_4$:Yb/Er	DNA	DNA delivery and imaging	[140]
	$NaYF_4$:Yb/Er	Organic molecule	Sensor	[141]
	β- $NaYF_4$:Yb,Tm	Organic molecule	Luminescence enhancement	[142]
Au nanorod	$NaYF_4$:Yb,Er	SiO_2	PDT	[143]
	$NaYF_4$:Yb/Er	SiO_2	PTT	[144]
	$NaGdF_4$:Yb/Er	DNA	Theranostic (UCL/CT/MRI/PA imaging and PTT/PDT combination therapy)	[145]
CuS nanoparticle	$NaYbF_4$: Er/Gd	SiO_2	Theranostic (UCL/CT/MRI imaging and radiation/photothermal synergistic therapy)	[146]
	$NaGdF_4$:Yb,Er@$NaGdF_4$:Yb@$NaNdF_4$	SiO_2	Theranostic (UCL/CT/MRI imaging and combined chemo-/photothermal therapy)	[147]
	$NaYF_4$:Yb,Er@$NaYF_4$:Yb@$NaNdF_4$:Yb@$NaYF_4$	SiO_2	Theranostic (UCL imaging and chemo/photothermal synergistic therapy)	[148]
TiO_2 nanoparticle	$NaYF_4$:Yb,Tm	SiO_2	Imaging and PDT	[149]
	$NaYF_4$:Yb,Tm@$NaGdF_4$:Yb	Organic molecule	PDT	[150]
	$NaYF_4$:Yb/Tm@$NaYF_4$:Yb@$NaNdF_4$:Yb@$NaYF_4$	Organic molecule	PDT	[151]
ZnO nanoparticle	$LiYF_4$:Ce	SiO_2	Synchronous radiotherapy and deep PDT	[152]
	$NaYF_4$:Yb,Er/$NaGdF_4$: Yb	SiO_2	Theranostic (UCL/CT/MRI imaging and on-demand chemotherapies)	[153]
Graphene oxide	$NaYF_4$:Yb,Er and $NaYF_4$: Mn, Yb, Er	Organic molecule	Drug delivery	[154]
	$NaYF_4$:Yb,Er,Tm/$NaYF_4$	Organic molecule	Theranostic (UCL imaging and PTT/PDT synergistic therapy)	[155]
MnO_2 nanosheet	$NaYF_4$:Yb/Tm@$NaYF_4$	Organic molecule	Sensor	[156]
	$NaYF_4$:Yb/Er/Tm	SiO_2	UCL Imaging and Oxygen-Elevated Synergetic Therapy	[157]
MoS nanosheet	$NaYF_4$:Yb,Er	Organic molecule	Theranostic (UCL imaging and PTT/PDT synergistic therapy)	[158]

group reported a multifunctional nanoplatform, which is developed by covalently grafting core-shell structured UCNPs with nanographene oxide (NGO) via bifunctional PEG [155]. The reason for selecting PEG as linker was twofold. On one hand, PEG has good compatibility with biological system, which renders NGO high aqueous solubility and stability in physiological solutions including serum. On the other hand, bonding UCNPs at the end of the long chain of PEG molecules can reduce the fluorescence quenching by NGO. Xu et al. constructed Au nanorods (NR) and UCNPs core-satellite nanoassemblies with two complementary oligonucleotides (DNA) as linkers [145]. The NR dimer was initially formed through binding two complementary thiolated-oligonucleotides (DNA1 and DNA2), then an amphiphilic diblock copolymer (PS-b-PAA) was used to encapsulate the dimer assemblies. After modifying by amino-terminated DNA (DNA3), NR dimer was integrated with UCNPs-Ce6-DNA1 by DNA hybridization. The DNA-driven assembly strategy is facile and general, which opens up a new avenue to construct hybrid theranostic nanoagents.

UCNPs for diagnostic imaging

UCNPs have been gaining more and more attention in the last few decades as the next generation fluorescent probes for diagnostic imaging owing to their superior features compared to traditional fluorescent probes, e.g. deep penetration, low autofluorescence from biosamples, excellent photostability, and low phototoxicity. Beyond that, incorporating multiple imaging moieties onto the UCNPs to construct integrated imaging systems, such as MRI, CT, PET, SPECT, and PAI has been widely developed since no single modality is perfect and sufficient to obtain all the necessary information for diagnosis. This section focuses on the recent developments in diagnostic imaging of UCNPs.

UCNPs for UCL imaging

UCL imaging, as an important branch of fluorescence imaging, has been developed rapidly in recently years from cellular imaging to small animal imaging [160–169]. For obtaining comprehensive morphological, anatomical, and physiological details for diagnosis, small animal models have been employed for in vivo imaging, which is the focus of this section.

Since Zhang et al. first demonstrated the deeper-tissue imaging advantages of UCNPs over QDs for small animal, [168] numerous works have been carried out to further increase the penetration depth of UCL imaging [162,170–174]. Zhao et al. reported Mn-doped $NaYF_4$:Yb/Er UCNPs with single-band red-emitting, which could apply as imaging probes for in vivo UCL imaging and extend the imaging depth to 15 mm [170]. Li and coworkers prepared sub-10 nm hexagonal $NaLuF_4$:Yb,Tm UCNPs, which is successfully used for in vivo UCL imaging of Kunming mouse with fur and black mouse with the penetrate depth up to ~2 cm [162]. Moreover, high-contrast UCL imaging of rabbit has been achieved. Very recently, Chen et al. successfully developed UCNP-mediated transcranial NIR optogenetic stimulation of specifically labeled neurons in deep brain areas (Fig. 3) [175]. The tissue-penetrating NIR light can locally converted to visible light for activating channelrhodopsin-expressing neurons. Moreover, the power of transcranial NIR irradiation can be tuned according to its depth for the stimulation of a specific brain region. The in vivo utility of UCNP-mediated NIR upconversion optogenetics was successfully demonstrated in ventral tegmental area (VTA) of the mouse brain, which located $\tilde{4}$.2 mm below the skull. After injection an adeno-associated virus (AAV) encoding ChR2-EYFP into the VTA of tyrosine hydroxylase (TH)–driven Cre recombinase (TH-Cre) transgenic mice for 4 weeks, blue-emitting $NaYF_4$:Yb/Tm@SiO_2 UCNPs was injected into the VTA. Then the anesthetized mice were exposed to transcranial pulsed NIR irradiation delivered from an optical fiber placed 2 mm above the skull. The results shows that neuronal excitation was only triggered by NIR light in ChR2-transfected mice in the presence of UCNPs. Importantly, the application of in vivo upconversion optogenetics has been extended to multiple modes of neural control, including inhibition, as well as to different brain regions. This is the first work about exploring the application of UCNPs in deep tissue.

With the development of UCNPs in bioimaging, researchers are keen on improving not only the penetration depth but also the quality of UCL imaging, i.e., the high sensitivity and resolution. Hao et al. achieved the highly sensitive tiny-tumor imaging through enhancing the UCL intensity [176]. Mg^{2+} doped $NaYF_4$:Yb/Er UCNPs were synthesized with simultaneous control of the phase and size. Compared with the Mg-free UCNPs, the overall UCL intensity of UCNPs doped with 20% Mg^{2+} is enhanced by ≈27.5 times. The obtained Mg-doped $NaYF_4$:Yb/Er UCNPs with size of 35 nm have been used as optical probes for highly sensitive tiny-tumor detection. In addition to doping other ions, Jin et al. significantly enhanced UCL intensity by using much higher activator concentrations under relatively high-irradiance excitation [177]. 8 mol% Tm^{3+} ions were doped into the $NaYF_4$ nanocrystals co-doped with 20 mol% Yb^{3+}, and the obtained significantly enhanced upconversion enabled the remote detection of a single nanocrystal using a fiber dip sensor. Such high brightness originates from a combination of high excitation intensity, increased activator concentration, and accelerated sensitizer-activator energy transfer rate arising from the decreased average minimum distance between adjacent Ln^{3+} ions. Recently, Jin's group harnessed these UCNPs doped with 8 % Tm^{3+} as molecular probes for low-power super-resolution stimulated emission depletion (STED), and obtained high resolution (28 nanometres, that is, 1/36th of the wavelength) by using synchronized 980 nm and 808 nm pulses as excitation/depletion [178]. Moreover, UCNPs offer saturation intensity two orders of magnitude lower than those of fluorescent probes currently employed in STED. He et al. also demonstrated two-color super-resolution imaging using UCNPs (resolution $\tilde{6}$6 nm) with similar method [179]. In addition, the super-resolution imaging of immunostained cytoskeleton structures of fixed cells (resolution $\tilde{8}$2 nm) using UCNPs was obtained (Fig. 4). These achievements broaden the applications of UCNPs for sub-diffraction microscopic imaging.

Despite significant achievements of UCNPs in UCL imaging in vivo have been made in the past decade, there still exist some daunting challenges that prevent their further bioapplications. The conventional Yb^{3+}-sensitized UCNPs are excited by 980 nm owing to the absorption of Yb^{3+}. However, this excitation band overlaps with the maximum absorption peak of water molecules, resulting in the significant attenuation while passing through biological samples. Moreover, continuous irradiation under 980 nm light would induce overheating effect to destruct the normal cell and tissue, which imposes challenges to the further applications of UCNPs in vivo. It is thus necessary to develop of a new type of UCNPs for in vivo imaging. Zhang et al. used 915 nm laser instead of 980 nm to excite the UCNPs, whereas the weaker emission was insufficient for further bioapplications [120]. Recently, Nd^{3+} ions, with a sharp absorption band at 808 nm, have been successfully introduced into UCNPs as new sensitizer [180–187]. The water absorption at 808 nm is about 20 times lower than that at 980 nm, which can minimize the heating effect and improve tissue penetrability. Yan et al. designed and synthesized Nd^{3+}-sensitized UCNPs ($NaGdF_4$:Er^{3+},Yb^{3+}@$NaGdF_4$:Yb^{3+},Nd^{3+}), and extend their excitation band to shorter wavelengths (808 nm, Fig. 5a) [181]. Separating spatially the Er^{3+} and Nd^{3+} in the core and shell could minimize deleterious energy transfer between Er^{3+} and Nd^{3+}, and the Yb^{3+} ions in both core and shell act as bridging ions for the energy transfer ($Nd^{3+}\rightarrow Yb^{3+}\rightarrow Er^{3+}$). The efficient emission was used for

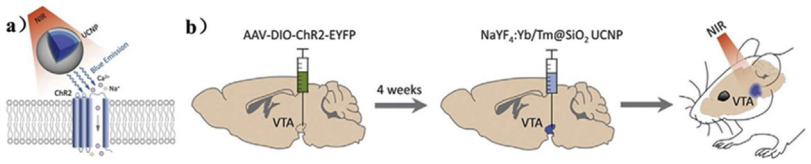

Fig. 3. UCNP-mediated NIR upconversion optogenetics for deep brain stimulation. a) Schematic principle of UCNP-mediated NIR upconversion optogenetics, and b) In vivo experimental scheme for transcranial NIR stimulation of the VTA in anesthetized mice. [Reference 175] printed with permission from Science.

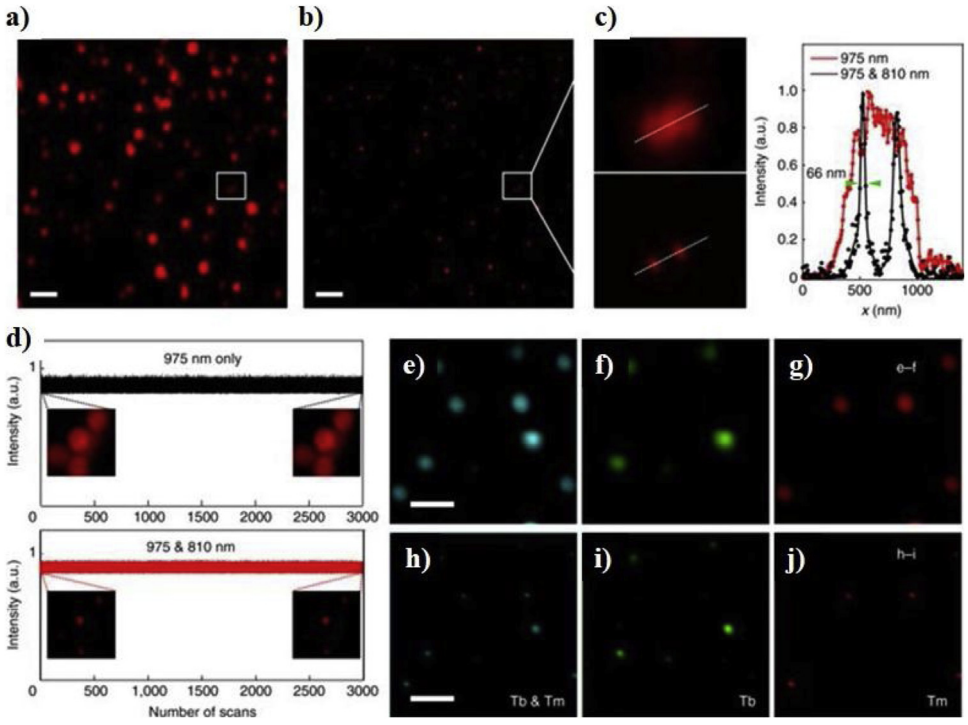

Fig. 4. Dual-color super-resolution microscopy using UCNPs. a) $NaYF_4$:18% Yb^{3+}, 10% Tm^{3+} (18.0 ± 1.8 nm in diameter) imaged by the multiphoton laser scanning microscope under 975-nm excitation solely. Scale bar: 2.5 μm. b) The corresponding super-resolution image of the same area under co-irradiation of a 975-nm Gaussian excitation beam and an 810-nm donut-shaped depletion beam. c) Magnified areas selected from a and b (marked by white squares) and the corresponding line profiles of the images, fitted with Gaussian functions. d) Intensity recording over the number of scans under 975-nm excitation solely and 975-nm and 810-nm co-irradiation. e-j) Dual-color imaging of $NaYF_4$:18% Yb^{3+}, 10% Tm^{3+} mixed with $NaGdF_4$:40%Yb^{3+}, 10% Tm^{3+} @$NaGdF_4$:15% Tb^{3+} (28.0 ± 2.1 nm in diameter). [Reference 179] printed with permission from Nature.

in vivo UCL imaging. After subcutaneously injected with Nd^{3+}-sensitized UCNPs in nude mouse, nearly the same photon flux as common UCNPs was detected with irradiation of 808 nm laser, implying that 808 nm laser excitation is efficient for in vivo applications (Fig. 5b). Importantly, the use of an 808 nm light source dramatically decreased the overheating effect (Fig. 5c), which minimizes the harm to the normal cells and tissue. After that, both Zhao's [188] and Andersson-Engels's [189] groups have further proved the significant improvement of penetration depth of Nd^{3+}-sensitized UCNPs 808 nm-excited UCNPs, demonstrating the potential of Nd^{3+}-sensitized UCNPs as new generation of probes for the effective bioimaging.

Very recently, several research groups made commendable efforts to exploit the bioimaging application of Nd^{3+}-sensitized UCNPs [190–195]. Lin and coworkers constructed core-shell structured Nd^{3+}-sensitized $NaYF_4$:Yb/Nd/Er@$NaYF_4$:Nd@$mSiO_2$ nanoparticles, and applied them as UCL imaging probes and anticancer drug carrier [195]. After injecting Nd^{3+}-sensitized UCNPs into the tumor in situ, the bright green emission was observed under irradiation with 808 nm laser. Short after, our group developed a core/satellite nanotheranostic agent (PDA@UCNPs) with polydopamine (PDA) as the core and core-shell-shell structured Nd^{3+}-sensitized UCNPs ($NaYF_4$:20%Yb^{3+}, 2%Er^{3+}/$NaYF_4$:10%Yb^{3+}, 10%Nd^{3+}/$NaYF_4$:20%Nd^{3+}) as the satellites (Fig. 6) [192]. The core-shell-shell structured design of Nd^{3+}-sensitized UCNPs enabled outstanding upconversion luminescence properties under the excitation of 808 nm. The obtained bright UCL emission was used for UCL imaging in vivo. The mouse bearing tumor was intratumorally injected with PDA@UCNPs, then imaged by a modified in vivo Maestro whole-body imaging system with an external 808 nm laser as the excitation source. An obviously UCL emission is observed from tumor on mouse after injection, and almost no auto-fluorescence is detected elsewhere. Moreover, Nd^{3+}-sensitized UCNPs could effectively reduce the overheating effect, thereby minimizing the harm to the tissue. Importantly, owing to the strong X-ray attenuation of Nd^{3+}, Nd^{3+}-sensitized UCNPs exhibited good performances as CT contrast both in vitro and in vivo, which is better than commercial used CT contrast agent. The UCL/CT dual modal imaging could be simultaneously performed with PDA@UCNPs in vivo, providing comprehensive information for tumor diagnosis.

UCNPs for multi-modality imaging

In vivo imaging of tumor that can visualize the region of tumor in a noninvasive manner makes diagnosis easier and provides more accurate information for the treatment. Despite UCL imaging has exhibited charming superiority as a tool for diagnosis of cancer, the relatively low penetration depth still limited their sensitivity in

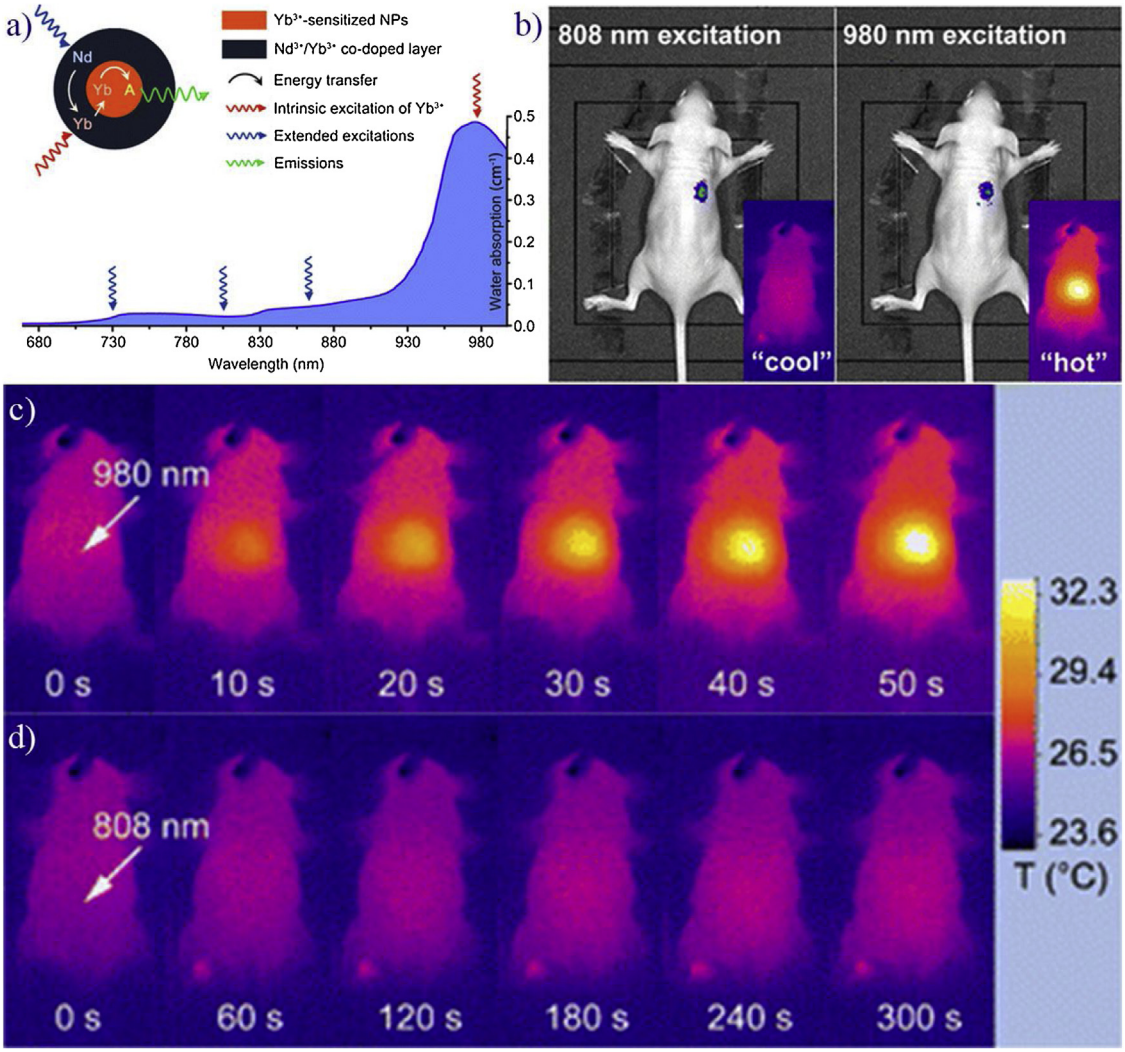

Fig. 5. a) Absorption of water in the NIR and the integration scheme of Nd^{3+}→Yb^{3+} →activator ET process by introducing Nd^{3+}/Yb^{3+} co-doped shell, b) In vivo UC imaging of a nude mouse subcutaneously injected with Er@Nd NPs irradiated with 980 nm and 808 nm laser, c) and d) The thermal images under irradiation with 980 nm and 808 nm for different time. [Reference 181] printed with permission from ACS.

Table 2
Comparison of clinical imaging modalities used in nanotheranostics.

Modality	Advantages	Disadvantages	Detection	Risk
MRI	High spatial resolution Unlimited tissue penetration	Relative low sensitivity High cost Long imaging time	Magnetic field	Harmless
CT	High spatial resolution Unlimited tissue penetration	Non quantitative	X-ray	Radiation
PET	High sensitivity Quantitative Unlimited tissue penetration	High cost	γ-ray	Radiation
SPECT	High sensitivity Quantitative Unlimited tissue penetration	Low spatial resolution	γ-ray	Radiation
PAI	High spatial resolution	Low sensitivity Low tissue penetration	Ultrasonic signal	Harmless
Fluorescence imaging	High sensitivity Multicolor imaging	Low tissue penetration Low spatial resolution	Fluorescence	Harmless

vivo. Other noninvasive imaging modalities, MRI, CT, PAI, PET, and SPECT, are useful tools in the diagnosis of various diseases. However, each imaging modality is not perfect, and has its own unique advantages along with intrinsic limitations (Table 2), e.g., MRI have good spatial resolution but relatively low sensitivity, which make single imaging modality unable to providing comprehensive diagnosis information. Therefore, multi-modal imaging has been developed rapidly and become a powerful tool for tumor diagnosis since it made use of the strengths of different imaging methods to give more accuracy information on tumors with both high resolution and sensitivity. In past decade, the considerable attentions have been paid to develop of UCNPs-based multi-modal imaging

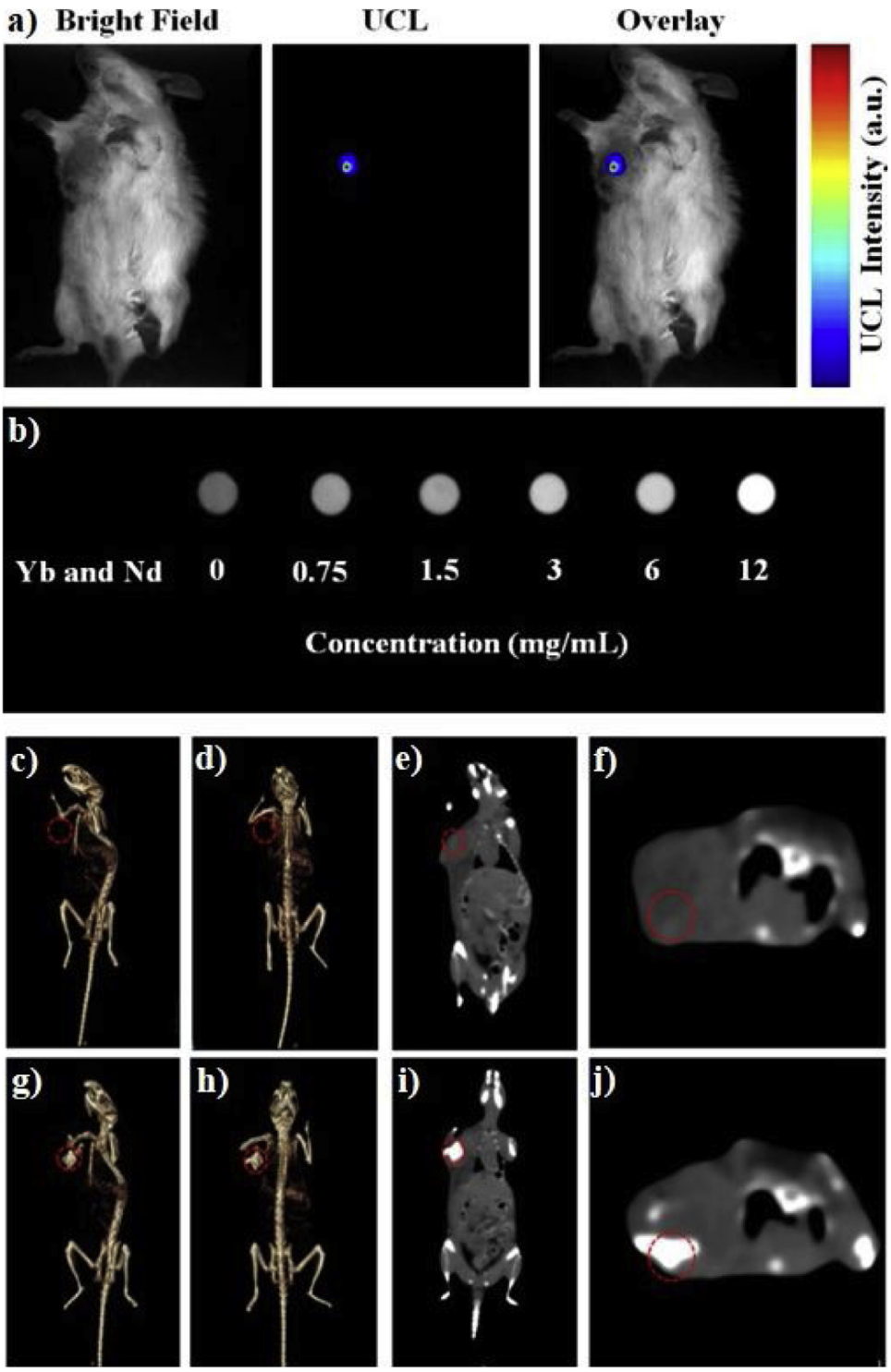

Fig. 6. a) In vivo upconversion luminescence imaging of a tumor-bearing Balb/c mouse after injection nanoparticles at the tumor site. Overlay of luminescence image and bright field image were also shown. b) CT images of solutions of PDA@UCNPs with different concentrations. c) CT images of a tumor-bearing Balb/c mouse: preinjection c-f) and after injection g-j) in situ. [Reference 192] printed with permission from Springer.

probes for tumor imaging. In this section, we describe some potentially useful designs and applications of UCNPs as multi-modality probes and their possible application for tumor imaging.

UCNPs for UCL/MRI imaging

MRI, as a routine diagnostic tool in clinical medicine, offers noninvasively the anatomic and metabolic/functional information with high spatial and temporal resolution. Several strategies have been developed to introduce MRI modality into UCNPs, such as introducing functional lanthanide ions into UCNPs and integration of UCNPs with paramagnetic materials, especially the stimuli-responsive paramagnetic materials.

Gd^{3+} ions have seven unpaired electrons in the ground state, which gives it a large paramagnetic moment. Therefore, Gd-based materials have been explored as the contrasts for MRI, such as $NaGdF_4$, [113,196–199] $KGdF_4$, [200] $BaGdF_5$, [201,202] and $GdVO_4$

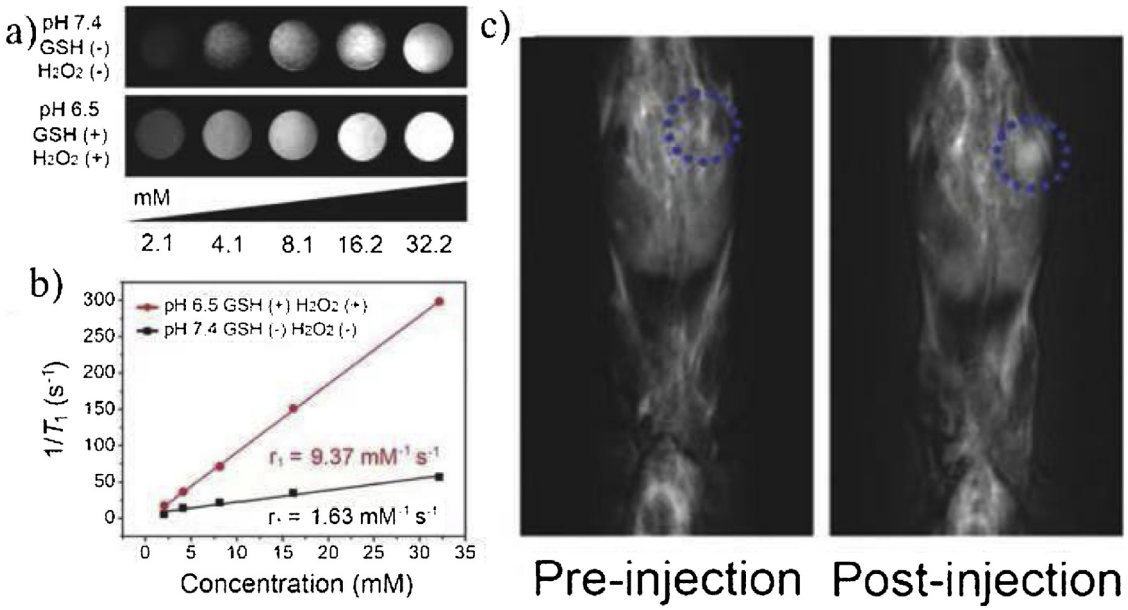

Fig. 7. a) In vitro T_1-weighted MR images of UCSM-PEG when incubated with PBS (pH 7.4, GSH 0×10^{-3} M, H_2O_2 0×10^{-6} M) and PBS (pH 6.5, GSH 10×10^{-3} M, H_2O_2 50×10^{-6} M) and b) corresponding relaxation rate r_1 versus concentrations of Mn and Gd. c) In vivo T_1-weighted MR images of tumor-bearing mice before and after injection of UCSM-PEG. [Reference 215] printed with permission from Wiley.

[203]. Shi and coworkers synthesized ultrasmall $NaGdF_4$@PLL nanodots (NDs) as a novel class of MR contrast agent, [196] which offers a high longitude relaxivity (6.42 $mM^{-1}s^{-1}$) for T_1-weighted MRI. Further in vivo animal experiments show the feasibility of $NaGdF_4$@PLL NDs as contrast agents for efficient kidney and brain tumor diagnosis. Besides, many paramagnetic lanthanide ions exhibit relatively short electronic transverse relaxation time that mainly affects T_2 weighted MRI, such as Dy^{3+}, [204,205] Ho^{3+}, [206,207] and Yb^{3+} [208,209]. For example, Hao et al. obtained a series of $NaYF_4$: Yb^{3+}, Tm^{3+} with different Yb^{3+} concentration [208]. When the Yb^{3+} concentration increases to 98%, NIR emission intensity is remarkably enhanced by 113 times. Simultaneously, the relaxation rate r_2 is calculated to be 2.61 mM^{-1} s^{-1}, especially r_2/r_1 ratio reach up to 326, which is larger than those of the clinical used T_2 contrast agents, such as Resovist, Feridex, and Combidex. More significantly, a small tumor down to 4 mm is detected in vivo via intravenous injection of these nanoprobes under both UC optical and T_2-weighted MRI modalities.

In addition to introduce the rare earth ion with magnetism properties, the integration of UCNPs with superparamagnetic nanoparticles can also impart the UCNPs nanocomposites with MRI ability, such as iron oxide [132,133,210–214] and manganese oxide (MnO_2) [157,215,216]. Especially MnO_2, it can degrade rapidly within the tumor microenvironment (TME) and release Mn^{2+} ions, endowing UCNPs with TME-responsive MRI capacity. Very recently, Lin et al. have successfully grown mesoporous MnO_2 shell on the surface of UCNPs coated with mesoporous silica via a facile ultrasonic way, and then modified with polyethylene glycol (UCSM-PEG) [215]. In TME, the fast degradation of mesoporous MnO_2 shell results in markedly enhanced T_1 -contrast MRI signals due to the released paramagnetic Mn^{2+} ions (Fig. 7), offering the nanosystem with the tumor-enhanced UCL/CT/MRI imaging capability.

UCNPs for dual-modality UCL/CT imaging

CT is a common used imaging tool for tumor diagnosis in clinical owing to its deep tissue penetration capability and high spatial resolution. An ideal CT contrast agent should contain electron dense elements with high atomic number, such as iodine-based CT contrast agent currently used in clinic, Bi, and Au. Lanthanide ions have higher atomic numbers than iodine and show excellent X-ray attenuation ability, thus arousing significant interests as CT contrast agents [121,217–219]. Lu and coworker first designed and synthesized Gd-doped $NaYbF_4$:Er nanoparticles with excellent X-ray attenuation ability, [121] which is superior to a clinical iodinate agent in present use and even more effective than currently available Au-, Pt-, Bi-, and Ta-based nanoparticles CT contrast agents under normal operating conditions (120 kVp). Thanks to the highest atomic number of Lu^{3+} ions among lanthanide elements, $NaLuF_4$ UCNPs recently have been developed as more efficient CT contrast agent [220,221]. Recently, our group reported Yb^{3+}/Er^{3+}-codoped Bi_2O_3 UCNPs as dual modality probe for UCL and CT imaging [222]. The obtained UCNPs as CT contrast agents exhibited significant enhancement of contrast efficacy than iodine-based contrast agent at different voltage setting (80-140 kVp) owing to the existence of both Bi^{3+} and Yb^{3+}. Integration UCNPs with other CT contrast agent is another effective strategy to construct bimodal imaging probes for UCL/CT imaging, such as Au and TaOx nanoparticles [137,223,224].

UCNPs for other imaging

Nuclear imaging techniques, including PET and SPECT, have the highest sensitivity at the picomolar level and tissue penetration, which could make up the shortcomings of UCL and other imaging modalities. Introducing radioactive isotopes into UCNPs endows them nuclear imaging capacity, such as ^{18}F and $^{153}Sm^{3+}$ ions. Li and coworkers successfully achieved UCL/PET dual-modality lymphatic node imaging and dual-modal UCL/SPECT blood pool imaging through this strategy [225,226].

PA imaging is a powerful tool for noninvasive visualization of tissue structures with high contrast, good spatial resolution, and deep imaging depth. Very recently, Paras N. Prasad et al. reported a new hierarchical nanotheronostic platform (UCNP@$mSiO_2$-ICG) with UCNPs ($NaYF_4$:18%Yb, 2%Er@$NaYF_4$:30%Nd, 10%Yb) as core and an additional mesoporous silica as shell containing sealed high concentration of ICG molecules [227]. Under NIR excitation at 800 nm, this nanoplatform can act as both UCL imaging and PA imaging agents in vitro and in vivo. Importantly, PA imaging experiments demonstrated that UCNP@$mSiO_2$-ICG could be delivered to

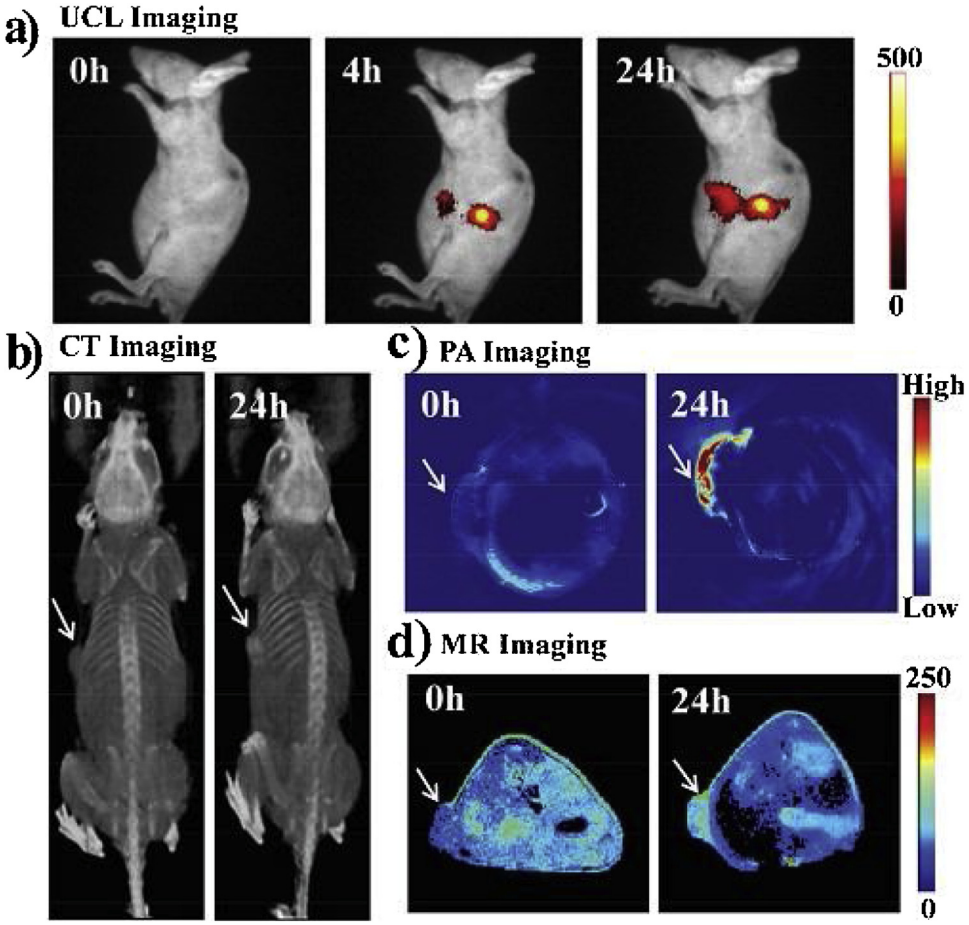

Fig. 8. In vivo multimodal imaging. a) UCL imaging, b) CT imaging, c) photoacoustic imaging, and d) T_1-MR imaging of HeLa tumor-bearing mice. [Reference 145] printed with permission from Wiley.

brain vessels with better angiography depth and longer circulation time.

Recently, the applications of UCNPs for multimodal bioimaging have aroused significant interests since the combination of different imaging modalities can take advantage of their respective merits to offset the limitation of single imaging modality, providing more reliable and accurate detection of tumor [204,228–231]. Our group synthesized core-shell structured $LiLuF_4$@$LiGdF_4$:Yb,Er/Tm@$LiGdF_4$ nanoparticles via a simple high boiling solvent process, which exhibited good performances as UCL/MRI/CT tri-modal imaging for tumor diagnosis [228]. Recently, Nie et al. fabricated UCNPs with multi-shell structure of $NaYF_4$:Yb:Er@$NaYF_4$:Yb@$NaNdF_4$:Yb@$NaYF_4$@$NaGdF_4$(CS2), and fuctionalized with exogenous PA imaging contrast agent indocyanine green (ICG) [230]. The obtained CS2-ICG offered a penetration depth up to 2.5 cm in turbid biological tissue under 800 nm excitation, and PA imaging depth was significantly improved from ≈4.8 to ≈10 mm. The animal experiments further demonstrated CS2-ICG could use as deep UCL/MRI/PA trimodal imaging probes for tumor. Very recently, Kuang et al. constructed core-satellite nanoassemblies through complementary base pairing. They chose Au nanorods dimer as core, and chlorin e6 (Ce6)-attached $NaGdF_4$:Yb, Er as satellite (NR dimer-UCNP-Ce6) [145]. Yb and Er, Gd, Yb, and Au nanorods dimer were responsible for UCL, MRI, CT, and PA imaging, respectively. After injection of NR dimer-UCNP-Ce6, the tumor can be visualized by those four imaging modalities. Importantly, these imaging modalities can provide detailed information of tumor (Fig. 8).

UCNPs for stimuli-responsive theranostics

For constructing stimuli-responsive theranostics, several kinds of stimuli-responsive cancer therapies have been integrated into UCNPs, ranging from chemotherapy, PDT, PTT to chemodynamic therapy (CDT), which are expect to further optimize the various factors of treatment based on the imaging information to attain personalized medicine. Except for providing diagnostic information of tumor, UCNPs in stimuli-responsive theranostics nanoplatform also perform other functions for therapy based on their wavelength-converting ability: (i) control the drug release by NIR light-induced photochemistry processes; (ii) excite the photosensitizer for PDT by NIR to avoid the harm of UV light and enhance the penetration depth in tissue; (iii) assist Fenton reaction to improve the efficiency of CDT; (iv) and monitor the distribution and accumulation of drugs. This section highlights various types of stimuli-responsive theranostics based on UCNPs, sorted according to the mechanism of response to a given stimulus (Table 3).

NIR light-responsive theranostics based on UCNPs

Light, as a noninvasive stimulus, has attracted much more attention and widely used for constructing responsive theranostics owing to its captivating features, such as adjustable wavelength, power, irradiation time, and spot size. Especially, phototriggered theranostics possess highly spatial and temporal precision, resulting in improved therapeutic efficacy and minimized side effects. However, the commonly used phototriggers are generally high energy UV or visible light featured with serious phototoxicity

Table 3
A summary of recent work on stimuli-responsive UCNPs theranostic nanoagents.

Trigger	Responsive link/agent	Imaging modality	Therapeutic modality	Ref.
NIR light	o-nitrobenzyl (NB)	UCL	Chemotherapy	[241]
NIR light	blue-light-cleavable ruthenium	UCL	Chemotherapy	[242]
NIR light	amino-coumarin derivative	UCL	Chemotherapy	[244]
NIR light	Pt (IV) pro-drugs	UCL/MRI/CT	Chemotherapy	[246]
NIR light	azobenzene groups	—	Chemotherapy	[247]
NIR light	azobenzene functionalized polymers	Luminescence imaging	Chemotherapy	[248]
NIR light	azobenzene molecules	—	Chemotherapy	[249]
NIR light	silicon phthalocyanine dihydroxide (SPCD)	UCL/CT/PET	Chemotherapy/PDT	[251]
NIR light	β-carboxyphthalocya-nine zinc or Rose Bengal	UCL/CT	PDT	[159]
NIR light	Ce6	UCL	PDT	[119]
NIR light/pH	Ce6	UCL/MRI	PDT	[126]
NIR light	Ce6	UCL	PDT/Immuno- therapy	[252]
NIR light	Rose Bengal	PAI	PDT	[253]
NIR light	Zn(II)-phthalocyanie	UCL	PDT	[118]
NIR light	Aminolevulinic acid	UCL	PDT	[256]
NIR light	Rose bengal	UCL/MRI	PDT	[191]
NIR light	Zr-based porphyrinic nanoscale MOFs (nMOFs)	UCL	Chemotherapy/PDT	[257]
NIR light	TiO_2	UCL/MRI/CT	PDT	[150]
NIR light	TiO_2	UCL/MRI/CT	PDT	[190]
NIR light	TiO_2	UCL	PDT	[149]
NIR light	g-C_3N_4	UCL/MRI/CT	PDT/PTT	[260]
NIR light	g-C_3N_4 quantum dots	—	PDT	[261]
NIR light	black phosphorus sheets	—	PDT	[262]
NIR light	Ce6 and MC540	UCL	PDT	[264]
NIR light	Ce6 and MC540	UCL/MRI/CT	PDT	[265]
NIR light	ZnPC and MC540	UCL	PDT	[266]
NIR light	carbon dots and ZnPC	CT/MRI/UCL	PTT/PDT/Chemotherapy	[272]
NIR light	Au nanorods	UCL	PTT/PDT	[275]
NIR light	Au nanoclusters	PAI/MRI/CT/UCL	PTT/PDT	[276]
NIR light	CuS NP	UCL/MRI/CT	radiotherapy /PTT	[146]
NIR light	MoS_2 nanosheet	UCL/MRI/CT	PTT/PDT	[277]
NIR light	polydopamine (PDA)	UCL/CT	PTT	[192]
NIR light	ICG	UCL	PDT/PTT	[281]
NIR light	$ZnFe_2O_4$	UCL/MRI/CT/PAI	PDT/Chemotherapy	[284]
pH	PAA shell	UCL	Chemotherapy	[292]
pH	hydrazone bonds	UCL/MRI/CT	Chemotherapy	[201]
pH	ZnO	UCL/MRI/CT	Chemotherapy	[293]
pH	DNA and Ce6	UCL	PDT	[294]
pH	Peptide and Pyropheophorbide a	UCL	PDT	[295]
GSH	disulfide bonds	UCL/MRI/PAI	PTT/Chemotherapy	[297]
GSH	disulfide bonds	—	PDT/Chemotherapy	[298]
GSH	Mn-doped silica	UCL/MRI/CT	Chemotherapy	[216]
ROS	thioketal linker	UCL	PDT/Chemotherapy	[301]
ROS	thioketal linker	UCL	PDT/Chemotherapy	[302]
ROS	MnO_2 nanosheets	UCL	PDT/radiotherapy	[157]
cathepsin B	Succinicacid–glycine –phenylalanine–leucine–glycine (SGFLG)	UCL	PDT/Chemotherapy	[304]
cathepsin B	cysteine and 2-cyanobenzothiazole	PAI/UCL	PDT/Chemotherapy	[305]
caspases-3	DEVD-DOX prodrug	UCL	PDT	[306]
Temperature	poly(N-isopropylacrylamide-co-methacrylic acid)	UCL	Chemotherapy	[308]
Temperature	P(NIPAm-co-MAA)	UCL/CT	PDT/PTT/Chemotherapy	[309]
Temperature	1,2-dipalmitoyl-sn-glycero-3-phosphocholine	UCL	PTT/Chemotherapy	[311]

and low tissue penetration depth because most of photosensitive materials are sensitive to the irradiation within this wavelength range. Spurred by these challenges, NIR light-responsive theranostics based on UCNPs have been fabricated and open the door for realizing NIR-controlled imaging and therapy since their unique upconversion luminescence properties enable UCNPs to trigger photoreactions of the photosensitive materials, excited the PS, and assist the Fenton reaction by NIR, thus offering enhanced penetration depth in biological tissues and negligible phototoxicity. According to the therapeutic function, NIR light-responsive theranostics based on UCNPs mainly include drug delivery system, PDT and photo-assisted CDT.

NIR light-responsive drug delivery system

To date, NIR light-responsive drug delivery system based on UCNPs deploy two main strategies to achieve NIR control over the delivery process, involving (i) NIR light-induced photolysis, and (ii) NIR light-induced photoisomerization.

(i) NIR light-induced photolysis. Based on photolysis strategy, bioactive molecules must be boned with photolytic materials via photolabile groups, and then loaded onto the UCNPs based nanocarriers. UCNPs convert NIR light to specific wavelength light (UV or visible light), which can trigger photolysis of photolytic materials, thereby releasing and activating bioactive molecules at the targeted site. In recently year, several photolysis reactions have been harnessed to control various bioactive molecules release from drug delivery system based on UCNPs, such as D-luciferin, [232] carboxylic acid, [233] nitric oxide (NO), [234,235] DOX, [138,236] siRNA [237], Pt complex [238,239] and cell adhesion molecules [240]. Here, we focus the molecules that can inhibit tumor growth.

DOX, as a widely used anti-cancer drug, has been successfully demonstrated the feasibility of the on-demanded release from UCNPs based nanocarriers triggered by NIR light. A representative work has been done by Liu's group [241]. They constructed the crosslinked $mSiO_2$ coated $NaYF_4$:Yb,Tm@$NaYF_4$ UCNPs drug delivery systems, in which photolabile molecule o-nitrobenzyl (NB) as the linker capped the pores of $mSiO_2$ for controlling DOX release.

Because the absorption profile of NB matches well with the emission bands of $NaYF_4$:Yb, Tm UCNPs, the photolysis of NB can be triggered by NIR light, thereby inducing the photo-controlled DOX release into the living cells. Very recently, Tan et al. further explored the applications of photoregulated drug delivery in vivo [242]. They first fabricated ultrasmall-superbright Nd^{3+}-sensitized $NaGdF_4$:Yb,Tm,Ca@$NaYbF_4$:Ca@$NaNdF_4$:Gd,Ca UCNPs through doping Ca^{2+} ions. After coating $mSiO_2$ on the surface of UCNPs, the blue-light-cleavable ruthenium (Ru), as the molecular valve, is grafted on the surface of UCNPs to prevent leakage of DOX before reaching the tumor. Upon 808 nm light irradiation, the upconverted blue light triggers the cleavage of Ru and uncaps the pores to release DOX, killing the cancer cells. The inhibition of tumor growth further demonstrates the therapeutic efficacy of light controllable release of DOX. Except for loading DOX into $mSiO_2$, DOX also boned with NB, and then attached onto the surface of UCNPs. Under irradiation with 980 nm light, the UV emission of the UCNPs induced photocleavage of NB, thus resealing the DOX from UCNPs based nanocarriers [243].

Another striking example was reported by Li and coworkers [244]. They developed a yolk-shell upconversion nanoparticle (YSUCNP) with $NaYF_4$:Yb,Tm@$NaLuF_4$ as inner yolks, which displayed intense NIR-to-UV emission and large pore volume (Fig. 9I). The anticancer drug chlorambucil, which was linked to the hydrophobized phototrigger of amino-coumarin derivative, could be loaded into the YSUCNP, exhibiting no premature release of drug under physiological conditions. The drug release could be triggered by continuous-wave 980 nm light in a controlled pattern. Furthermore, phototriggered drug release in animal models has been successfully performed for the first time. This work points out the direction for phototriggered drug delivery system in future practical application.

As other kinds of antitumor drugs, Pt (II) complexes including cisplatin, carboplatin, and oxaliplatin have been successfully applied to treat various types of cancer. Unfortunately, the serious toxic side-effects and drug resistance hinder their further applications in clinical practice. To surmount these problems, Pt (IV) complexes as promising pro-drugs of Pt (II) have aroused considerable interests owing to their good chemical inertness, low cytotoxicity for normal tissues, and redox properties. Importantly, UV light can effectively induce photoactivate Pt (IV) complexes to release cytotoxic Pt (II) components. Recently, in light of the harm of UV light, many efforts have aimed at constructing UCNPs nanocarriers for Pt (IV) prodrug delivery and releasing cytotoxic Pt (II) mediate by NIR. For instance, Xing et al. reported a NIR light-activated nanoplatform based on silica-coated $NaYF_4$:Yb,Tm UCNPs conjugated with a photoactivatable Pt (IV) prodrug and an apoptosis sensing peptide with a flanking activatable FRET pair consisting of a far-red fluorescence donor Cy5 and a NIR quencher Qsy21 for the remote control of antitumor platinum prodrug activation and simultaneously for real-time imaging of apoptosis induced by activated cytotoxicity [245]. Upon NIR light irradiation, the converted emission from UCNPs@SiO_2 could locally activate the Pt (IV) prodrug and thus efficiently induced potent antitumor cytotoxcity in both cisplatin-sensitive and resistant tumor cells. Moreover, such NIR light-controlled tumor inactivation triggers the cellular apoptosis, which can be imaging in real time by the restoring NIR fluorescence owing to the cleaving of the NIR imaging peptide probe from the nanoparticle surface by highly activated caspase. This work not only provide a promising strategy to remotely control the localized activation of the Pt (IV) prodrug at the target tumor sites, but more importantly, the developed a tumor markers to image in real time and evaluate the antitumor therapy at the cellular level. Lin and coworkers further investigated the theranostic applications of photoregulated Pt (IV) prodrug in vivo (Fig. 9II) [246]. Core-shell structured $NaYF_4$:Yb^{3+}/Tm^{3+}@$NaGdF_4$:Yb^{3+} UCNPs were used as nanocarriers, and conjugated with Pt (IV) prodrugs on their surface. The UCNPs can activate the pro-drug to high toxicity Pt (II) drug under irradiation with NIR light, which not only can kill cancer cells but also suppress tumor growth in the animal model. Meanwhile, this system can realize UCL/MR/CT trimodality imaging, which could provide complete information. This work provides the strategy of harness NIR-to-UV UCNPs to active Pt (IV) prodrug in vivo for the first time, which paves the way for practical applications of photoactivated Pt (IV) prodrug.

(ii) NIR light-induced photoisomerization. Apart from photolysis process, photochromism phenomenon also has been harnessed to design of the UCNPs-based light-initiated drug delivery systems because the molecular structure or conformation of photochromic compounds can change reversibly along with a change of absorption spectrum upon exposure to certain wavelengths of light, especially UV light. As mentioned above, in view of the weaknesses of using direct UV or visible light to induce the photoreaction, NIR has emerged as an appealing alternative to trigger photochemical isomerization through upconversion process. To date, various photochromic compounds have been demonstrated to achieve the reversible transformation in the molecular structure with the assistant of UCNPs, such as dithienylethene derivatives, azobenzene derivatives, and spiropyran derivatives. Based on these investigations, phototrigerred UCNPs-based drug delivery systems through photochromism process have been successfully developed. Shi and coworkers reported a NIR light-triggered anticancer drug delivery system based on $mSiO_2$-coated $NaYF_4$:TmYb@$NaYF_4$ UCNPs [247]. The azobenzene groups (azo) as "stirrer" were first installed into the channel of $mSiO_2$ shell. Upon 980 nm irradiation, simultaneous UV and visible light emitted by the UCNPs induced the reversible transformation of azo between trans- and cis-isomer, leading to a continuous rotation-inversion movement to propels the release of DOX. Very recently, Zhao et al. constructed nanocapsules based on azobenzene functionalized polymers and up/downconversion nanoparticles (U/DCNPs) by layer-by-layer co-assembly strategy (Fig. 9III) [248]. The nanocapsules (ca. 180 nm) could decompose to small U/DCNPs (ca. 20 nm) and release the drug under irradiation with 980 nm NIR since the converted UV/visible light by U/DCNPs can trigger the photoisomerization of azobenzene groups in the framework, resulting in high tumor accumulation and treatment outcome as well as fast elimination. Such strategy lays solid foundations towards a novel platform for next generation nanotherapeutics with both spatial and temporal external control.

Another striking example was reported by Zhao and coworkers, who first synthesized dual-compartment Janus mesoporous silica nanocomposites (UCNP@SiO_2@$mSiO_2$&PMO) [249]. The Janus nanocomposites possess the unique dual independent mesopores with capacity of loading hydrophobicity/hydrophilicity drugs. After modifying with light-sensitive azo molecules and heat-sensitive 1-tetradecanol molecules, the Janus mesoporous silica nanocomposites can be realized heat and NIR light bimodal triggered dual-drugs release, and the achieved cancer cell killing efficiency is significantly higher than that for the single triggered drugs delivery system. This work provides a new concepts and architecture for the design of upconverting nanocarriers for multiple drug delivery and combined therapy.

NIR light-triggered photodynamic therapy based UCNPs

PDT that employs a PS to generate the singlet oxygen ($^1O_2$) or other reactive oxygen species (ROS) by irradiating with an appropriate excitation light has been clinically approved for the treatment of several types of solid cancer, and aroused significant research interests in the past decade. However, conventional PDT mainly utilizes the visible or even UV light to excite the PS, which exhibits poor penetration depth due to the light absorption and scattering in biological tissues, confining to treat the tumors

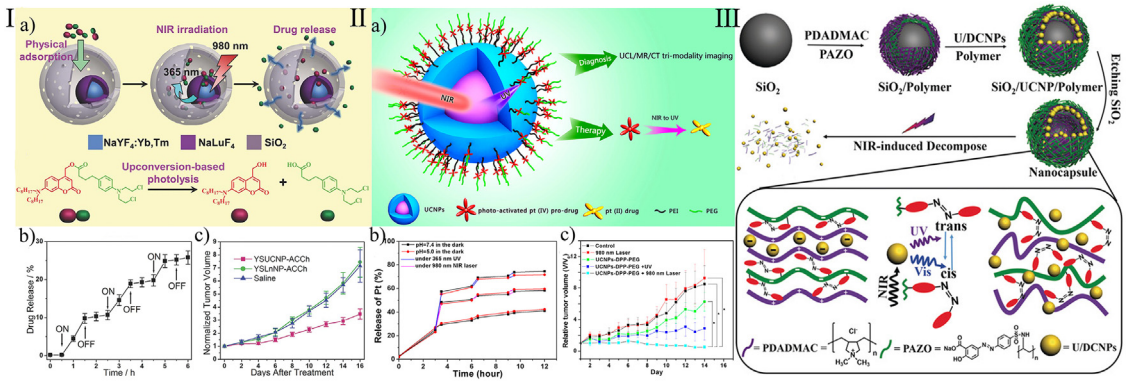

Fig. 9. (I) a) Schematic illustration of the NIR-regulated upconversion-based PDD, b) the photolysis of the prodrug under upconversion emission from the YSUCNPs, c) the photo-regulated release of chlorambucil (drug) from YSUCNP-ACCh controlled by a 980 nm laser, ("ON" and "OFF" indicate the initiation and termination of laser irradiation, respectively, and d) The release profiles of chlorambucil from YSUCNP-ACCh and YSLnNP-ACCh (control material) in PBS solution (pH = 7.5) under CW 980 nm irradiation. [Reference 244] printed with permission from Wiley. (II) a) Schematic illustration of the characterization of UCNP-DPP-PEG nanoparticles, b) Release profile of UCNP-DPP-PEG nanoparticles under different pH values (7.4 and 5.0) alternately changing the illumination conditions between 980 nm NIR irradiation (or 365 nm UV) and in the dark conditions, and c) In vivo tumor volume changes of Balb/c mice on different groups after various treatments, 980 nm laser irradiation for 30 min, UV (365 nm) irradiation for 30 min, or without any irradiation. [Reference 246] printed with permission from ACS. (III) Illustration of the fabrication of the up/downconversion nanoparticle (U/DCNP) functionalized hollow polymer nanocapsules and the near-infrared light induced decomposing process from 180 nm nanocapsules to scattered polymers and 20 nm U/DCNPs. [Reference 248] printed with permission from Wiley.

under the skin and leading to less efficacious to internal or large tumors. NIR light, within the "window of optical transparency" (750-1100 nm) of tissue, not only can afford significantly deeper penetration depths than the visible light, but also exhibit a low phototoxicity to normal tissues. Motivated by the unique capability of converting NIR light into UV-visible light, UCNPs-based PDT have gained a great deal of attention in recent years. Since Zhang first reported $mSiO_2$ coated UCNPs for NIR triggered cancer PDT, a lot of researches have been demonstrated the success of UCNPs-based PDT for cancer therapy at cellular level [250]. In this section, we focus on the recent advance of UCNPs-based PDT triggered by NIR for cancer therapy in vivo. Except for light, PS molecules and oxygen within the tissue at tumor site are the other key components in PDT process. The development of UCNPs-based PDT will be reviewed from these two directions below.

Photosensitizers. In UCNPs-based PDT process, the selection and attachment of PS to the UCNPs is of prime importance for the success of the treatment. The PS molecules can be excited from a ground state to a high-energy state, and then transfer the energy to neighboring oxygen to generate $^1O_2$ or ROS. Therefore, it is necessary that the UCNPs emission should match well with the absorption of PS for efficient energy transfer. Meanwhile, sufficient amount of PS in close proximity to the UCNPs is required for sufficient ROS generation. The widely used photosensitizers involve mainly two categories: (i) organic photosensitizers including zinc(II) phthalocyanine (ZnPc), merocyanine 540, mesotetraphenyl porphine (TPP), methylene blue (MB), rose bengal (RB), Chlorine6 (Ce6), tris(bipyridine)ruthenium(II), aluminum phthalocyanine (AlC4Pc), silicon phthalocyanine dihydroxide (SPCD), porphyrin, etc. (ii) semiconductors and photocatalys, such as titanium dioxide (TiO_2), graphitic carbon nitride (g-C_3N_4), ZnO, black phosphorus and fullerene.

Organic photosensitizers. As for organic photosensitizers, the appropriate strategy for loading of PS molecules on to UCNPs is vital to efficient energy transfer from UCNPs to PS. Silica encapsulation is the most popular approach to construct UCNPs-based PDT system. Recently, Shi and coworkers fabricated a UCNPs-based PDT system composed of $NaYF_4$:Yb^{3+}/Er^{3+}/Gd^{3+} UCNPs core and double silica shells, that is, middle dense and outer mesoporous silica layers for loading PS (SPCD) and pro-drug (TPZ) that toxic under hypoxic conditions [251]. Upon irradiation with NIR light, the upconverted red light matched with the absorption spectrum of SPCD, resulting in efficient energy transfer from UCNPs to PS. The generated large amount of ROS can suppress tumor growth. In the meanwhile, the creation of hypoxic microenvironment induced the activation of TPZ, achieving a high-effective synergistic tumor therapy. In order to further increase the loading capacity, rattle-structured UCNP-silica nanocomposites have been synthesized with the core of β-$NaLuF_4$:Gd/Yb/Er and the shell of benzene-bridged organosilica (Fig. 10a) [159]. Rattle structure and aromatic bridging groups increase the storage of PS, avoid their aggregation, and promote energy transfer owing to the shortening distance between UCNPs and PS, which are critical for improving PDT efficacy. Moreover, the UCNPs core can act as bimodal contrast for UC/CT imaging, making the nanocomposites highly promising for theranostic.

Non-covalent physical adsorption is another very simple strategy to load PS molecules on UCNPs, which is proposed by Liu's group. Ce6 molecules were loaded into the hydrophobic region of PEG functionalized $NaYF_4$:Yb, Er UCNPs for PDT [119]. Compared to the traditional PDT relying on visible light excitation, the obtained UCNPs-based PDT system exhibited much deeper tissue penetration depth, and thus the excellent tumor destruction was achieved. Based on this strategy, they constructed a UCNPs-based PDT system (UCNP@2xCe6-DMMA-PEG) by layer-by-layer self-assembly process, which is highly sensitive to the environmental pH [126]. More nanocomposites were uptake by cancer cell at pH 6.8, and accumulated in the tumor after either intratumor injection or intravenous administration owing to the slightly acidic tumor microenvironment, resulting in enhanced PDT cancer-killing efficacy both in vitro and in vivo. Recently, Liu et al. used the same UCNPs-PEG nanocoposites for delivering both PS Ce6 and immune adjuvant imiquimod (R837). Under NIR irradiation, the effective photodynamic destruction of tumors generated a pool of tumor-associated antigens, which are able to promote strong antitumor immune responses in the presence of those R837-containing nanoparticles as the adjuvant (Fig. 10b) [252]. Moreover, the PDT with UCNP-Ce6-R837 in combination with the cytotoxic T-lymphocyte-associated protein 4 (CTLA-4) checkpoint blockade not only shows excellent efficacy in eliminating tumors exposed to the NIR laser but also results in strong antitumor immunities to inhibit the growth of distant tumors left behind after PDT treatment. This work demonstrated the great potency of inte-

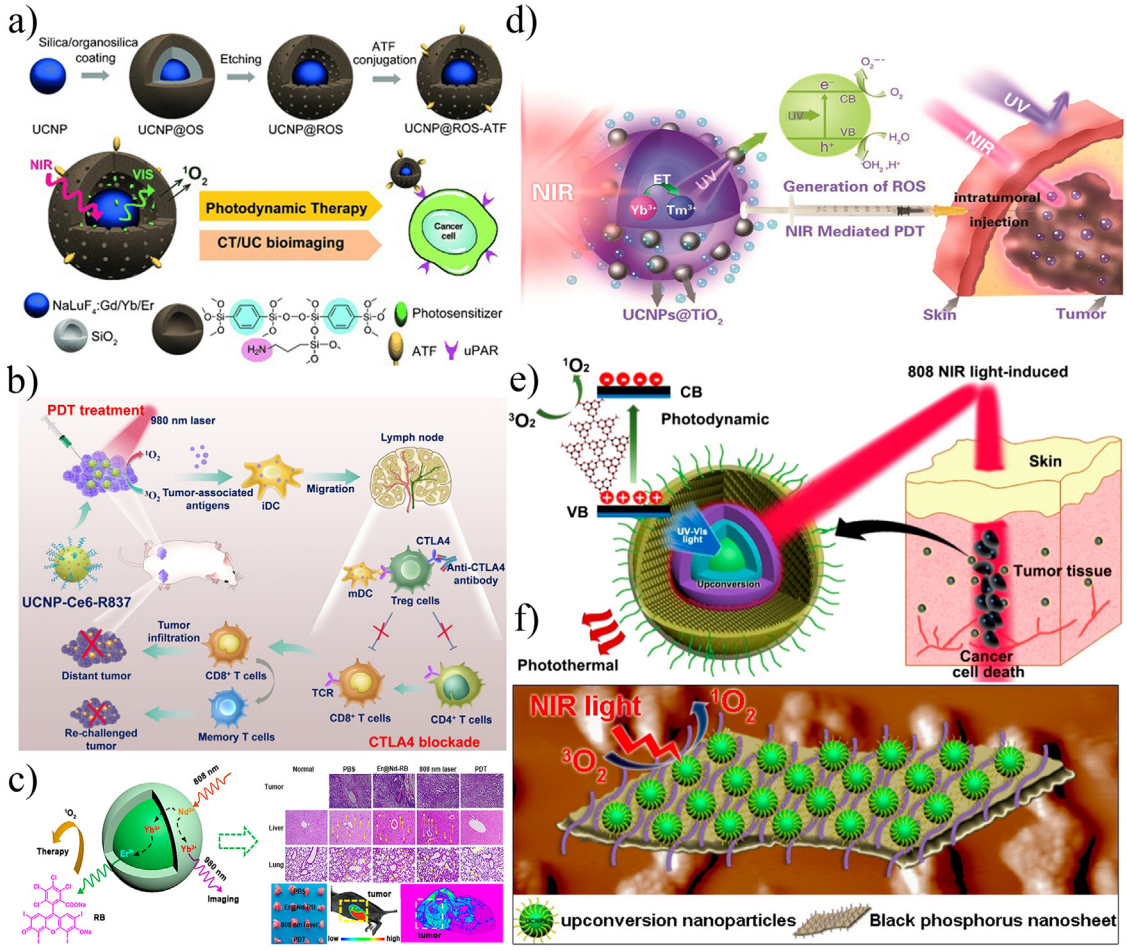

Fig. 10. a) Illustration of multifunctional nano-bioprobes based on rattle-structured organosilica-shelled UCNPs. [Reference 159] printed with permission from Wiley. b) Scheme summarizing the mechanisms of combining NIR-mediated PDT with CTLA-4 checkpoint blockade for cancer immunotherapy. UCNP-Ce6-R837 nanoparticles under NIR light would enable eff ;ective photodynamic destruction of tumors. The generated tumor-associated antigens in the presence of those nanoparticles as the adjuvant are able to promote strong antitumor immune responses, which with the help of a CTLA-4 checkpoint blockade would eliminate primary tumors under direct NIR exposure, inhibit the growth of distant tumors left behind after PDT, and further yield a long-term immune memory to prevent tumor reoccurrence. [Reference 252] printed with permission from ACS. c) Schematic of the dual-band luminescent LNPs in application for PDT, together with NIR imaging and MRI. [Reference 191] printed with permission from ACS. d) Schematic illustration of potential mechanism of UCNPs@TiO_2-based NIR light mediated PDT treatment. [Reference 150] printed with permission from ACS. e) The mechanism of the charge tansfer and the ROS generation of UCNPs@g-C_3N_4-PEG nanocomposite upon 808 nm NIR light irradiation. [Reference 260] printed with permission from ACS. f) UCNPs-BPS composite for 808 nm excited photodynamic therapy. [Reference 262] printed with permission from ACS.

grating UCNPs-based PDT with cancer immunotherapy. Generally, UCNPs-based PDT needs to exposure to NIR for long time during the therapy. Very recently, Zhang et al. constructed a NIR rechargeable "optical battery" for irradiation-free PDT by embedding upconversion materials, persistent luminescence materials, PS into biocompatible polydimethylsiloxane [253]. As long as the PDT "optical battery" is charged by 980-nm NIR laser for 5 s, it can produced green persistent luminescence to excite the photosensitizer and generate cytotoxic singlet oxygen for continuous irradiation-free PDT (~30 min) without external irradiation. Such NIR rechargeable "optical battery" may give rise to next generation of intelligent stimuli-responsive nanomedicine and noninvasive photo bio-stimulation research for future clinical applications.

However, the PS molecules physically entrapped or encapsulated inside the silica network or the hydrophobic layer suffered from prematurely release during the circulation in the blood, resulting in reduced PDT efficiency and unwanted side effects. Covalent bonding of PS molecules on the surface of UCNPs is a promising strategy to ameliorate these hurdles [191,254,255]. Zhang and coworkers covalently bonded ZnPc on the surface of $NaYF_4$:Yb^{3+}, Er^{3+} UCNPs for PDT, which significantly shortened the distance and enhanced the energy transfer between UCNPs and ZnPc [118]. The high tumor inhibitory ratio of approximately 80.1% was obtained in animal model. Han et al. developed a UCNP-PDT system with high Yb doped UCNPs as core, CaF_2 as shell, and conjugated the prodrug 5-ALA (ALA-r-$NaYF_4$:Yb,Er@CaF_2 UCNPs) for deep-set tumors treatment [256]. The obtained UCNPs shows a high absolute upconversion quantum yield of 3.2% in red-emission, which is 15-fold stronger than the known optimal β-phase core/shell UCNPs. Such strong emission caused high singlet oxygen generation, resulting in significant PDT effect in deep-set tumor (>1.2 cm). This work marks a major step forward in photodynamic therapy utilizing UCNPs to effectively access deep-set tumors. However, owing to the absorption of UC emissions by photosensitizers to generate singlet oxygen for PDT, the imaging signals from UCNPs are significantly weakened. Yan et al. reported Nd^{3+} sensitized UCNPs with dual-band visible and NIR emissions for PDT and imaging under a single 808 nm excitation (Fig. 10c) [191]. Such theranostics nanoplatforms not only effectively inhibited the growth and metastase of pulmonary and hepatic tumor, but also avoided the overheating effect induced by the laser irradiation. Importantly, NIR emissions deriving from Yb^{3+} could realize the imaging of tumor, guiding the PDT. Very recently, the PS molecules (Zr-based porphyrinic nanoscale metal – organic frameworks, nMOFs) have been success-

fully grown on the surface of UCNPs through selective anisotropic growth [257]. Such heterostructure endows UCMOF with high production of singlet oxygen under NIR light irradiation owing to the direct resonance energy transfer from the UCNPs to nMOFs. Moreover, the porous channels of the nMOF enable an efficient cancer treatment strategy by combining chemotherapy and NIR-induced PDT.

Inorganic photosensitizers. In recent years, some inorganic nanoparticles, including TiO_2, g-C_3N_4, ZnO, graphene quantum dots and black phosphorus, have been explored as PS for constructing UCNPs based-PDT systems owing to their unique advantages, such as more stable and a longer duration of action in an organism comparing to the organic PS. For instants, TiO_2 featured with minimal dark cytotoxicity but serious cytotoxicity triggered by UV light has been used as a potential photosensitizer in UCNPs based-PDT systems [258,259]. Lin and coworkers fabricated core-shell structured composites with $NaYF_4$:Yb^{3+},Tm^{3+}@$NaGdF_4$:Yb^{3+} UCNPs core and TiO_2 crystallized shells (UCNPs@TiO_2 NCs, Fig. 10d) [150]. UCNPs@TiO_2 NCs can efficiently generate intracellular ROS under 980 nm NIR laser excitation, inducing apoptotic cancer cell death in vitro and effective tumor inhibition. Compared to previous UCNP-based organic PS PDT systems, the novelty of this work involves: (i) the covalent linking of TiO_2 as a PS by themselves with high loading can effectively prevent PS molecules from leaking and self-aggregating, and (ii) TiO_2 shells were coated directly on the surfaces of UCNPs, ensuring maximum energy transfer from UCNPs to TiO_2 so as to facilitate the generation and release of ROS. To solve the issue of limited penetration depth and overheating of the excited 980 nm NIR light, the same group developed a multifunctional TiO_2 nanoparticles decorated Nd^{3+}-sensitized UCNPs for 808 nm NIR light mediated PDT [190]. The core-multishell structured $NaGdF_4$:Yb/Tm@$NaGdF_4$:Yb@$NaNdF_4$:Yb@$NaGdF_4$ UCNPs completely eliminate the deleterious cross-relaxation between the activated Tm^{3+} and sensitized Nd^{3+} by adding an inner quenching shield layer, thus proving strong UCL emission for PDT upon the 808 nm laser excitation. The existence of $mSiO_2$ shell offer large surface area for loading a large amount of TiO_2 PS, producing a significant amount of ROS to effectively kill tumor cells. Compared with 980 nm and UV irradiations, 808 nm NIR light-mediated PDT shows much higher antitumor efficacy due to the higher tissue penetration depth. For controlling the amount of TiO_2 PS loaded in UCNPs, Zhang et al. designed core-shell structured nanocomposite in which a single monodisperse $NaYF_4$:Yb,Tm UCNPs core is surrounded by a thin layer of TiO_2, the amount of which can be precisely controlled constructs and achieving stable loading of sufficient amount of PS [149].

Owing to the relatively narrow band gap (2.7 eV), g-C_3N_4 can be responsive to UV-vis region light and activate molecular oxygen to produce more active radicals for PDT. In recent years, g-C_3N_4 has been wide used as PS in UCNPs-based PDT systems. A novel UCNPs@g-C_3N_4-PEG nanocomposite was first fabricated via a template etching process for the 808 nm mediated PDT (Fig. 10e) [260]. The upconverted UV and visible lights from the $NaGdF_4$:Yb/Tm@$NaGdF_4$:Yb@$NaNdF_4$:Yb upconversion core upon 808 nm NIR light irradiation excite the electrons of g-C_3N_4 to produce a large amount of ROS for PDT. The PDT combined with the PTT effect derived from Nd^{3+} in UCNPs cause remarkable tumor inhibiting effect in vitro and in vivo. Very recently, g-C_3N_4 quantum dots (QDs) have combined with $NaYF_4$:Yb^{3+}/Tm^{3+} UCNPs via the positive ligand poly(L-lysine) for PDT [261]. g-C_3N_4 QDs not only acted as PS for NIR light-mediated PDT, but also realized blue-to-green visible light for imaging.

Apart from the above motioned PS, black phosphorus sheets (BPS) as PS have been exploited for PDT [262]. After modifying with PEG-NH_2, ultrathin BPS were integrated with the small $NaGdF_4$:Yb,Er@Yb@Nd@Yb UCNPs by electrostatic interaction (Fig. 10f). Upon 808 nm NIR light irradiation, the UCNPs-BPS composite show the strongest tumor inhibition effect owing to their greater generation capability than those of 650 and 980 nm irradiations.

Two types of photosensitizers. More recently, for improving the treatment effect of PDT, two types of PS molecules have been incorporated into a single nanoplatform [263]. Zhang et al. first incorporated ZnPc and MC540 into a single nanoplatform, and excited by two UC emission peaks of $NaYF_4$:Yb/Er under 980 nm NIR irradiation, which exhibited a greater PDT efficacy due to fully utilizing the upconverted energy to generate of $^1O_2$ comparing to the single-PS loaded PDT system [264]. The significant tumor regression of melanoma tumors was observed in the animal model. After that, Lin et al. fabricated IR-808-sensitized $NaGdF_4$:Yb,Er@$NaGdF_4$:Nd,Yb UCNPs, and coated with $mSiO_2$ for loading two PS Ce6 and MC540 through covalent bond and electrostatic interaction, respectively [265]. The ultrabright red and green UCL under low 808 nm excitation can be activate the two PS to generate cytotoxic ROS for antitumor therapy. Importantly, dual-photosensitizer UCNPs nanostructure exhibits higher PDT efficacy than those of the single-load nanosystem. Very recently, a mesenchymal stem-cell-membrane-camouflaged mesoporous silica-encapsulated β-$NaYF_4$:Yb^{3+},Er^{3+} UCNPs (SUCNPs@SiO_2) have been developed as an intravenous injectable photodynamic antitumor platform [266]. Two PSs (ZnPC and MC540) are highly loaded and simultaneously activated by a single 980 nm laser. The obtained SUCNPs@SiO_2 not only possesses good stability and biocompatibility but also displays intravenous injectability, immune escape capabilities, prolonged blood circulation time, and the tumor targeting functionalities of stem cells. More importantly, tumor growth was effectively inhibited owing to the high PS loading capacity and effective accumulation in tumors. This work paves the way for the development of bioactive cellular components as a platform for targeted PDT.

Oxygen environment at tumor site. As we have mentioned above, PDT employs PS to activate the transformation of surrounding O_2 at tumor site into cytotoxic $^1O_2$, causing the destruction of cancer cells. This process involves significant O_2 consumption, leading to drastically decreased therapeutic efficacy of PDT during continuing treatment. Therefore, it is critical desired to develop specific O_2 delivery system for overcoming the tumor hypoxia and improving the treatment effect. Very recently, Zhang et al. fabricated core-multi shell structured $NaGdF_4$:Yb,Er@$NaYF_4$:Yb@$NaGdF_4$:Yb,Nd@$NaYF_4$@$NaGdF_4$:Yb,Tm@$NaYF_4$ UCNPs functionalized with a novel ultrasensitive site-specific hypoxia probe (HP) and PS RB, and subsequently installed on the red blood cell (RBC) surfaces to obtain the RBC microcarriers (Fig. 11a) [267]. Upon 980 nm NIR excitation, the inactive HP can be transformed into active state specifically to trigger the O_2 release from oxygenated hemoglobin in a hypoxic condition. Owing to the increasing of O_2 amount, the PDT efficiency can be enhanced greatly under 808 nm NIR irradiation, which is further demonstrated by remarkably regressed the solid tumor volumes. Very recently, some catalysts have been used to catalyze and decompose H_2O_2 to generate O_2 for enhanced PDT effects on hypoxia solid tumors, such as manganese dioxide (MnO_2) nanosheets, [268,269] catalase, [270] and cerium oxide [271]. Zhang et al. constructed multifunctional UCNPs@TiO_2@MnO_2 nanocomposites (UTMs) for O_2 self-supplemented and ROS circulating amplified PDT (Fig. 11b) [268]. MnO_2 nanosheets can generate O_2 in tumor microenvironment (mild acid and excessive H_2O_2) to overcome tumor hypoxia for superior PDT efficacy, and obtained Mn^{2+} ions by decomposition can realize stimuli-enhanced T_1-weighted MRI. Meanwhile,

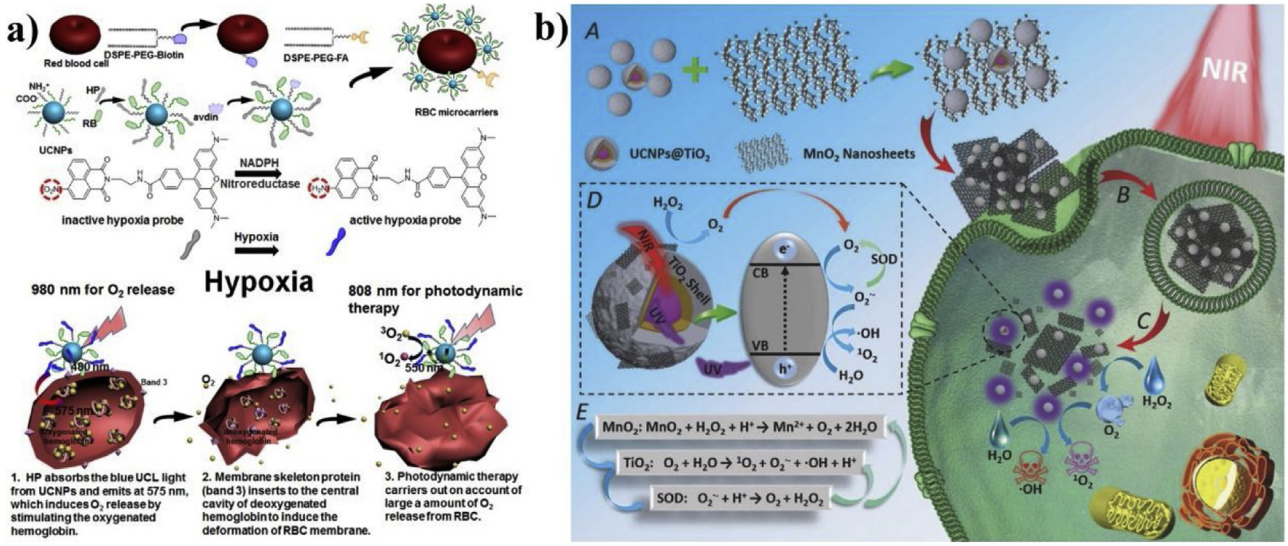

Fig. 11. a) Schematic illustration stepwise engineering of NIR-controlled orthogonal excitation-emission UCNPs anchored RBC microcarrier and O_2 release followed by RBC membrane deformation under 980-nm excitation to enhance PDT under 808-nm NIR excitation. [Reference 267] printed with permission from Elsevier. b) Schematic illustration of UTMs for O_2 self-supplemented and ROS circulating amplified PDT. [Reference 268] printed with permission from Wiley.

the quenched upconversion luminescence of UCNPs by MnO_2 nanosheets recovered for UCL imaging in tumor and activated TiO_2 nanoshells to produce cytotoxic $^1O_2$ and ·OH for PDT. Importantly, H_2O_2 and O_2 were regenerated by catalyzing intracellular superoxide dismutase, resulting in the circulate amplifying the ROS generation with a significantly enhanced PDT outcome. Owing to the catalase-like activities and photocatalyst features of cerium oxide nanoparticle, it also could realize O_2-evolving to improve the efficiency of PDT. Zhang et al. reported lanthanide ion-doped mesoporous hollow cerium oxide upconversion nanoparticles (Ce-UCNPs), which can not only realize in situ oxygen-producing through catalyzing the decomposition of the endogenous H_2O_2 of tumor but also convert NIR light to UV emission to trigger the triggered PDT simultaneously [271]. These works open up an exciting new area in oxygen-producing O_2 in situ to overcome hypoxic tumor.

NIR light-triggered photothermal therapy based UCNPs

PTT has attracted considerable attention over the years as one of the most promising alternative to current clinical cancer treatments (including surgery, radiotherapy, and chemotherapy) owing to its high efficiency and selectivity, minimal invasiveness, and favorable biosafety to normal tissues. Under NIR laser irradiation, photothermal agents absorbed the light to generate heat, resulting in the thermal ablation of tumor. Currently numerous nanomaterials with strong NIR absorption and high photothermal conversion efficiency have been successfully employed as photothermal agents for PTT, such as various of gold nanostructures, metal chalcogenides nanoparticles, carbon nanomaterials, and organic polymers. For UCNPs based PTT studies, UCNPs are combined with these mentioned photothermal agents to offer imaging guided PTT, which is regarded as an effective theranostic strategy. However, two different wavelengths NIR lights are usually required to implement imaging and therapy, respectively, which makes real-time monitoring and evaluation of treatment efficiency difficult. In this section, we will survey on the recent advance of UCNPs-based PTT nanoplatforms triggered by a single NIR light according to the different PTT agents.

Carbon nanomaterials. Recently, carbon nanomaterials emerged as promising agents for PTT owing to their intrinsic high NIR absorbance, such as graphene, [155] carbon dots [272] and carbon shells [273]. Lin's group designed and constructed the multifunctional GdOF:Ln@SiO_2 mesoporous capsules with DOX and ZnPc into the SiO_2 shell for PDT and chemotherapy, and then attached carbon dots on the surface of SiO_2 shell, which not only serve as the photothermal agents for PTT, but also prevent the DOX release during the delivery process (Fig. 12a) [272]. The smart design of the structure make the nanocomposites applied as both multiple imaging (CT, MRI, UCL, photothermal) agent and drug carriers for multiple anticancer therapy (PDT, PTT, and chemotherapy). The animal experiment indicated the cancer can be markedly inhibited with organs undamaged.

Au nanostructure. Different structured Au nanomatierls have been widely used as photothermal agents thanks to their capacity of inducing surface plasmon resonance (SPR), including nanoshells, [132] nanorods, [274,275] and nanoclusters [276]. For instance, Liu et al. prepared a hybrid plasmonic upconversion nanostructure (AuNR@UCNPs) by assembling UCNPs onto the surface of gold nanorods through electrostatic adsorption method [275]. Under 808 nm NIR light irradiation, the upconversion emissions could not only trigger AuNRs to generate heat for PTT through controlling the aspect ratio of AuNRs due to the match of the surface plasmon resonance peaks of with emissions of UCNPs, but also excite the photosensitizer capsulated in the mesoporous silica layer to generate ROS for PDT. This nanocomposite is a new generation of theranostic platform, which can be applied to imaging and combined PTT with PDT under single 808 nm NIR laser irradiation. Recently, captopril-stabilized Au nanoclusters (Au25) acted as both photothermal agents and new photothermal agents have been modified on the surface of mesoporous silica coated β-$NaGdF_4$:Yb/Er@β-$NaGdF_4$:Yb@β-$NaNdF_4$:Yb UCNPs [276]. Under the irradiation of 808 nm light, the newly formed Au25 shell exhibited a considerable photothermal effect and the production of $^1O_2$, leading to excellent tumor growth inhibition efficacy. Importantly, the 808 nm NIR light not only effectively triggered simultaneous PDT/PTT, but also conquered overheating effect of the conventional 980 nm laser.

Metal chalcogenides. Metal chalcogenides featured with high photothermal conversion efficiency and good thermal stabil-

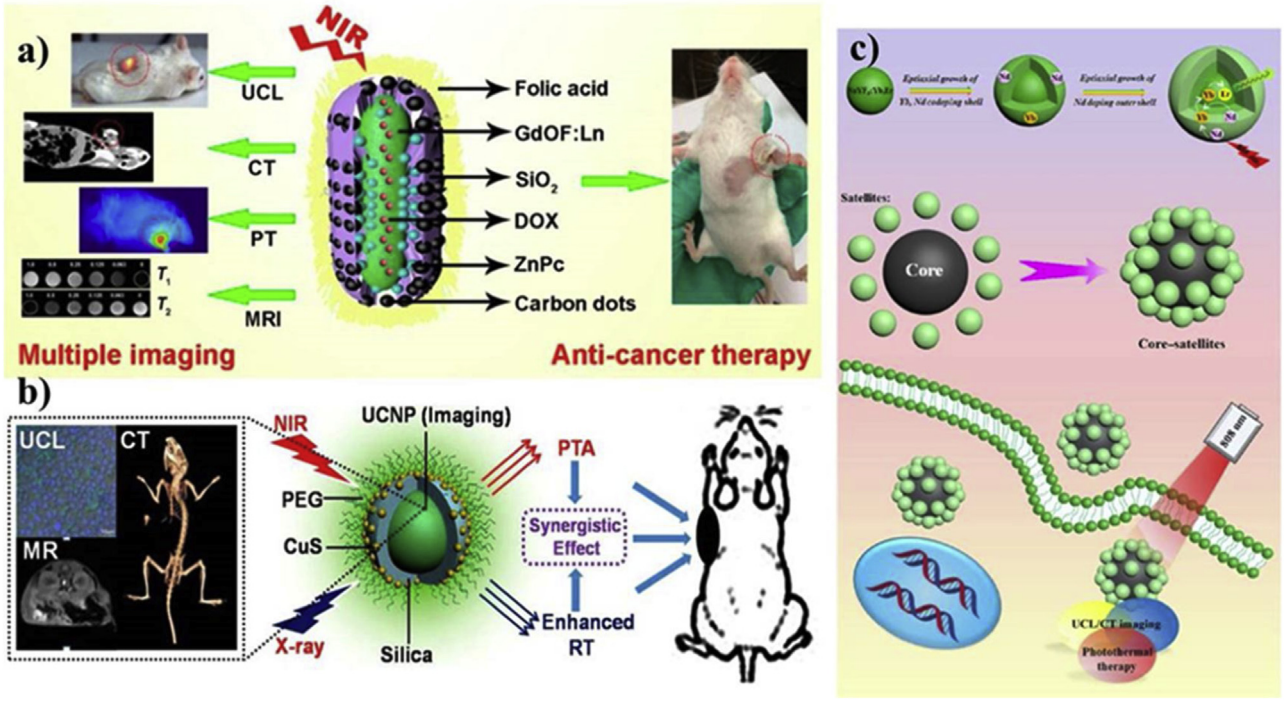

Fig. 12. a) Schematic illustration for the bio-application of GdOF:Ln@SiO_2-ZnPc-CDs microcapsule for multiple imaging and anti-tumor therapy. [Reference 272] printed with permission from ACS. b) The CSNT for UCL/MR/CT trimodal imaging guided enhanced RT/PTA synergistic therapy. [Reference 146] printed with permission from ACS. c) Schematic illustration for the design and synthesis of core/satellite nanotheranostic PDA@UCNPs for dual modal imaging guided PTT. [Reference 192] printed with permission from Springer.

ity have been regarded as prospective photothermal agents for PTT. CuS and djurleite $Cu_{2-x}S$ are the representatives among them [146–148]. Shi and coworkers developed a new type of multifunctional nanotheranostic with silica-coated UCNPs ($NaYbF_4$:2%Er^{3+}/20%Gd^{3+}@SiO_2-NH_2) as the core and ultrasmall CuS NPs as the satellites for synergistic radiotherapy and PTT (CSNT, Fig. 12b) [146]. Upon irradiation with 980 nm NIR, the temperature of CSNT solution increased remarkably, suggesting that the NIR laser had been transformed into heat by the CSNTs. Furthermore, the presence of high Z elements (Yb, Gd, and Er) in CSNTs could cause a large local radiation dose-enhancement around the NPs, demonstrating that CSNTs could also be used as radiosensitizers. The excellent tumor inhibitory has been confirmed in the animal model. The other striking example is MoS_2 nanosheets [277]. After functionalized with IR-808 dye and Ce6, UCNPs were grafted on the MoS_2 nanosheet with PTT and PDT combined in one nanosystem triggered by 808 nm NIR laser. Owing to the higher absorption coeffcients of NIR dye, core-shell structured UCNPs-IR808 exhibited superbright visible emission under low 808 nm light excitation, which could excite Ce6 to produce ROS for efficient PDT. Simultaneously, upon 808 nm laser irradiation, the MoS_2 nanosheet can not only generate local hyperthermia to inhibit the tumor growth, but also synergistically improve the PDT.

Organic polymer. Although the above mentioned inorganic PTT agents have exhibited good photothermal performance, the long-term safety concern of these agents seriously hampers their further clinical implementation because they are not biodegradable. To overcome this problem, some organic PTT agents with strong NIR light absorbance have aroused significant interests, such as polydopamine (PDA), [123,192,278,279] polymer polypyrrole (PPy), [280] and indocyanine green (ICG) [281,282]. Among them, PDA, as the main composition of melanin, not only exhibits good biodegradability and no long-term toxicity, but also provides a higher photothermal conversion efficiency of 40% than those of previously reported PTT agents. Our group developed a novel multifunctional core/satellite nanotheranostic (PDA@UCNPs) with PDA as core and core–shell–shell structured Nd^{3+}-sensitized UCNPs as satellite for in vivo imaging guidance photothermal therapy using single 808 nm laser irradiation (Fig. 12c) [192]. The core–shell–shell structured design endowed UCNPs with outstanding upconversion luminescence properties and strong X-ray attenuation, thereby making the nanotheranostics potential candidates for excellent UCL/CT dual modal imaging. Apart from PDA, ICG is another star Food and Drug Administration (FDA)-approved drug, which can be triggered by 808-nm irradiation to produce both a photothermal effect and cytotoxic ROS [281]. Lin and coworkers prepared PDA coated $NaYF_4$:Yb,Er@$NaYF_4$:Yb UCNPs, and loaded ICG on the surface of PDA via electrostatic adsorption, hydrophobic interaction and π–π stacking. Such nanocomposites (UPI) can ablate cancer cells effectively with 808 nm irradiation, revealing their great potential as a NIR-mediated imaging and dual-modal therapeutic platform.

NIR light-assisted chemodynamic therapy based UCNPs

As another important ROS-based cancer treatment strategy, CDT has been aroused significant interests, which utilizes Fenton reaction to convert intracellular H_2O_2 into harmful ·OH. Unfortunately, the Fenton reaction requires strict reaction condition, e.g. low pH value (pH = 3 – 4), resulting in its low efficiency in tumor microenvironment (pH~6.5). It is well recognized that irradiation with UV light can improve the Fenton reaction. However, low penetration depth and potential tissue damage of UV light restrict its further application in tumor therapy. UCNPs can convert NIR with deeper tissue penetration into UV light, which could act as UV source to assist Fenton reaction, thereby improving the generation of ·OH. Shi and coworkers reported a photochemotherapy agent (UCSRF) for cancer therapy using NIR-assisted tumor-specific Fenton reactions, consisting of UCNP cores for converting NIR light to UV or visible photons to assist photo-Fenton reaction, mesoporous silica shell

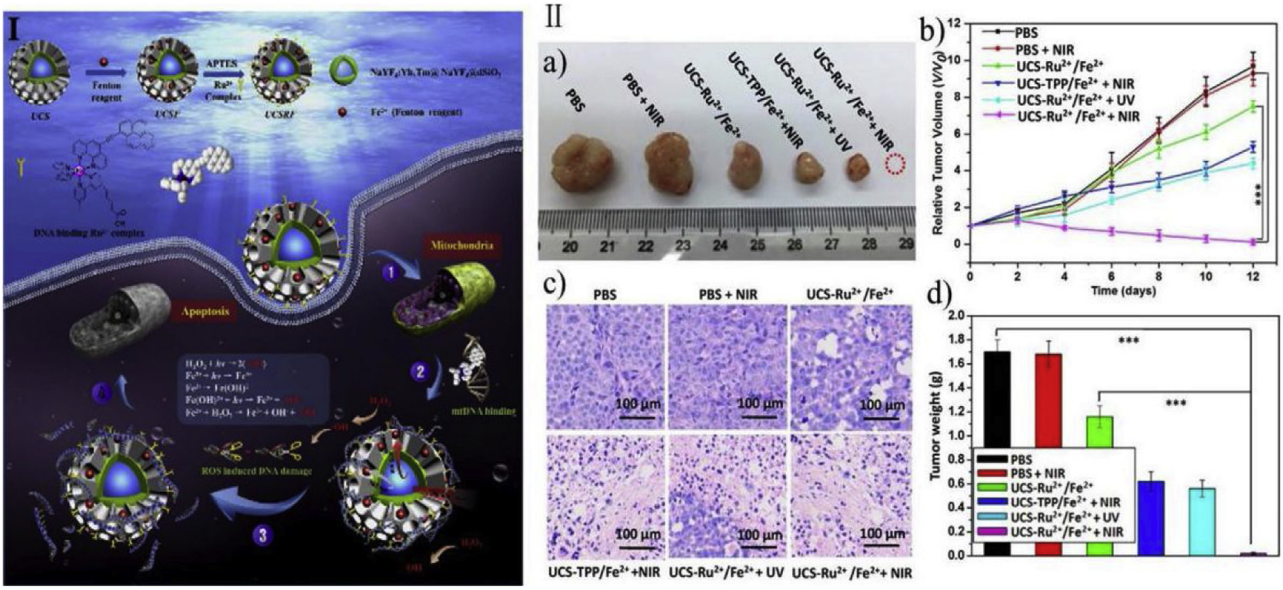

Fig. 13. I) Schematic illustrations for the synthetic procedures of UCSRF and a mitochondrial DNA-targeted and NIR-initiated photochemical therapy (PCT) of cancer based on a photo-Fenton reaction. II) In vivo anticancer effect of UCSRF for tumor-bearing mice. a) Tumor photos of mice in 12 days of different treatments. b) Relative tumor volumes of different treatments in 12 days of treatments. c) H&E-staining of the tumor tissue section harvested from different groups of mice in 3 days post irradiation. d) Tumor weights of different groups in 12 days of treatment. Error bars show standard deviations of results (five mice each group) in the same condition. Using the Student's two-tailed t-test to perform Statistical analysis (***$P < 0.001$) compared to control groups without UCSRF nanoparticles or NIR irradiation. [Reference 283] printed with permission from Elsevier.

as Fenton reagent (Fe^{2+}) carrier, and Ru^{2+} complex co-conjugated on the surface of mesoporous silica shell to bind mitochondrial DNA (Fig. 13I) [283]. Under NIR irradiation, UCSRF accumulated in intratumoral mitochondrion, and reacted with H_2O_2 to efficiently generate localized ·OH radicals that caused mitochondrial DNA damage. Such strategy showed much enhanced and tumor-specific therapeutic efficacy due to the capacity of ROS targeting with mitochondrial DNA (Fig. 13II).

Lately, Yang et al. constructed a multifunctional nanoplatform based on $ZnFe_2O_4$ functionalized UCNPs (UCPZ) that combined PDT and CDT triggered by NIR [284]. $ZnFe_2O_4$ nanoparticles not only act as photosensitizers for PDT, but also can react with excess H_2O_2 in cancer cells to generate ·OH for CDT. Furthermore, the linker Pt(IV) prodrugs can be reduced to high virulent Pt(II) by glutathione in the cancer cells, which further improved the outcome of the collaborative cancer treatment.

pH-responsive theranostics based on UCNPs

Thanks to the high rate of glycolysis in cancer cells, the pH in tumors is lower than in normal tissues. It is demonstrated that the pH of normal tissues and blood is approximately 7.4, whereas that in a tumor microenvironment is between 6.0 and 7.0. At the subcellular level, late endosomes and lysosomes exhibit much lower pH ranging from 4.5 to 5.5. Such pH gradient makes pH-responsive theranostics feasible to achieve "turn on" imaging and therapy in tumor site, improving the outcome of therapy and alleviating the side effect. A number of pH-responsive theranostics based on UCNPs have been explored in recent years, including pH-responsive drug delivery system and pH-driven tumor-targeting for PDT.

pH-responsive drug delivery system based UCNPs

Recent years have witnessed the rapid pace of research and development of pH-responsive drug delivery system based on UCNPs for gaining drug controllable release. Several design and constructing of pH-responsive drug release strategies have been investigated. One important design strategy is to introduce charge-conversional polymer on the surface of UCNPs, which contains negative charge under neutral and weakly basic conditions but switch to being positively charged in a slightly acidic environment, such as PAA [203,285–287], 2, 3-dimethylmaleic anhydride (DMMA) [288], naturally modified nonionic alginate-based polymers, [289] carboxylatebased pillar [5] arene (WP5), [290] and poly(DL-lactic-co-glycolic acid)(PLGA) [291]. For instance, Lin and coworkers have successfully prepared a series of PAA fictionalized UCNPs as pH-responsive drug delivery systems, including PAA@$GdVO_4$:Ln^{3+}, $NaYF_4$:Yb,Er@$NaYF_4$:Yb@$NaNdF_4$:Yb@$NaYF_4$:Yb@PAA, and $NaYF_4$:Yb, Er@$NaYF_4$:Yb@$NaNdF_4$:Yb@$NaYF_4$:Yb-CuS@PAA. Taking the Nd^{3+}-sensitized UCNPs as an example, core-shell structured $NaYF_4$:Yb,Er@$NaYF_4$:Yb@$NaNdF_4$:Yb@$NaYF_4$:Yb UCNPs have been developed by varying the shell number, core size, and host lattices, which exhibits significantly improved UCL intensity (Fig. 14I) [292]. After functionalized by PAA, a pH-responsive nanocarrier has been obtained, and their loading and control drug release capacities were superior to that of UCNP@$mSiO_2$. Ultrahigh drug storage capacity and sensitive pH-responsive drug release properties make UCNPs@PAA as promising pH-dependent drug delivery systems for chemotherapy.

The pH-sensitive linkers that can be cleaved with decreasing pH value, such as acetal bond, hydrazine bond, hydrazone bond, and ester bond, have provided opportunities for constructing pH-responsive drug delivery systems based on UCNPs. Recently, a new pH-responsive drug delivery system based on ultra-small $BaGdF_5$:Yb/Tm@$BaGdF_5$:Yb (sub-10 nm) was reported, in which DOX were conjugated to the surface of UCNPs by hydrazone bonds [201]. At neutral pH, the linkers remain intact and inhibit DOX release, resulting in low side-effect of chemotherapeutics to normal tissues, while the cleavage of hydrazone bonds in acidic environment allows the release of DOX, realizing pH-triggered drug release.

Apart from these strategies, some acidic-decomposable inorganic materials have recently been reported as gatekeepers to control drug release, offering opportunities to design promising specific carriers for therapeutic agents. Our group have constructed a multifunctional nanotheranostic agent with UCNPs ($NaYF_4$:20%Yb^{3+}, 2%Er^{3+}/$NaGdF_4$:2%Yb^{3+}) as the core, and a mesoporous silica layer as the outer shell with ZnO as "gatekeeper"

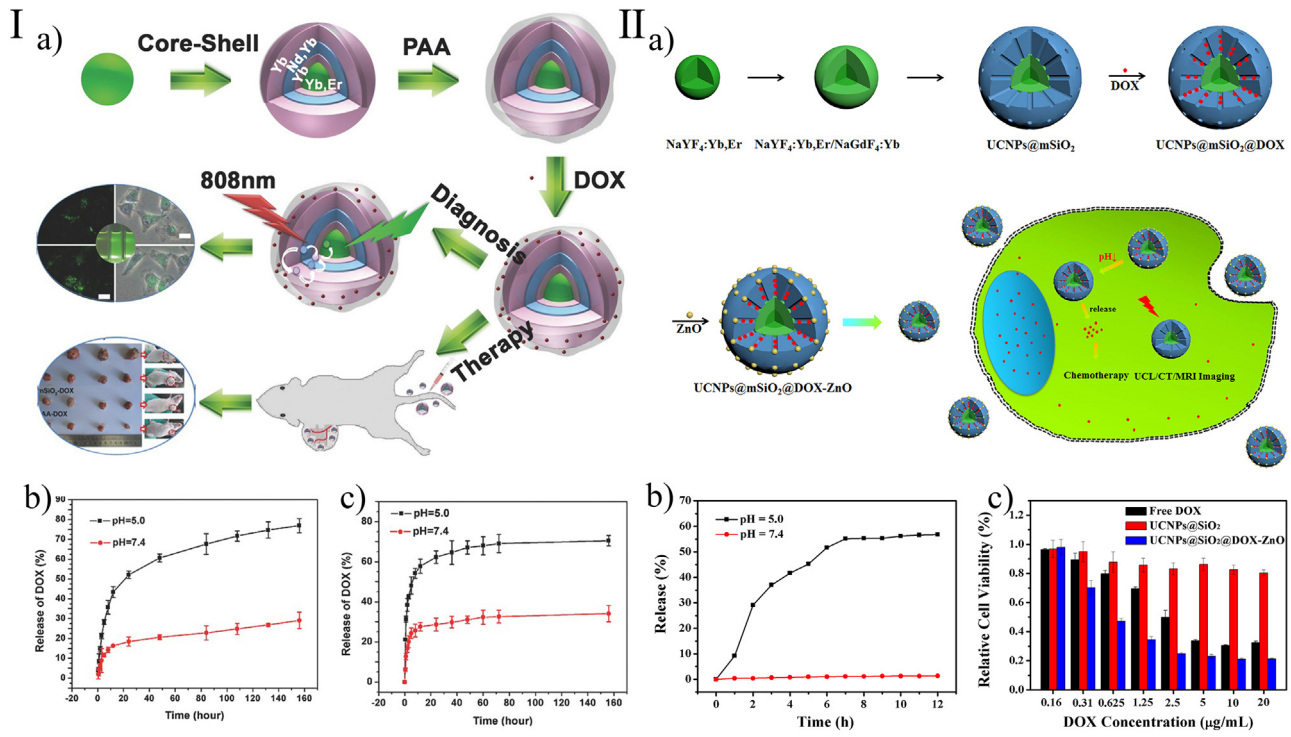

Fig. 14. I) Schematic illustration of a) the synthesis of core–shell structured UCNP@PAA multifunctional nanoparticles and subsequent bio-applications in UCL imaging and anti-cancer therapy, b, c) Cumulative DOX release from b) UCNP@PAA and c) UCNP@$mSiO_2$ at pH = 5.0 (black line) and pH = 7.4 (red line) PBS buffer. [Reference 292] printed with permission from Wiley. II) Schematic illustration of a) the synthesis of UCNPs@$mSiO_2$@DOX-ZnO for multi-modality bioimaging guided pH-triggered chemotherapy, b) Release profiles of UCNPs@$mSiO_2$@DOX-ZnO at pH 7.4 and 5.0, and c) Cell viability of HeLa cells incubated with free DOX, UCNPs@$mSiO_2$, UCNPs@$mSiO_2$-ZnO, and UCNPs@$mSiO_2$@DOX-ZnO for 24 h, respectively. [Reference 293] printed with permission from Wiley.

for pH-triggered drug delivery (UCNPs@$mSiO_2$-ZnO, Fig. 14II) [293]. After internalization into HeLa cells, ZnO can be efficiently dissolved rapidly in the acidic intracellular compartments, followed by loaded DOX release from $mSiO_2$ shell. Importantly, ZnO is non-toxic towards normal tissues but cytotoxic towards tumors after dissolution, enhancing the anti-cancer effect. The pH-triggered on-demand drug release not only improves the therapeutic effectiveness but also effectually reduces adverse side effects of drugs. Combining UCL/MR/CT multimodal imaging with specific pH-triggered on-demand drug release has a great potential for simultaneous diagnosis and therapy of cancer.

pH-driven tumor-targeting for PDT

Targeting is critical for tumor diagnosis and therapy, and generally divided two types: passive targeting and active targeting. Recently, more attention has been paid to active targeting through modifying UCNPs with tumor-selective agents that can recognize the unique receptors overexpressed or present on tumor cells owing to the limited target capacity of passive targeting. Folic acid (FA) is a widely used targeting agent due to its high stability, non-immunogenic character, and feasibility to conjugate with functional groups. However, the expression of folate receptors (FRs) in normal tissues will lead to unexpected targeting and unsatisfactory therapeutic effect. Tang et al. developed a pre-protective strategy for precise tumor targeting and efficient PDT [294]. A switchable DNA/upconversion nanocomposite (UCNPs@PAA–DNA) was constructed by modifying two kinds of DNA sequences with different lengths on the surface of UCNPs. FA groups on the shorter DNA sequences are protected by the longer DNA sequences in normal tissues, avoiding unexpected uptake. Whereas, UCNPs@PAA–DNA reached the tumor region, the longer DNA would fold in the acidic tumor microenvironment, and FA groups were exposed to achieve the targeting with cancer cell. At the same time, the photosensitizer Ce6 on the longer DNA gets close to the surface of UCNPs, improving the treatment outcome of PDT. This pre-protective strategy provides new insights for precise targeting and highly efficient cancer therapy.

Other pH-responsive targeting molecules are also employed to construct upconversion nanotheranostics for pH-driven tumor-targeted PDT. Wang et al. used the pH low insertion peptide (pHLIP) to functionalize an Nd^{3+} sensitized UCNP for precise targeting and efficient PDT [295]. pHLIP can bring cargo specifically into cancer cells under an acidic environment, realizing the effective active-targeting and efficient PDT.

Glutathione-responsive theranostics based on UCNPs

Owing to the difference of the concentration of tripeptide glutathione (GSH) in the extracellular fluids (20 – 40 μM) and intracellular microenvironment (0.5–10 mM), GSH has been recognized as a specific pathological trigger for constructing stimuli-responsive theranostics. To date, a variety of GSH-responsive theranostics based on UCNPs have been developed, which mainly rely on the strategies of cleavage of disulfide bonds, thiol exchange reaction, and so on.

Among them, the disulfide-based processes is the most employed strategy, which operated by cleavage of disulfide bonds with GSH and subsequent release of the drug. Wu et al. reported a novel amphiphilic fluorinated block copolymer (poly(oligo ethylene glycol methyl ether methacrylate (OEGMA)-co-2-(N,N-dimethylamino)ethyl methacrylate (DMAEMA))-b-2-((2-methacryloyloxy ethyl) disulfanyl)ethyl 3,5-bis(trifluoromethyl) benzoate (MESEF)) through reversible addition-fragmentation chain transfer polymerization (RAFT) polymerization, and constructed hybrid colloidal nanoclusters by self-assemble with hydrophobic UCNPs and DOX, which exhibited

good pH-/redox-dual-responsive controllable drug release behavior via both the cleavage of disulfide by GSH and the protonation of amino groups by acidic environment [296]. By taking advantage of the cleavage of disulfide bonds by GSH, Du et al. grafted the gatekeeper CuS on the surface of mesoporous upconversion nanoparticles (mUCNPs) through disulfide bond as a cleavable linker, and functionalized with targeted molecule HA (mUCNPs@DOX/CuS/HA) for UCL/MR/PA guided chemotherapy and PTT [297]. Compared to without HA, more mUCNPs@DOX/CuS/HA nanoparticles (nealy 98%) were uptaken by cells after incubation 4 h, predicting better treatment efficiency. In tumor microenvironment, 71% of DOX were released from mUCNPs@DOX/CuS/HA nanoparticles, whereas 21% of DOX were released without GSH. Moreover, CuS nanoparticle can act as photothermal agent for PTT, leading to the synergistic effect of chemotherapy and thermal therapy.

GSH-mediated thiol exchange reaction of disulfide bonds is another strategy to develop the GSH-responsive nanotheranostics. The pivotal factor of successfully constructing GSH-responsive nanotheranostics is making them enter into the cytoplasm where abundant GSH could take effect to trigger the theranostics rather than trapping within endolysosomes. Liu et al. reported a GSH-responsive polyprodrug vesicles that could escape from endosomal and enter into the cytoplasm through NIR-activated photochemical internalization [298]. The amphiphilic polyprodrugs of poly(N,N-dimethylacrylamide-co-EoS)-b-PCPTM were synthesized via sequential reversible addition-fragmentation chain transfer polymerization, and then self-assembled into hybrid vesicles in the presence of hydrophobic oleic acid (OA)-stabilized UCNPs ($NaYF_4$:Yb/Er), leading to the generation of $^1O_2$ through the energy transfer between UCNPs and PS EoS moieties. The $^1O_2$ molecules could not only kill the cancer cell by PDT, but also disrupt the membranes of endolysosomes and thus facilitate the nanovesicles to escape from endolysosomes and enter into the cytosol, leading to the GSH-triggered camptothecin release in the cytosol. The integration of PDT module improved the therapeutic performance not only by the synergistic effect of PDT and chemotherapy but also through the photochemical internalization effect. Therefore, it is a feasible strategy to elevate the treatment effect by introducing PDT module into the design of GSH-responsive nanotheranostics.

GSH in tumor microenvironments can also make Mn ions doped silica nanoshell biodegradation, leading to GSH-responsive nanotheranostics [216]. Lin and coworkers synthesized yolk-structured Mn-doped upconversion nanocapsules (Mn-UCNCs) with UCNPs as core and Mn-doped silica as shell, which is responsive to mild reductive and acidic tumor condition. This tumor-sensitive degradation of the shell not only facilitates DOX release in the tumor location but also allows faster nanoparticle diffusion and deeper tumor penetration, thus realizing efficient particle distribution and improved chemotherapy. At the same time, the released Mn^{2+} improved the MRI effect derived from the UCNPs, endow Mn-UCNCs with superior multiple imaging functions.

ROS-responsive theranostics based on UCNPs

In addition to common $^1O_2$, H_2O_2, and ·OH, ROS in biological system include superoxide ($O_2{\cdot}^-$), hypochlorous acid (HOCl), and peroxynitrite ($ONOO^-$), which have an important impact on a variety of biological events including cell signaling, homeostasis, proliferation and aging [299]. Owing to the higher concentrations of ROS in cancer cells than that in normal cells, ROS have been employed as a promising stimulus to explore stimuli-responsive theranostics.

Especially $^1O_2$ molecules, they not only can kill the cancer cell by PDT, but also can cleave the thioketal linker to construct ROS-responsive theranostics. UCNPs are able to excite photosensitizers to generate $^1O_2$ molecules by NIR, with potent applications in PDT. Therefore, more attention has been focused on the development of ROS-responsive theranostics based on UCNPs in the recent years [300–302]. Cui et al. constructed a new multifunctional UCNPs theranostic system through loading mPEG-COOH, PS Ce6, and ROS-cleavable thioketal-conjugated camptothecin on the surface of UCNPs (Fig. 15I) [301]. Under 980 nm laser irradiation, Ce6 could be activated by UCL and produced $^1O_2$ molecules that can be used for PDT and to cleave the thioketal linker in thioketal-conjugated camptothecin to release camptothecin for chemotherapy. Moreover, the emission of Ce6 between 650-750 nm was employed for near-infrared fluorescence imaging. Such ROS-responsive theranostic owns great potential in applications on simultaneous lung cancer fluorescent imaging, ROS-activated chemotherapy and PDT in the near future. Qu and coworker also take advantage of the feature of ROS that can break down the thioketal linker to control drug release to construct a ROS-responsive theranostic (Fig. 15II) [302]. After coating $mSiO_2$ on the surface of the core–shell nanostructured $NaYF_4$:Yb,Er@$NaYF_4$ nanoparticles, the PS Ce6 and DOX were loaded, and then the thioketal linkers were capped on the outside of the nanocomposites by a simple silane coupling reaction, preventing the drug premature release. Upon NIR irradiation, the generated ROS through exciting Ce6 by visible light emission (derived from UCNP) not only brought about irreversible damage to the cancer tissue to achieve PDT, but also broken down the "gate" thioketal linker to control drug release. Therefore, introducing PDT model into ROS-responsive theranostics based on UCNPs, controllable chemotherapy and PDT can be achieved at the same time, which enhanced the curative effect owing to the synergistic effect.

H_2O_2 is another common stimulus for developing ROS-responsive theranostics, whose level is higher in the tumor microenvironment than in the normal tissue. In tumor microenvironment, acidic H_2O_2 can reduce MnO_2 nanosheets into Mn^{2+} and O_2, which enhances the diagnostic accuracy and treatment effect of oxygen-dependent therapy, such as PDT. Taking advantage of this information, multifunctional UCNPs have been introduced on the surface of MnO_2 nanosheets to constructing intelligent theranostic nanosystems for H_2O_2-responsive UCL imaging and oxygen-elevated synergetic radio/photodynamic therapy (Fig. 15III) [157]. UCNPs ($NaYF_4$:Yb/Er/Tm) were coated by photosensitizer (SPCD)-incorporated $dSiO_2$ (UCSs), preventing the leakage of SPCD molecules and facilitating the generation of $^1O_2$ through the red luminescence energy transfer from UCNPs to SPCD. Then MnO_2 nanosheets were wrapped out onto the surface of all UCSs, resulting in the quenching of UCL of UCSs. In the normal tissues, the UCL of UCSs kept quenching by MnO_2 nanosheets, whereas the UCL recovered in the tumor microenvironment owing to acidic H_2O_2-induced reduction of MnO_2, achieving concurrent pH-/H_2O_2-responsive UCL imaging for diagnosis. On the other hand, the generated O_2 by MnO_2-H_2O_2 redox reaction improved the therapeutic effect of synergetic radio/photodynamic therapy.

Enzyme-responsive theranostics based on UCNPs

Enzymes are a kind of important biocatalysts, taking part in almost all biological and metabolic processes in the cells. Due to their high specific and selectivity, enzymes have recently acted as promising triggers to design and construct responsive theranostics. Below, we focused on recent progress concerning enzyme-responsive theranostics based on UCNPs, including cathepsin B- and caspases-activated strategies.

Cathepsin B, as a member of lysosomal proteases family, is regarded as a potential biomarker because it overexpressed in varieties of cancer, such as breast cancer and pancreatic cancer [303]. Moreover, cathepsin B has been widely used as the trigger for imag-

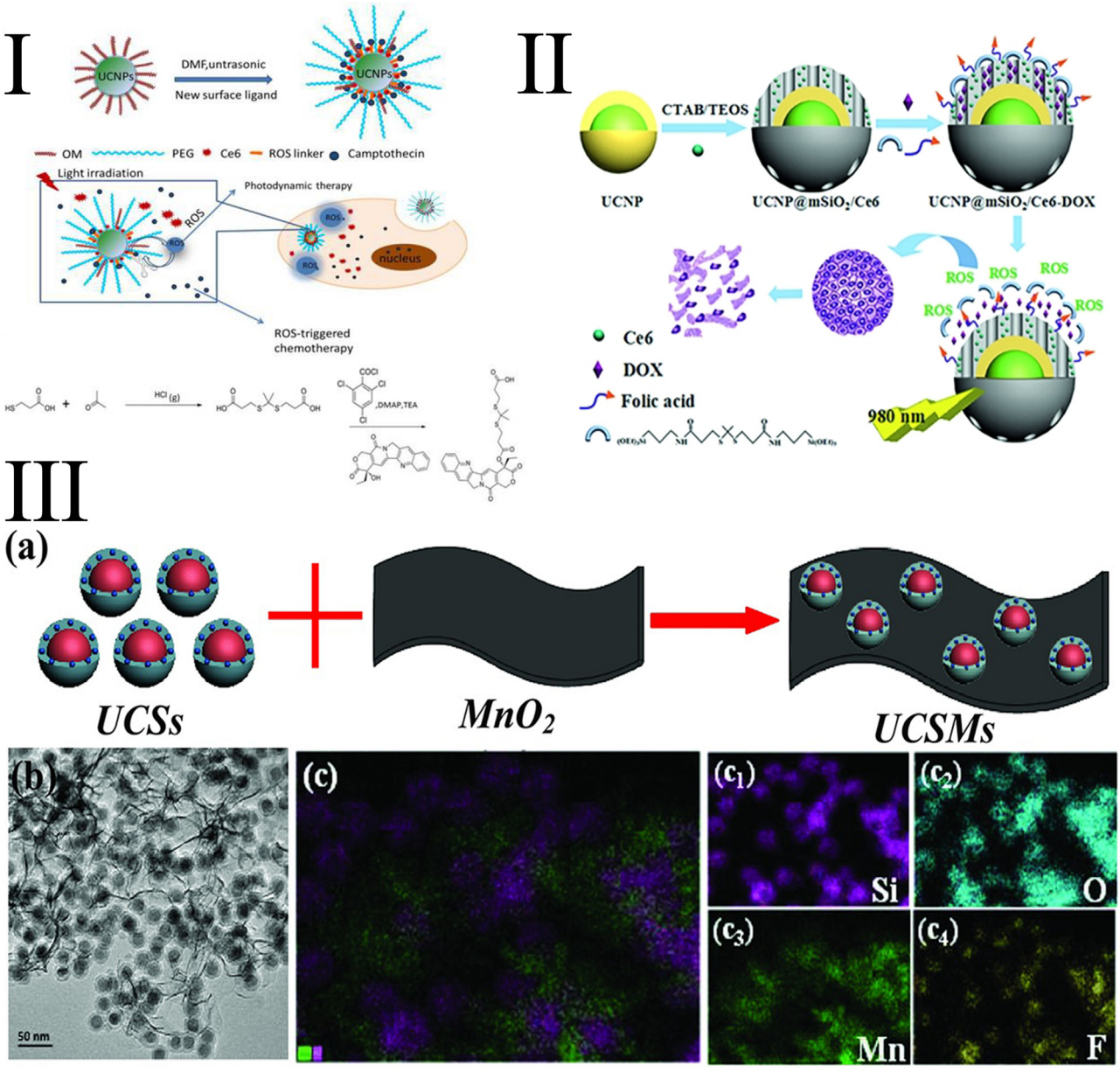

Fig. 15. I) Schematic illustration of the preparation of Ce6-CPT-UCNPs and concept of the light-regulated ROS-activated Ce6-CPT-UCNPs. [Reference 301] printed with permission from Theranostics. II) Schematic illustration of the synthesis and the controlled release process. [Reference 302] printed with permission from Wiley. III) Schematic illumination of (a) the construction of intelligent MnO_2 nanosheets anchored with upconversion nanoprobes (UCSMs). (b) TEM images of UCSMs. (c) STEM image and the corresponding element mapping of UCSMs. [Reference 157] printed with permission from Wiley.

ing and drug release at tumor site owing to its capacity of selectively cleave the peptide with specific unit, i.e. Gly-Phe-Leu-Gly or Arg-Arg-Lys. Qu and coworkers developed a cathepsin B responsive UCNPs nanostructure for drug release and PDT [304]. In 2016, Xing et al. reported a cathepsin B triggered cross-linking of UCNPs system for effective tumor localization and theranostics (Fig. 16) [305]. Nd^{3+}-doped UCNPs have been synthesized and exhibited good upconverted luminescences properties upon excitation at 808 nm. An enzyme-responsive peptide, Ac-FKC(StBu)AC(SH)-CBT containing a side-protected cysteine and 2-cyanobenzothiazole (CBT) was designed for specific reaction with cathepsin B, and connected on the surface of Ce6-modified UCNPs (CRUN). Cathepsin B could cleave the peptides and induce covalent cross-linking between the exposed cysteine and CBT on neighbouring particles, which not only triggered the accumulation of UCNPs into tumour site, but also enhanced light upconverting emission. Improved upconverted luminescences properties further amplifies the singlet oxygen generation from Ce6, thus increasing the PDT efficacy. Both in vitro and in vivo theranostic studies demonstrated that enzyme-responsive localization of light-converted rare-earth nanostructures could significantly inhibit the tumour growth in process of PDT treatment. This strategy provide a promising solution for effective site-specific tumour imaging and treatment.

Caspases have been proven to be associated with cell apoptosis, therefore many efforts have been devoted to develop caspase responsive nanoparticles for monitoring the therapeutic process. Very recently, Hu et al. constructed caspase-3 responsive functionalized UCNPs (CFUNs) through self-assembly of caspase-3 responsive DOX prodrug tethered with DEVD peptide (DEVD-DOX), UCNPs, a PS (pyropheophorbide-a methyl ester, MPPa), and tumor-targeting cRGD-PEG-DSPE [306]. This system integrated three-in-one function: NIR triggered photosensitizer to generate

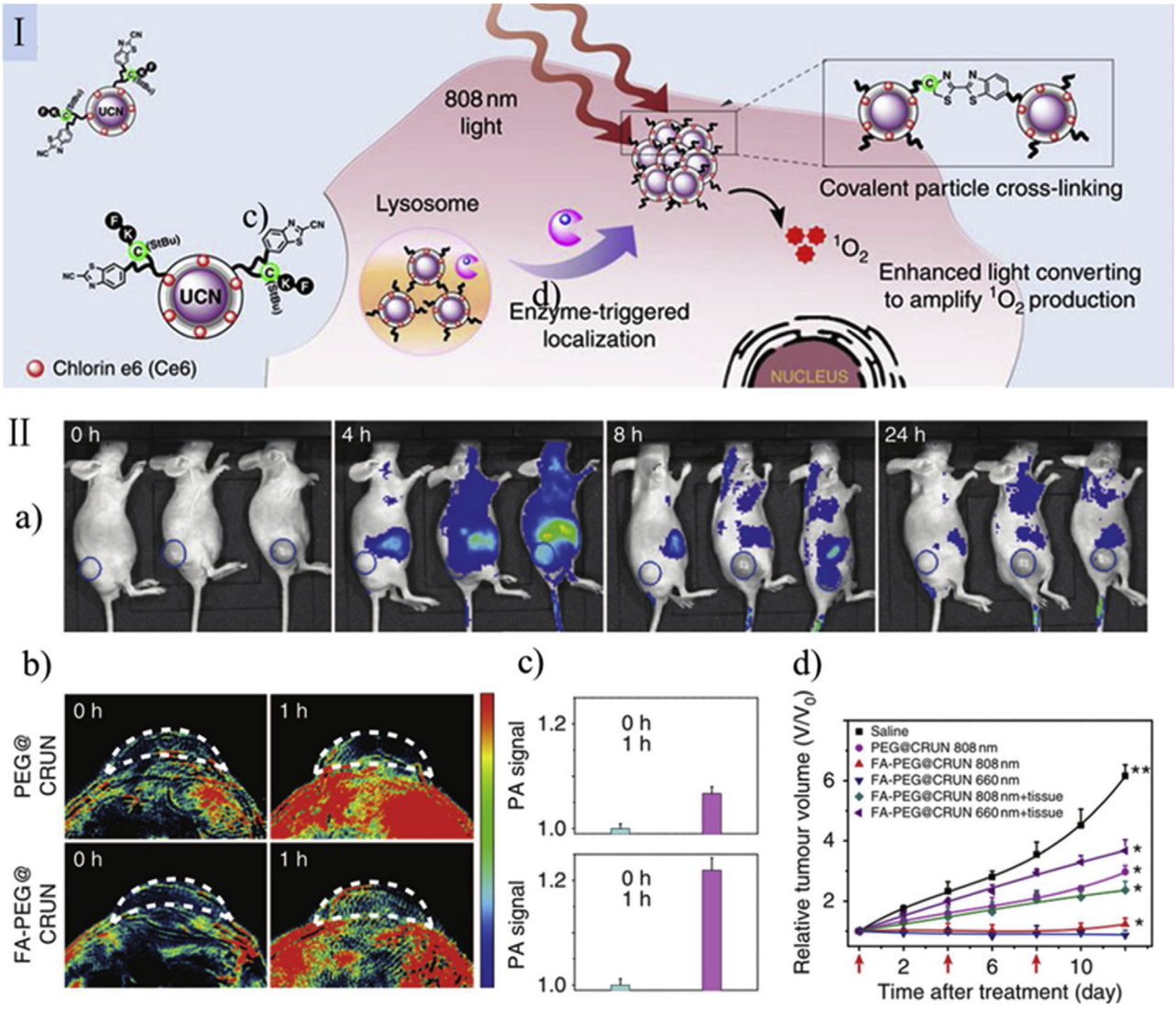

Fig. 16. I) Illustration of the microenvironment-sensitive strategy for covalent cross-linking of peptide-premodified UCNs in tumor areas. II) a) Fluorescence imaging of tumors (blue circle) in living mice at different time intervals after injection. b) PA imaging signals in the tumor region at different time intervals after intravenous injection. c) Tumor volumes change as a function of time in treated groups to evaluate the effectiveness of PDT treatment in vivo. [Reference 305] printed with permission from Nature.

ROS causing photo-dynamic damage along with caspase-3 activation, subsequent caspase-3 responsive drug release, and cascade chemotherapeutic activation. Such sequential and repetitive processes could enhance and amplify the therapeutic efficiency by apoptotic activation to neighboring tumor tissues. This strategy may pave the way for novel cascade tumor therapy that is favorable to overcome drug resistance and heterogeneity in tumor therapy.

Temperature-responsive theranostics based on UCNPs

The temperature in tumor is higher than that of normal tissues owing to the high rates of aerobic glycolysis and fast proliferation [307]. Based on the temperature difference, developing the temperature-responsive theranostics has attracted more and more attentions. Among them, temperature-sensitive polymers have been widely used to control the antitumor drugs release through their structure change in response to the temperature in the tumor [308–310]. Lin et al. described a thermo/pH dual-responsive drug delivery system based on UCNPs [308]. Mesoporous silica coated UCNPs were acted as DOX carriers, and temperature sensitive poly(N-isopropylacrylamide-co-methacrylic acid) [P(NIPAm-co-MAA)] polymer brushes were grafted onto the channel and outer shell of the mesoporous silica scafford. The obtained hybrid nanocarriers were capable to respond to the slight difference of temperature/pH between tumor tissue and healthy tissue in the simulated physiological conditions, and control the drug release on-demand. Furthermore, photothermal effects caused by NIR irradation also promoted the release of DOX molecules. In 2015, Yang and coworkers utilized the same sensitive polymer [P(NIPAm-co-MAA)] developed a nano-theranostic by conjugating photosensitive $Au_{25}(SR)_{18}$-(SR refers to thiolate) clusters, and anti-cancer drug DOX onto the surface of mesoporous silica coated core-shell UCNPs [309]. $Au_{25}(SR)_{18}$ clusters have contributed to temperature-responsive drug delivery owing to their good photothermal effect under NIR irradiation. The in vitro and in vivo results reveal the excellent anti-cancer therapeutic effect of synergistic PTT and chemotherapy.

Although combination of chemotherapy and PTT can enhance the treatment effect, these two treatment modes are initiated at the same time in most reported works due to the fact that drug release is activated by photothermal effect. However, as evidenced by a number of studies, giving chemodrug (doxorubicin) prior to thermal therapy results in better antitumor effect than simultaneous intake. Very recently, Li et al. developed a temperature sensi-

tive upconversion nanocomposite for programming chemotherapy and PTT combination therapy [311]. The temperature responsive upconversion nanosystem contains photothermal agent and thermal responsive drug release unit (1,2-dipalmitoyl-sn-glycero-3-phosphocholine, abbreviated as DPPC). Eigen temperature during photothermal process is monitoring by sensitive upconversion luminescence of Er^{3+} with the excitation of 980 nm laser. Power density of 730 nm laser, corresponding to photothermal effect, is tuned in light of UCL feedback to schedule chemotherapy and PTT sequentially. This work provides a non-invasive method to precisely modulate the process of combination therapy and a new strategy for designing next generation of cancer therapy.

Conclusions and perspectives

UCNPs have been widely developed in theranostics applications thus far thanks to their intriguing properties. However, most of UCNPs nanotheranostics are lack of the capacity to carry on their therapeutic function in response to targeted tumor instead of healthy tissues. In this review, we summarized the advancements of stimuli-driven turn on nanotheranostics based on UCNPs for tumor-specific imaging and therapy, covering internal stimuli (e.g., pH, GSH, ROS, enzyme, and temperature) and external stimuli (e.g., NIR). Rational engineering of UCNPs nanotheranostics plays a crucial role to achieve precision imaging and therapy of tumor through responding to a variety of stimuli, especially cancer-associated triggers. Although many efforts have been devoted to explore the stimuli-responsive UCNPs nanotheranostics, there are still many challenges that need to be addressed for promoting the future translational clinical applications.

Firstly, the UCL efficiency is still unsatisfactory for further application in vivo. The relative low UCL efficiency (usually less than 1%) is mainly ascribed to the low absorption cross sections of lanthanide ions and the energy losses through nonradiative transitions. Although many strategies have been used to address this challenge, such as constructing core-shell structure, regional doping, surface plasmon resonance-enhanced effects, etc. The preparation of UCNPs with high efficient still remains as a grand challenge. Exploiting NIR antenna that can transfer energy to Ln^{3+} luminescent centers might be of great help to improve the upconversion efficiency of UCNPs.

Second, the limited light penetration depth of UCNPs in tissues is another concern for either imaging or phototriggered therapy. Although Nd^{3+}-Yb^{3+} combined sensitized UCNPs have been developed, which can be excited by 808 nm NIR, resolving the problem of 980 nm NIR strongly absorbed by water, the effective penetration depth is still limited to a few centimeters, restricting their applications in the superficial tumors. Fluorescent imaging in the second near-infrared window (NIR-II) has been considered to probe deep tissue owing to the minimum auto-fluorescence and tissue scattering. Recently, the novel Er^{3+} sensitized UCNPs are reported with both excitation (1530 nm) and emission (1180 nm) located in the NIR-II window, which is promising for the theranostic of deep-set tumor [312]. In addition, developing some medical devices is greatly demanded, such as introducing the optical fibers to delivery NIR light into deep lesions.

Thirdly, the biosafety concern of UCNPs nanotheranostic is crucial importance for their future clinical applications. Despite numerous investigations have been demonstrated that UCNPs based nanotheranostic agents exhibited good biocompatibility with no obvious toxicity in animal model, the systematic and rigorous evaluations of the potential long-term toxicity including biodistribution, transformation, and excretion should be investigated in the future. Importantly, in light of the dose depend toxicity of UCNPs, the safe dose also needs further investigation, guiding the future clinical applications.

Fourth, NIR exhibits several advantages as a external stimulus in design and constructing theranostic systems, but it is necessary to precisely irradiate the laser at the tumor site. Therefore, it is required that the tumors must be accurately localized firstly and monitored in real time, which could reduce the damage to surrounding tissues. In contrast, the utilization of the cancer-associated stimuli that based on the differences between cancer cells and normal cells to construct theranostic indicates more mild, stable and precise. In fact, most reported pH triggered theranostics that responds to acidic conditions (pH < 6.5), which do not match with the pH value in the tumor microenvironments (pH 6.5 to 6.9). Therefore, it is urgent and significant to explore new cancer-associated stimuli to construct UCNPs nanotheranostic for precise cancer imaging and therapy in the coming years, i.e. over-expressed proteins or specific metal ions.

Finally, although constructing of stimuli-responsive UCNPs nanotheranostic agents by integrating with multimodal imaging and therapy functions into a single nanoplatform exhibited potent potential application for the accurate early diagnosis and efficient in situ therapy of cancer, the engineering and investigation of UCNPs based nanotheranostic agents is still in the infant stage. We believe that elaborately design and synthesis the smart stimuli-responsive UCNPs nanotheranostic will make significant contribute to the development of precise cancer theranostics in the future.

Acknowledgements

This work was supported by the financial aid from the National Natural Science Foundation of China (Grant Nos. 51502284, 51372242, 21521092, 21590794, 21635007, 21210001 and 81571737), the Hong Kong, Macao and Taiwan Science and Technology Cooperation Special Project of Ministry of Science and Technology of China (No. 2014DFT10310), the Program of Science and Technology Development Plan of Jilin Province of China (No. 20140201007GX), the National Key Basic Research Program of China (No. 2014CB643802), the Strategic Priority Research Program of the Chinese Academy of Sciences (Grant No. XDB20030300), the Key Research Program of Frontier Sciences, CAS (YZDY-SSW-JSC018), and the Jilin Province Foundation (20150520007JH and 20170101186JC).

References

[1] R. Siegel, D. Naishadham, A. Jemal, CA: a cancer journal for clinicians 63 (2013) 11–30.
[2] C.E. Meacham, S.J. Morrison, Nature 501 (2013) 328–337.
[3] R.A. Burrell, N. McGranahan, J. Bartek, C. Swanton, Nature 501 (2013) 338–345.
[4] V. Almendro, A. Marusyk, K. Polyak, Annual review of pathology 8 (2013) 277–302.
[5] J. Xie, S. Lee, X. Chen, Advanced drug delivery reviews 62 (2010) 1064–1079.
[6] I. Petak, R. Schwab, L. Orfi, L. Kopper, G. Keri, Nature reviews. Drug discovery 9 (2010) 523–535.
[7] F.M. Kievit, M. Zhang, Advanced materials (Deerfield Beach, Fla.) 23 (2011), H217-247.
[8] S.M. Janib, A.S. Moses, J.A. MacKay, Advanced drug delivery reviews 62 (2010) 1052–1063.
[9] M.E. Davis, Z.G. Chen, D.M. Shin, Nature reviews. Drug discovery 7 (2008) 771–782.
[10] R. Bardhan, S. Lal, A. Joshi, N.J. Halas, Accounts of chemical research 44 (2011) 936–946.
[11] V.I. Shubayev, T.R. Pisanic 2nd, S. Jin, Advanced drug delivery reviews 61 (2009) 467–477.
[12] M. Shevtsov, G. Multhoff, Current drug metabolism 17 (2016) 737–744.
[13] M.K. Lima-Tenorio, E.A. Pineda, N.M. Ahmad, H. Fessi, A. Elaissari, International journal of pharmaceutics 493 (2015) 313–327.
[14] M. Angelakeris, Biochimica et biophysica acta (2017).
[15] Y. Volkov, Biochemical and biophysical research communications 468 (2015) 419–427.
[16] S.K. Tripathi, G. Kaur, R.K. Khurana, S. Kapoor, B. Singh, Critical reviews in therapeutic drug carrier systems 32 (2015) 461–502.
[17] K.L. Schroeder, R.V. Goreham, T. Nann, Pharmaceutical research 33 (2016) 2337–2357.

[18] A.C. Sintov, C. Velasco-Aguirre, E. Gallardo-Toledo, E. Araya, M.J. Kogan, International review of neurobiology 130 (2016) 199–227.
[19] H. Sharma, P.K. Mishra, S. Talegaonkar, B. Vaidya, Drug discovery today 20 (2015) 1143–1151.
[20] P.D. Pietro, G. Strano, L. Zuccarello, C. Satriano, Current topics in medicinal chemistry 16 (2016) 3069–3102.
[21] G. Paramasivam, N. Kayambu, A.M. Rabel, A.K. Sundramoorthy, A. Sundaramurthy, Acta biomaterialia 49 (2017) 45–65.
[22] L.A. Dykman, N.G. Khlebtsov, Biomaterials 108 (2016) 13–34.
[23] R.K. Singh, K.D. Patel, K.W. Leong, H.W. Kim, ACS applied materials & interfaces 9 (2017) 10309–10337.
[24] G. Lin, P. Mi, C. Chu, J. Zhang, G. Liu, Advanced science (Weinheim, Baden-Wurttemberg, Germany) 3 (2016) 1600134.
[25] Z. Li, J.C. Barnes, A. Bosoy, J.F. Stoddart, J.I. Zink, Chemical Society reviews 41 (2012) 2590–2605.
[26] Y. Feng, N. Panwar, D.J.H. Tng, S.C. Tjin, K. Wang, K.T. Yong, Coord. Chem. Rev. 319 (2016) 86–109.
[27] K. Yang, L. Feng, X. Shi, Z. Liu, Chemical Society reviews 42 (2013) 530–547.
[28] R. Sao, R. Vaish, N. Sinha, Journal of nanoscience and nanotechnology 15 (2015) 1960–1972.
[29] M. Orecchioni, R. Cabizza, A. Bianco, L.G. Delogu, Theranostics 5 (2015) 710–723.
[30] K. Albert, H.Y. Hsu, Molecules (Basel, Switzerland) 21 (2016) 1585.
[31] X. Yue, Q. Zhang, Z. Dai, Advanced drug delivery reviews (2017).
[32] Z. Wang, G. Niu, X. Chen, Pharmaceutical research 31 (2014) 1358–1376.
[33] C.G. Qian, Y.L. Chen, P.J. Feng, X.Z. Xiao, M. Dong, J.C. Yu, Q.Y. Hu, Q.D. Shen, Z. Gu, Acta pharmacologica Sinica 38 (2017) 764–781.
[34] O.I. Parisi, L. Scrivano, M.S. Sinicropi, N. Picci, F. Puoci, Mini reviews in medicinal chemistry 16 (2016) 754–761.
[35] K. Pant, O. Sedlacek, R.A. Nadar, M. Hruby, H. Stephan, Advanced healthcare materials 6 (2017).
[36] C. Oerlemans, W. Bult, M. Bos, G. Storm, J.F. Nijsen, W.E. Hennink, Pharmaceutical research 27 (2010) 2569–2589.
[37] B.T. Luk, L. Zhang, ACS applied materials & interfaces 6 (2014) 21859–21873.
[38] H. Xing, K. Hwang, Y. Lu, Theranostics 6 (2016) 1336–1352.
[39] B.T. Luk, R.H. Fang, L. Zhang, Theranostics 2 (2012) 1117–1126.
[40] W.T. Al-Jamal, K. Kostarelos, Accounts of chemical research 44 (2011) 1094–1104.
[41] A.S. Abu Lila, T. Ishida, Biological & pharmaceutical bulletin 40 (2017) 1–10.
[42] X.R. Song, X. Wang, S.X. Yu, J. Cao, S.H. Li, J. Li, G. Liu, H.H. Yang, X. Chen, Advanced materials (Deerfield Beach, Fla.) 27 (2015) 3285–3291.
[43] S.S. Chou, B. Kaehr, J. Kim, B.M. Foley, M. De, P.E. Hopkins, J. Huang, C.J. Brinker, V.P. Dravid, Angewandte Chemie (International ed. in English) 52 (2013) 4160–4164.
[44] M. Chhowalla, H.S. Shin, G. Eda, L.J. Li, K.P. Loh, H. Zhang, Nature chemistry 5 (2013) 263–275.
[45] L. Cheng, J. Liu, X. Gu, H. Gong, X. Shi, T. Liu, C. Wang, X. Wang, G. Liu, H. Xing, W. Bu, B. Sun, Z. Liu, Advanced materials (Deerfield Beach, Fla.) 26 (2014) 1886–1893.
[46] Z. Chen, Q. Wang, H. Wang, L. Zhang, G. Song, L. Song, J. Hu, H. Wang, J. Liu, M. Zhu, D. Zhao, Advanced materials (Deerfield Beach, Fla.) 25 (2013) 2095–2100.
[47] J. Zhang, R.E. Campbell, A.Y. Ting, R.Y. Tsien, Nature reviews. Molecular cell biology 3 (2002) 906–918.
[48] E. Schrock, S. du Manoir, T. Veldman, B. Schoell, J. Wienberg, M.A. Ferguson-Smith, Y. Ning, D.H. Ledbetter, I. Bar-Am, D. Soenksen, Y. Garini, T. Ried, Science (New York, N.Y.) 273 (1996) 494–497.
[49] X. Wu, H. Liu, J. Liu, K.N. Haley, J.A. Treadway, J.P. Larson, N. Ge, F. Peale, M.P. Bruchez, Nature biotechnology 21 (2003) 41–46.
[50] D.R. Larson, W.R. Zipfel, R.M. Williams, S.W. Clark, M.P. Bruchez, F.W. Wise, W.W. Webb, Science (New York, N.Y.) 300 (2003) 1434–1436.
[51] S. Kim, Y.T. Lim, E.G. Soltesz, A.M. De Grand, J. Lee, A. Nakayama, J.A. Parker, T. Mihaljevic, R.G. Laurence, D.M. Dor, L.H. Cohn, M.G. Bawendi, J.V. Frangioni, Nature biotechnology 22 (2004) 93–97.
[52] J.K. Jaiswal, H. Mattoussi, J.M. Mauro, S.M. Simon, Nature biotechnology 21 (2003) 47–51.
[53] Q. Zhao, F. Li, C. Huang, Chemical Society reviews 39 (2010) 3007–3030.
[54] Q. Zhao, C. Huang, F. Li, Chemical Society reviews 40 (2011) 2508–2524.
[55] S.V. Eliseeva, J.C. Bunzli, Chemical Society reviews 39 (2010) 189–227.
[56] N.C. Shaner, P.A. Steinbach, R.Y. Tsien, Nature methods 2 (2005) 905–909.
[57] N.C. Shaner, R.E. Campbell, P.A. Steinbach, B.N. Giepmans, A.E. Palmer, R.Y. Tsien, Nature biotechnology 22 (2004) 1567–1572.
[58] T. Nagai, K. Ibata, E.S. Park, M. Kubota, K. Mikoshiba, A. Miyawaki, Nature biotechnology 20 (2002) 87–90.
[59] E. Betzig, G.H. Patterson, R. Sougrat, O.W. Lindwasser, S. Olenych, J.S. Bonifacino, M.W. Davidson, J. Lippincott-Schwartz, H.F. Hess, Science (New York, N.Y.) 313 (2006) 1642–1645.
[60] D. Wu, A.B. Descalzo, F. Weik, F. Emmerling, Z. Shen, X.Z. You, K. Rurack, Angewandte Chemie (International ed. in English) 47 (2008) 193–197.
[61] S.A. Hilderbrand, R. Weissleder, Current opinion in chemical biology 14 (2010) 71–79.
[62] Y. Du, B. Xu, T. Fu, M. Cai, F. Li, Y. Zhang, Q. Wang, Journal of the American Chemical Society 132 (2010) 1470–1471.
[63] J. Zhou, M. Yu, Y. Sun, X. Zhang, X. Zhu, Z. Wu, D. Wu, F. Li, Biomaterials 32 (2011) 1148–1156.
[64] J. Zhou, Y. Sun, X. Du, L. Xiong, H. Hu, F. Li, Biomaterials 31 (2010) 3287–3295.
[65] J. Zhou, Z. Liu, F. Li, Chemical Society reviews 41 (2012) 1323–1349.
[66] F. Zhang, G.B. Braun, Y. Shi, Y. Zhang, X. Sun, N.O. Reich, D. Zhao, G. Stucky, Journal of the American Chemical Society 132 (2010) 2850–2851.
[67] L. Xiong, T. Yang, Y. Yang, C. Xu, F. Li, Biomaterials 31 (2010) 7078–7085.
[68] L. Xiong, Z. Chen, Q. Tian, T. Cao, C. Xu, F. Li, Analytical chemistry 81 (2009) 8687–8694.
[69] M. Wang, C.C. Mi, W.X. Wang, C.H. Liu, Y.F. Wu, Z.R. Xu, C.B. Mao, S.K. Xu, ACS nano 3 (2009) 1580–1586.
[70] F. Wang, X. Liu, Chemical Society reviews 38 (2009) 976–989.
[71] F. Wang, D. Banerjee, Y. Liu, X. Chen, X. Liu, The Analyst 135 (2010) 1839–1854.
[72] C. Wang, L. Cheng, Z. Liu, Biomaterials 32 (2011) 1110–1120.
[73] M. Haase, H. Schafer, Angewandte Chemie (International ed. in English) 50 (2011) 5808–5829.
[74] R. Abdul Jalil, Y. Zhang, Biomaterials 29 (2008) 4122–4128.
[75] F. Auzel, Chemical reviews 104 (2004) 139–173.
[76] Y. Sun, X. Zhu, J. Peng, F. Li, ACS nano 7 (2013) 11290–11300.
[77] Z. Liu, F. Pu, S. Huang, Q. Yuan, J. Ren, X. Qu, Biomaterials 34 (2013) 1712–1721.
[78] W. Fan, B. Shen, W. Bu, F. Chen, K. Zhao, S. Zhang, L. Zhou, W. Peng, Q. Xiao, H. Xing, J. Liu, D. Ni, Q. He, J. Shi, Journal of the American Chemical Society 135 (2013) 6494–6503.
[79] L. Cheng, C. Wang, Z. Liu, Nanoscale 5 (2013) 23–37.
[80] J. Zhou, Q. Liu, W. Feng, Y. Sun, F. Li, Chemical reviews 115 (2015) 395–465.
[81] W. Zheng, P. Huang, D. Tu, E. Ma, H. Zhu, X. Chen, Chemical Society reviews 44 (2015) 1379–1415.
[82] L.D. Sun, Y.F. Wang, C.H. Yan, Accounts of chemical research 47 (2014) 1001–1009.
[83] A. Sedlmeier, H.H. Gorris, Chemical Society reviews 44 (2015) 1526–1560.
[84] L. Prodi, E. Rampazzo, F. Rastrelli, A. Speghini, N. Zaccheroni, Chemical Society reviews 44 (2015) 4922–4952.
[85] Y.I. Park, K.T. Lee, Y.D. Suh, T. Hyeon, Chemical Society reviews 44 (2015) 1302–1317.
[86] V. Muhr, S. Wilhelm, T. Hirsch, O.S. Wolfbeis, Accounts of chemical research 47 (2014) 3481–3493.
[87] X. Liu, C.H. Yan, J.A. Capobianco, Chemical Society reviews 44 (2015) 1299–1301.
[88] X. Li, F. Zhang, D. Zhao, Chemical Society reviews 44 (2015) 1346–1378.
[89] W. Fan, W. Bu, J. Shi, Advanced materials (Deerfield Beach, Fla.) 28 (2016) 3987–4011.
[90] H. Dong, S.R. Du, X.Y. Zheng, G.M. Lyu, L.D. Sun, L.D. Li, P.Z. Zhang, C. Zhang, C.H. Yan, Chemical reviews 115 (2015) 10725–10815.
[91] X. Chen, D. Peng, Q. Ju, F. Wang, Chemical Society reviews 44 (2015) 1318–1330.
[92] G. Chen, H. Agren, T.Y. Ohulchanskyy, P.N. Prasad, Chemical Society reviews 44 (2015) 1680–1713.
[93] X. Li, F. Zhang, D. Zhao, Nano Today 8 (2013) 643–676.
[94] W. Xu, X. Chen, H. Song, Nano Today 17 (2017) 54–78.
[95] Z. Gu, L. Yan, G. Tian, S. Li, Z. Chai, Y. Zhao, Advanced materials (Deerfield Beach, Fla.) 25 (2013) 3758–3779.
[96] G. Chen, H. Qiu, P.N. Prasad, X. Chen, Chemical reviews 114 (2014) 5161–5214.
[97] Z. Li, Y. Zhang, Angewandte Chemie (International ed. in English) 45 (2006) 7732–7735.
[98] F. Li, C. Li, X. Liu, Y. Chen, T. Bai, L. Wang, Z. Shi, S. Feng, Chemistry (Weinheim an der Bergstrasse, Germany) 18 (2012) 11641–11646.
[99] S. Jiang, Y. Zhang, K.M. Lim, E.K. Sim, L. Ye, Nanotechnology 20 (2009) 155101.
[100] J. Liu, W. Bu, S. Zhang, F. Chen, H. Xing, L. Pan, L. Zhou, W. Peng, J. Shi, Chemistry (Weinheim an der Bergstrasse, Germany) 18 (2012) 2335–2341.
[101] L. Sun, T. Liu, Y. Qiu, J. Liu, L. Shi, O.S. Wolfbeis, Microchimica Acta 181 (2014) 775–781.
[102] C. Li, D. Yang, P. Ma, Y. Chen, Y. Wu, Z. Hou, Y. Dai, J. Zhao, C. Sui, J. Lin, Small (Weinheim an der Bergstrasse, Germany) 9 (2013) 4150–4159.
[103] H.S. Qian, H.C. Guo, P.C. Ho, R. Mahendran, Y. Zhang, Small (Weinheim an der Bergstrasse, Germany) 5 (2009) 2285–2290.
[104] B. Liu, C. Li, D. Yang, Z. Hou, P.a. Ma, Z. Cheng, H. Lian, S. Huang, J. Lin, European Journal of Inorganic Chemistry 2014 (2014) 1906–1913.
[105] Z. Xu, C. Li, P. Ma, Z. Hou, D. Yang, X. Kang, J. Lin, Nanoscale 3 (2011) 661–667.
[106] Y. Zhu, T. Ikoma, N. Hanagata, S. Kaskel, Small (Weinheim an der Bergstrasse, Germany) 6 (2010) 471–478.
[107] F. Tang, L. Li, D. Chen, Advanced materials (Deerfield Beach, Fla.) 24 (2012) 1504–1534.
[108] L. Zhang, T. Wang, L. Yang, C. Liu, C. Wang, H. Liu, Y.A. Wang, Z. Su, Chemistry (Weinheim an der Bergstrasse, Germany) 18 (2012) 12512–12521.
[109] J. Liu, J. Bu, W. Bu, S. Zhang, L. Pan, W. Fan, F. Chen, L. Zhou, W. Peng, K. Zhao, J. Du, J. Shi, Angewandte Chemie (International ed. in English) 53 (2014) 4551–4555.
[110] Z. Cheng, J. Lin, Macromolecular rapid communications 36 (2015) 790–827.
[111] B. Pegaz, E. Debefve, J.P. Ballini, Y.N. Konan-Kouakou, H. van den Bergh, Journal of photochemistry and photobiology. B, Biology 85 (2006) 216–222.
[112] R. Naccache, F. Vetrone, V. Mahalingam, L.A. Cuccia, J.A. Capobianco, Chem. Mat. 21 (2009) 717–723.

[113] Q. Chen, C. Wang, L. Cheng, W. He, Z. Cheng, Z. Liu, Biomaterials 35 (2014) 2915–2923.
[114] J. Wang, T. Wei, X. Li, B. Zhang, J. Wang, C. Huang, Q. Yuan, Angewandte Chemie (International ed. in English) 53 (2014) 1616–1620.
[115] G. Chen, T.Y. Ohulchanskyy, W.C. Law, H. Agren, P.N. Prasad, Nanoscale 3 (2011) 2003–2008.
[116] J. Jin, Y.J. Gu, C.W. Man, J. Cheng, Z. Xu, Y. Zhang, H. Wang, V.H. Lee, S.H. Cheng, W.T. Wong, ACS nano 5 (2011) 7838–7847.
[117] Y. Dai, H. Xiao, J. Liu, Q. Yuan, P. Ma, D. Yang, C. Li, Z. Cheng, Z. Hou, P. Yang, J. Lin, Journal of the American Chemical Society 135 (2013) 18920–18929.
[118] L. Xia, X. Kong, X. Liu, L. Tu, Y. Zhang, Y. Chang, K. Liu, D. Shen, H. Zhao, H. Zhang, Biomaterials 35 (2014) 4146–4156.
[119] C. Wang, H. Tao, L. Cheng, Z. Liu, Biomaterials 32 (2011) 6145–6154.
[120] Q. Zhan, J. Qian, H. Liang, G. Somesfalean, D. Wang, S. He, Z. Zhang, S. Andersson-Engels, ACS nano 5 (2011) 3744–3757.
[121] Y. Liu, K. Ai, J. Liu, Q. Yuan, Y. He, L. Lu, Angewandte Chemie (International ed. in English) 51 (2012) 1437–1442.
[122] L.L. Li, R. Zhang, L. Yin, K. Zheng, W. Qin, P.R. Selvin, Y. Lu, Angewandte Chemie (International ed. in English) 51 (2012) 6121–6125.
[123] F. Liu, X. He, Z. Lei, L. Liu, J. Zhang, H. You, H. Zhang, Z. Wang, Advanced healthcare materials 4 (2015) 559–568.
[124] G. Tian, W. Yin, J. Jin, X. Zhang, G. Xing, S. Li, Z. Gu, Y. Zhao, Journal of Materials Chemistry B 2 (2014) 1379–1389.
[125] W. Ren, G. Tian, S. Jian, Z. Gu, L. Zhou, L. Yan, S. Jin, W. Yin, Y. Zhao, Rsc Advances 2 (2012) 7037–7041.
[126] C. Wang, L. Cheng, Y. Liu, X. Wang, X. Ma, Z. Deng, Y. Li, Z. Liu, Advanced Functional Materials 23 (2013) 3077–3086.
[127] W. Zhang, F. Ding, S.Y. Chou, Advanced materials (Deerfield Beach, Fla.) 24 (2012), Op236-241.
[128] S. Schietinger, T. Aichele, H.Q. Wang, T. Nann, O. Benson, Nano letters 10 (2010) 134–138.
[129] W. Ge, X.R. Zhang, M. Liu, Z.W. Lei, R.J. Knize, Y. Lu, Theranostics 3 (2013) 282–288.
[130] W. Xu, X. Chen, H. Song, Nano Today 17 (2017) 54–78.
[131] B. Dong, S. Xu, J. Sun, S. Bi, D. Li, X. Bai, Y. Wang, L. Wang, H. Song, Journal of Materials Chemistry 21 (2011) 6193–6200.
[132] L. Cheng, K. Yang, Y. Li, X. Zeng, M. Shao, S.T. Lee, Z. Liu, Biomaterials 33 (2012) 2215–2222.
[133] L. Cheng, K. Yang, Y. Li, J. Chen, C. Wang, M. Shao, S.T. Lee, Z. Liu, Angewandte Chemie (International ed. in English) 50 (2011) 7385–7390.
[134] C. Mi, J. Zhang, H. Gao, X. Wu, M. Wang, Y. Wu, Y. Di, Z. Xu, C. Mao, S. Xu, Nanoscale 2 (2010) 1141–1148.
[135] D. Hu, M. Chen, Y. Gao, F. Li, L. Wu, Journal of Materials Chemistry 21 (2011) 11276–11282.
[136] J. Shen, L.D. Sun, Y.W. Zhang, C.H. Yan, Chemical communications (Cambridge, England) 46 (2010) 5731–5733.
[137] H. Xing, W. Bu, S. Zhang, X. Zheng, M. Li, F. Chen, Q. He, L. Zhou, W. Peng, Y. Hua, J. Shi, Biomaterials 33 (2012) 1079–1089.
[138] S. Han, A. Samanta, X. Xie, L. Huang, J. Peng, S.J. Park, D.B.L. Teh, Y. Choi, Y.T. Chang, A.H. All, Y. Yang, B. Xing, X. Liu, Advanced materials (Deerfield Beach, Fla.) (2017) 29.
[139] L. Song, N. Zhao, F.-J. Xu,Advanced Functional Materials 27 (2017), 1701255.
[140] L.L. Li, P. Wu, K. Hwang, Y. Lu, Journal of the American Chemical Society 135 (2013) 2411–2414.
[141] H.P. Zhou, C.H. Xu, W. Sun, C.H. Yan, Advanced Functional Materials 19 (2009) 3892–3900.
[142] N. Liu, W. Qin, G. Qin, T. Jiang, D. Zhao, Chemical communications (Cambridge, England) 47 (2011) 7671–7673.
[143] C.W. Chen, Y.C. Chan, M. Hsiao, R.S. Liu, ACS applied materials & interfaces 8 (2016) 32108–32119.
[144] C.W. Chen, P.H. Lee, Y.C. Chan, M. Hsiao, C.H. Chen, P.C. Wu, P.R. Wu, D.P. Tsai, D. Tu, X.Y. Chen, R.S. Liu, Journal of Materials Chemistry B 3 (2015) 8293–8302.
[145] M. Sun, L. Xu, W. Ma, X. Wu, H. Kuang, L. Wang, C. Xu, Advanced materials (Deerfield Beach, Fla.) 28 (2016) 898–904.
[146] Q. Xiao, X. Zheng, W. Bu, W. Ge, S. Zhang, F. Chen, H. Xing, Q. Ren, W. Fan, K. Zhao, Y. Hua, J. Shi, Journal of the American Chemical Society 135 (2013) 13041–13048.
[147] G. Yang, R. Lv, F. He, F. Qu, S. Gai, S. Du, Z. Wei, P. Yang, Nanoscale 7 (2015) 13747–13758.
[148] B. Liu, C.X. Li, Z.X. Xie, Z.Y. Hou, Z.Y. Cheng, D.Y. Jin, J. Lin, Dalton Trans. 45 (2016) 13061–13069.
[149] S.S. Lucky, N. Muhammad Idris, Z. Li, K. Huang, K.C. Soo, Y. Zhang, ACS nano 9 (2015) 191–205.
[150] Z. Hou, Y. Zhang, K. Deng, Y. Chen, X. Li, X. Deng, Z. Cheng, H. Lian, C. Li, J. Lin, ACS nano 9 (2015) 2584–2599.
[151] Z. Hou, K. Deng, C. Li, X. Deng, H. Lian, Z. Cheng, D. Jin, J. Lin, Biomaterials 101 (2016) 32–46.
[152] C. Zhang, K. Zhao, W. Bu, D. Ni, Y. Liu, J. Feng, J. Shi, Angewandte Chemie (International ed. in English) 54 (2015) 1770–1774.
[153] Y. Wang, S. Song, J. Liu, D. Liu, H. Zhang, Angewandte Chemie (International ed. in English) 54 (2015) 536–540.
[154] L. Yan, Y.N. Chang, L.N. Zhao, Z.J. Gu, X.X. Liu, G. Tian, L.J. Zhou, W.L. Ren, S. Jin, W.Y. Yin, H.Q. Chang, G.M. Xing, X.F. Gao, Y.L. Zhao, Carbon 57 (2013) 120–129.
[155] Y. Wang, H. Wang, D. Liu, S. Song, X. Wang, H. Zhang, Biomaterials 34 (2013) 7715–7724.
[156] R.R. Deng, X.J. Xie, M. Vendrell, Y.T. Chang, X.G. Liu, Journal of the American Chemical Society 133 (2011) 20168–20171.
[157] W. Fan, W. Bu, B. Shen, Q. He, Z. Cui, Y. Liu, X. Zheng, K. Zhao, J. Shi, Advanced materials (Deerfield Beach, Fla.) 27 (2015) 4155–4161.
[158] J. Han, H. Xia, Y. Wu, S.N. Kong, A. Deivasigamani, R. Xu, K.M. Hui, Y. Kang, Nanoscale 8 (2016) 7861–7865.
[159] S. Lu, D. Tu, P. Hu, J. Xu, R. Li, M. Wang, Z. Chen, M. Huang, X. Chen, Angewandte Chemie (International ed. in English) 54 (2015) 7915–7919.
[160] Y. Zhang, F. Zheng, T. Yang, W. Zhou, Y. Liu, N. Man, L. Zhang, N. Jin, Q. Dou, Y. Zhang, Z. Li, L.P. Wen, Nature materials 11 (2012) 817–826.
[161] L. Yu, Y. Lu, N. Man, S.H. Yu, L.P. Wen, Small (Weinheim an der Bergstrasse, Germany) 5 (2009) 2784–2787.
[162] T. Yang, Y. Sun, Q. Liu, W. Feng, P. Yang, F. Li, Biomaterials 33 (2012) 3733–3742.
[163] F. Vetrone, R. Naccache, A. Juarranz de la Fuente, F. Sanz-Rodriguez, A. Blazquez-Castro, E.M. Rodriguez, D. Jaque, J.G. Sole, J.A. Capobianco, Nanoscale 2 (2010) 495–498.
[164] J. Shan, J. Chen, J. Meng, J. Collins, W. Soboyejo, J.S. Friedberg, Y. Ju, Journal of Applied Physics (2008) 104.
[165] Y.I. Park, J.H. Kim, K.T. Lee, K.-S. Jeon, H. Bin Na, J.H. Yu, H.M. Kim, N. Lee, S.H. Choi, S.-I. Baik, H. Kim, S.P. Park, B.-J. Park, Y.W. Kim, S.H. Lee, S.-Y. Yoon, I.C. Song, W.K. Moon, Y.D. Suh, T. Hyeon, Advanced Materials 21 (2009) 4467-+.
[166] H. Hu, M.X. Yu, F.Y. Li, Z.G. Chen, X. Gao, L.Q. Xiong, C.H. Huang, Chem. Mat. 20 (2008) 7003–7009.
[167] N.N. Dong, M. Pedroni, F. Piccinelli, G. Conti, A. Sbarbati, J.E. Ramirez-Hernandez, L.M. Maestro, M.C. Iglesias-de la Cruz, F. Sanz-Rodriguez, A. Juarranz, F. Chen, F. Vetrone, J.A. Capobianco, J.G. Sole, M. Bettinelli, D. Jaque, A. Speghini, ACS nano 5 (2011) 8665–8671.
[168] D.K. Chatterjee, A.J. Rufaihah, Y. Zhang, Biomaterials 29 (2008) 937–943.
[169] Y. Bai, Y. Wang, K. Yang, X. Zhang, Y. Song, C.H. Wang, Optics Communications 281 (2008) 5448–5452.
[170] G. Tian, Z. Gu, L. Zhou, W. Yin, X. Liu, L. Yan, S. Jin, W. Ren, G. Xing, S. Li, Y. Zhao, Advanced materials (Deerfield Beach, Fla.) 24 (2012) 1226–1231.
[171] J. Pichaandi, J.C. Boyer, K.R. Delaney, F. van Veggel, J. Phys. Chem. C 115 (2011) 19054–19064.
[172] M. Nyk, R. Kumar, T.Y. Ohulchanskyy, E.J. Bergey, P.N. Prasad, Nano letters 8 (2008) 3834–3838.
[173] Q. Liu, Y. Sun, T. Yang, W. Feng, C. Li, F. Li, Journal of the American Chemical Society 133 (2011) 17122–17125.
[174] L.A. Cheng, K. Yang, S.A. Zhang, M.W. Shao, S.T. Lee, Z.A. Liu, Nano Res. 3 (2010) 722–732.
[175] S. Chen, A.Z. Weitemier, X. Zeng, L. He, X. Wang, Y. Tao, A.J.Y. Huang, Y. Hashimotodani, M. Kano, H. Iwasaki, L.K. Parajuli, S. Okabe, D.B.L. Teh, A.H. All, I. Tsutsui-Kimura, K.F. Tanaka, X. Liu, T.J. McHugh, Science 359 (2018) 679–684.
[176] Y. Li, X. Li, Z. Xue, M. Jiang, S. Zeng, J. Hao, Advanced healthcare materials 6 (2017).
[177] J. Zhao, D. Jin, E.P. Schartner, Y. Lu, Y. Liu, A.V. Zvyagin, L. Zhang, J.M. Dawes, P. Xi, J.A. Piper, E.M. Goldys, T.M. Monro, Nature nanotechnology 8 (2013) 729–734.
[178] Y. Liu, Y. Lu, X. Yang, X. Zheng, S. Wen, F. Wang, X. Vidal, J. Zhao, D. Liu, Z. Zhou, C. Ma, J. Zhou, J.A. Piper, P. Xi, D. Jin, Nature 543 (2017) 229–233.
[179] Q. Zhan, H. Liu, B. Wang, Q. Wu, R. Pu, C. Zhou, B. Huang, X. Peng, H. Agren, S. He, Nature communications 8 (2017) 1058.
[180] X. Xie, N. Gao, R. Deng, Q. Sun, Q.H. Xu, X. Liu, Journal of the American Chemical Society 135 (2013) 12608–12611.
[181] Y.F. Wang, G.Y. Liu, L.D. Sun, J.W. Xiao, J.C. Zhou, C.H. Yan, ACS nano 7 (2013) 7200–7206.
[182] J. Shen, G. Chen, A.-M. Vu, W. Fan, O.S. Bilsel, C.-C. Chang, G. Han, Advanced Optical Materials 1 (2013) 644–650.
[183] M. Pokhrel, L.C. Mimun, B. Yust, G.A. Kumar, A. Dhanale, L. Tang, D.K. Sardar, Nanoscale 6 (2014) 1667–1674.
[184] M.K. Jayakumar, N.M. Idris, K. Huang, Y. Zhang, Nanoscale 6 (2014) 8441–8443.
[185] F. He, C. Li, X. Zhang, Y. Chen, X. Deng, B. Liu, Z. Hou, S. Huang, D. Jin, J. Lin, Dalton transactions (Cambridge, England : 2003) 45 (2016) 1708–1716.
[186] A. Bagheri, H. Arandiyan, C. Boyer, M. Lim, Advanced science (Weinheim, Baden-Wurttemberg, Germany) 3 (2016) 1500437.
[187] Y. Zhong, G. Tian, Z. Gu, Y. Yang, L. Gu, Y. Zhao, Y. Ma, J. Yao, Advanced materials (Deerfield Beach, Fla.) 26 (2014) 2831–2837.
[188] Y. Zhao, Q. Zhan, J. Liu, S. He, Biomedical optics express 6 (2015) 838–848.
[189] H. Soderlund, M. Mousavi, H. Liu, S. Andersson-Engels, Journal of biomedical optics 20 (2015) 86008.
[190] G. Yang, D. Yang, P. Yang, R. Lv, C. Li, C. Zhong, F. He, S. Gai, J. Lin, Chem. Mat. 27 (2015) 7957–7968.
[191] Y. Li, J. Tang, D.X. Pan, L.D. Sun, C. Chen, Y. Liu, Y.F. Wang, S. Shi, C.H. Yan, ACS nano 10 (2016) 2766–2773.
[192] X. Ding, J. Liu, D. Liu, J. Li, F. Wang, L. Li, Y. Wang, S. Song, H. Zhang, Nano Res. (2017).
[193] Y. Chen, B. Liu, X. Deng, S. Huang, Z. Hou, C. Li, J. Lin, Nanoscale 7 (2015) 8574–8583.
[194] F. Ai, Q. Ju, X. Zhang, X. Chen, F. Wang, G. Zhu, Scientific reports 5 (2015) 10785.

[195] B. Liu, Y.Y. Chen, C.X. Li, F. He, Z.Y. Hou, S.S. Huang, H.M. Zhu, X.Y. Chen, J. Lin, Advanced Functional Materials 25 (2015) 4717–4729.
[196] H. Xing, S. Zhang, W. Bu, X. Zheng, L. Wang, Q. Xiao, D. Ni, J. Zhang, L. Zhou, W. Peng, K. Zhao, Y. Hua, J. Shi, Advanced Materials 26 (2014) 3867–3872.
[197] D. Ni, Z. Shen, J. Zhang, C. Zhang, R. Wu, J. Liu, M. Yi, J. Wang, Z. Yao, W. Bu, J. Shi, ACS nano 10 (2016) 3783–3790.
[198] D. Ma, L. Meng, Y. Chen, M. Hu, Y. Chen, C. Huang, J. Shang, R. Wang, Y. Guo, J. Yang, ACS applied materials & interfaces 7 (2015) 16257–16265.
[199] X. Jin, F. Fang, J. Liu, C. Jiang, X. Han, Z. Song, J. Chen, G. Sun, H. Lei, L. Lu, Nanoscale 7 (2015) 15680–15688.
[200] Q. Ju, D. Tu, Y. Liu, R. Li, H. Zhu, J. Chen, Z. Chen, M. Huang, X. Chen, Journal of the American Chemical Society 134 (2012) 1323–1330.
[201] D. Yang, Y. Dai, J. Liu, Y. Zhou, Y. Chen, C. Li, P.a. Ma, J. Lin, Biomaterials 35 (2014) 2011–2023.
[202] Y. Feng, H. Chen, L. Ma, B. Shao, S. Zhao, Z. Wang, H. You, ACS applied materials & interfaces 9 (2017) 15096–15102.
[203] X. Kang, D. Yang, Y. Dai, M. Shang, Z. Cheng, X. Zhang, H. Lian, P. Ma, J. Lin, Nanoscale 5 (2013) 253–261.
[204] Y. Li, Y. Gu, W. Yuan, T. Cao, K. Li, S. Yang, Z. Zhou, F. Li, ACS applied materials & interfaces 8 (2016) 19208–19216.
[205] Y. Liu, Q. Guo, X. Zhu, W. Feng, L. Wang, L. Ma, G. Zhang, J. Zhou, F. Li, Advanced Functional Materials 26 (2016) 5120–5130.
[206] D. Ni, W. Bu, S. Zhang, X. Zheng, M. Li, H. Xing, Q. Xiao, Y. Liu, Y. Hua, L. Zhou, W. Peng, K. Zhao, J. Shi, Advanced Functional Materials 24 (2014) 6613–6620.
[207] D. Ni, J. Zhang, W. Bu, C. Zhang, Z. Yao, H. Xing, J. Wang, F. Duan, Y. Liu, W. Fan, X. Feng, J. Shi, Biomaterials 76 (2016) 218–225.
[208] Z. Yi, X. Li, Z. Xue, X. Liang, W. Lu, H. Peng, H. Liu, S. Zeng, J. Hao, Advanced Functional Materials 25 (2015) 7119–7129.
[209] Z. Xue, Z. Yi, X. Li, Y. Li, M. Jiang, H. Liu, S. Zeng, Biomaterials 115 (2017) 90–103.
[210] F. Chen, S. Zhang, W. Bu, X. Liu, Y. Chen, Q. He, M. Zhu, L. Zhang, L. Zhou, W. Peng, J. Shi, Chemistry (Weinheim an der Bergstrasse, Germany) 16 (2010) 11254–11260.
[211] L. Zeng, L. Luo, Y. Pan, S. Luo, G. Lu, A. Wu, Nanoscale 7 (2015) 8946–8954.
[212] B. Liu, C. Li, P. Ma, Y. Chen, Y. Zhang, Z. Hou, S. Huang, J. Lin, Nanoscale 7 (2015) 1839–1848.
[213] Y. Li, J. Tang, L. He, Y. Liu, Y. Liu, C. Chen, Z. Tang, Advanced materials (Deerfield Beach, Fla.) 27 (2015) 4075–4080.
[214] L. Feng, D. Yang, F. He, S. Gai, C. Li, Y. Dai, P. Yang, Advanced healthcare materials (2017).
[215] J. Xu, W. Han, P. Yang, T. Jia, S. Dong, H. Bi, A. Gulzar, D. Yang, S. Gai, F. He, J. Lin, C. Li, Advanced Functional Materials 28 (2018) 1803804.
[216] J. Xu, F. He, Z. Cheng, R. Lv, Y. Dai, A. Gulzar, B. Liu, H. Bi, D. Yang, S. Gai, P. Yang, J. Lin, Chem. Mat. 29 (2017) 7615–7628.
[217] G. Tian, X. Zheng, X. Zhang, W. Yin, J. Yu, D. Wang, Z. Zhang, X. Yang, Z. Gu, Y. Zhao, Biomaterials 40 (2015) 107–116.
[218] G. Gao, C. Zhang, Z. Zhou, X. Zhang, J. Ma, C. Li, W. Jin, D. Cui, Nanoscale 5 (2013) 351–362.
[219] H. Liu, W. Lu, H. Wang, L. Rao, Z. Yi, S. Zeng, J. Hao, Nanoscale 5 (2013) 6023–6029.
[220] J. Zhou, X. Zhu, M. Chen, Y. Sun, F. Li, Biomaterials 33 (2012) 6201–6210.
[221] Y. Sun, J. Peng, W. Feng, F. Li, Theranostics 3 (2013) 346–353.
[222] P. Lei, P. Zhang, Q. Yuan, Z. Wang, L. Dong, S. Song, X. Xu, X. Liu, J. Feng, H. Zhang, ACS applied materials & interfaces 7 (2015) 26346–26354.
[223] M. Rai, S.K. Singh, A.K. Singh, R. Prasad, B. Koch, K. Mishra, S.B. Rai, ACS applied materials & interfaces 7 (2015) 15339–15350.
[224] Q. Xiao, W. Bu, Q. Ren, S. Zhang, H. Xing, F. Chen, M. Li, X. Zheng, Y. Hua, L. Zhou, W. Peng, H. Qu, Z. Wang, K. Zhao, J. Shi, Biomaterials 33 (2012) 7530–7539.
[225] Y. Yang, Y. Sun, T. Cao, J. Peng, Y. Liu, Y. Wu, W. Feng, Y. Zhang, F. Li, Biomaterials 34 (2013) 774–783.
[226] Y. Sun, M. Yu, S. Liang, Y. Zhang, C. Li, T. Mou, W. Yang, X. Zhang, B. Li, C. Huang, F. Li, Biomaterials 32 (2011) 2999–3007.
[227] R. Lv, D. Wang, L. Xiao, G. Chen, J. Xia, P.N. Prasad, Scientific reports 7 (2017).
[228] X. Zhai, P. Lei, P. Zhang, Z. Wang, S. Song, X. Xu, X. Liu, J. Feng, H. Zhang, Biomaterials 65 (2015) 115–123.
[229] J.W. Shen, C.X. Yang, L.X. Dong, H.R. Sun, K. Gao, X.P. Yan, Analytical chemistry 85 (2013) 12166–12172.
[230] Y. Liu, N. Kang, J. Lv, Z. Zhou, Q. Zhao, L. Ma, Z. Chen, L. Ren, L. Nie, Advanced Materials 28 (2016) 6411-+.
[231] Q. Liu, Y. Sun, C. Li, J. Zhou, C. Li, T. Yang, X. Zhang, T. Yi, D. Wu, F. Li, ACS nano 5 (2011) 3146–3157.
[232] N. Niu, F. He, P. Ma, S. Gai, G. Yang, F. Qu, Y. Wang, J. Xu, P. Yang, ACS applied materials & interfaces 6 (2014) 3250–3262.
[233] C.J. Carling, F. Nourmohammadian, J.C. Boyer, N.R. Branda, Angewandte Chemie (International ed. in English) 49 (2010) 3782–3785.
[234] J.V. Garcia, J. Yang, D. Shen, C. Yao, X. Li, R. Wang, G.D. Stucky, D. Zhao, P.C. Ford, F. Zhang, Small (Weinheim an der Bergstrasse, Germany) 8 (2012) 3800–3805.
[235] P.T. Burks, J.V. Garcia, R. GonzalezIrias, J.T. Tillman, M. Niu, A.A. Mikhailovsky, J. Zhang, F. Zhang, P.C. Ford, Journal of the American Chemical Society 135 (2013) 18145–18152.
[236] Y.H. Chien, Y.L. Chou, S.W. Wang, S.T. Hung, M.C. Liau, Y.J. Chao, C.H. Su, C.S. Yeh, ACS nano 7 (2013) 8516–8528.
[237] Y. Yang, F. Liu, X. Liu, B. Xing, Nanoscale 5 (2013) 231–238.
[238] S. Perfahl, M.M. Natile, H.S. Mohamad, C.A. Helm, C. Schulzke, G. Natile, P.J. Bednarski, Molecular pharmaceutics 13 (2016) 2346–2362.
[239] X. Deng, Y. Dai, J. Liu, Y. Zhou, P. Ma, Z. Cheng, Y. Chen, K. Deng, X. Li, Z. Hou, C. Li, J. Lin, Biomaterials 50 (2015) 154–163.
[240] W. Li, J. Wang, J. Ren, X. Qu, Journal of the American Chemical Society 136 (2014) 2248–2251.
[241] Y. Yang, B. Velmurugan, X. Liu, B. Xing, Small (Weinheim an der Bergstrasse, Germany) 9 (2013) 2937–2944.
[242] Y. Zhang, Z. Yu, J. Li, Y. Ao, J. Xue, Z. Zeng, X. Yang, T. Tan, ACS nano 11 (2017) 2846–2857.
[243] P.T. Wong, D. Chen, S. Tang, S. Yanik, M. Payne, J. Mukherjee, A. Coulter, K. Tang, K. Tao, K. Sun, J.R. Baker Jr, S.K. Choi, Small (Weinheim an der Bergstrasse, Germany) 11 (2015) 6078–6090.
[244] L. Zhao, J. Peng, Q. Huang, C. Li, M. Chen, Y. Sun, Q. Lin, L. Zhu, F. Li, Advanced Functional Materials 24 (2014) 363–371.
[245] Y. Min, J. Li, F. Liu, E.K.L. Yeow, B. Xing, Angewandte Chemie-International Edition 53 (2014) 1012–1016.
[246] Y. Dai, H. Xiao, J. Liu, Q. Yuan, P.a. Ma, D. Yang, C. Li, Z. Cheng, Z. Hou, P. Yang, J. Lin, Journal of the American Chemical Society 135 (2013) 18920–18929.
[247] J. Liu, W. Bu, L. Pan, J. Shi, Angewandte Chemie-International Edition 52 (2013) 4375–4379.
[248] T. Zhao, P. Wang, Q. Li, A.A. Al-Khalaf, W.N. Hozzein, F. Zhang, X. Li, D. Zhao, Angewandte Chemie (International ed. in English) 57 (2018) 2611–2615.
[249] X. Li, L. Zhou, Y. Wei, A.M. El-Toni, F. Zhang, D. Zhao, Journal of the American Chemical Society 136 (2014) 15086–15092.
[250] P. Zhang, W. Steelant, M. Kumar, M. Scholfield, Journal of the American Chemical Society 129 (2007) 4526–4527.
[251] Y. Liu, Y. Liu, W. Bu, C. Cheng, C. Zuo, Q. Xiao, Y. Sun, D. Ni, C. Zhang, J. Liu, J. Shi, Angewandte Chemie (International ed. in English) 54 (2015) 8105–8109.
[252] J. Xu, L. Xu, C. Wang, R. Yang, Q. Zhuang, X. Han, Z. Dong, W. Zhu, R. Peng, Z. Liu, ACS nano 11 (2017) 4463–4474.
[253] L. Hu, P. Wang, M. Zhao, L. Liu, L. Zhou, B. Li, F.H. Albaqami, A.M. El-Toni, X. Li, Y. Xie, X. Sun, F. Zhang, Biomaterials 163 (2018) 154–162.
[254] L. Zeng, Y. Pan, R. Zou, J. Zhang, Y. Tian, Z. Teng, S. Wang, W. Ren, X. Xiao, J. Zhang, L. Zhang, A. Li, G. Lu, A. Wu, Biomaterials 103 (2016) 116–127.
[255] F. Lu, L. Yang, Y. Ding, J.-J. Zhu, Advanced Functional Materials 26 (2016) 4778–4785.
[256] A. Punjabi, X. Wu, A. Tokatli-Apollon, M. El-Rifai, H. Lee, Y. Zhang, C. Wang, Z. Liu, E.M. Chan, C. Duan, G. Han, ACS nano 8 (2014) 10621–10630.
[257] Y. Li, Z. Di, J. Gao, P. Cheng, C. Di, G. Zhang, B. Liu, X. Shi, L.D. Sun, L. Li, C.H. Yan, Journal of the American Chemical Society 139 (2017) 13804–13810.
[258] Z. Yu, Q. Sun, W. Pan, N. Li, B. Tang, ACS nano 9 (2015) 11064–11074.
[259] L. Zhang, L. Zeng, Y. Pan, S. Luo, W. Ren, A. Gong, X. Ma, H. Liang, G. Lu, A. Wu, Biomaterials 44 (2015) 82–90.
[260] L. Feng, F. He, B. Liu, G. Yang, S. Gai, P. Yang, C. Li, Y. Dai, R. Lv, J. Lin, Chem. Mat. 28 (2016) 7935–7946.
[261] M.H. Chan, C.W. Chen, I.J. Lee, Y.C. Chan, D. Tu, M. Hsiao, C.H. Chen, X. Chen, R.S. Liu, Inorganic chemistry 55 (2016) 10267–10277.
[262] R. Lv, D. Yang, P. Yang, J. Xu, F. He, S. Gai, C. Li, Y. Dai, G. Yang, J. Lin, Chem. Mat. 28 (2016) 4724–4734.
[263] Z. Yu, W. Pan, N. Li, B. Tang, Chemical Science 7 (2016) 4237–4244.
[264] N.M. Idris, M.K. Gnanasammandhan, J. Zhang, P.C. Ho, R. Mahendran, Y. Zhang, Nature medicine 18 (2012) 1580–1585.
[265] J. Xu, P. Yang, M. Sun, H. Bi, B. Liu, D. Yang, S. Gai, F. He, J. Lin, ACS nano 11 (2017) 4133–4144.
[266] C. Gao, Z. Lin, Z. Wu, X. Lin, Q. He, ACS applied materials & interfaces 8 (2016) 34252–34260.
[267] P. Wang, X. Li, C. Yao, W. Wang, M. Zhao, A.M. El-Toni, F. Zhang, Biomaterials 125 (2017) 90–100.
[268] C. Zhang, W.-H. Chen, L.-H. Liu, W.-X. Qiu, W.-Y. Yu, X.-Z. Zhang, Advanced Functional Materials 27 (2017) 1700626.
[269] T. Gu, L. Cheng, F. Gong, J. Xu, X. Li, G. Han, Z. Liu, ACS applied materials & interfaces 10 (2018) 15494–15503.
[270] H.-J. Cai, T.-T. Shen, J. Zhang, C.-F. Shan, J.-G. Jia, X. Li, W.-S. Liu, Y. Tang, Journal of Materials Chemistry B 5 (2017) 2390–2394.
[271] C. Yao, W. Wang, P. Wang, M. Zhao, X. Li, F. Zhang, Advanced materials (Deerfield Beach, Fla.) 30 (2018).
[272] R. Lv, P. Yang, F. He, S. Gai, C. Li, Y. Dai, G. Yang, J. Lin, ACS nano 9 (2015) 1630–1647.
[273] X. Zhu, W. Feng, J. Chang, Y.W. Tan, J. Li, M. Chen, Y. Sun, F. Li, Nature communications 7 (2016) 10437.
[274] C. Wang, L. Xu, J. Xu, D. Yang, B. Liu, S. Gai, F. He, P. Yang, Dalton Trans. 46 (2017) 12147–12157.
[275] M.-H. Chan, S.-P. Chen, C.-W. Chen, Y.-C. Chan, R.J. Lin, D.P. Tsai, M. Hsiao, R.-J. Chung, X. Chen, R.-S. Liu, The Journal of Physical Chemistry C 122 (2018) 2402–2412.
[276] F. He, G. Yang, P. Yang, Y. Yu, R. Lv, C. Li, Y. Dai, S. Gai, J. Lin, Advanced Functional Materials 25 (2015) 3966–3976.
[277] J. Xu, A. Gulzar, Y. Liu, H. Bi, S. Gai, B. Liu, D. Yang, F. He, P. Yang, Small (Weinheim an der Bergstrasse, Germany) 13 (2017).
[278] T. Liu, S. Li, Y. Liu, Q. Guo, L. Wang, D. Liu, J. Zhou, Journal of Materials Chemistry B 4 (2016) 2697–2705.
[279] R. Lv, P. Yang, G. Chen, S. Gai, J. Xu, P.N. Prasad, Scientific reports 7 (2017) 13562.
[280] X. Huang, B. Li, C. Peng, G. Song, Y. Peng, Z. Xiao, X. Liu, J. Yang, L. Yu, J. Hu, Nanoscale 8 (2016) 1040–1048.

[281] B. Liu, C. Li, B. Xing, P. Yang, J. Lin, Journal of Materials Chemistry B 4 (2016) 4884–4894.
[282] Y. Liu, L. Li, Q. Guo, L. Wang, D. Liu, Z. Wei, J. Zhou, Theranostics 6 (2016) 1491–1505.
[283] P. Hu, T. Wu, W. Fan, L. Chen, Y. Liu, D. Ni, W. Bu, J. Shi, Biomaterials 141 (2017) 86–95.
[284] H. Bi, Y. Dai, P. Yang, J. Xu, D. Yang, S. Gai, F. He, B. Liu, C. Zhong, G. An, J. Lin, Small (Weinheim an der Bergstrasse, Germany) 14 (2018) 1703809.
[285] L. Li, C. Liu, L. Zhang, T. Wang, H. Yu, C. Wang, Z. Su, Nanoscale 5 (2013) 2249–2253.
[286] X. Jia, J. Yin, D. He, X. He, K. Wang, M. Chen, Y. Li, Journal of biomedical nanotechnology 9 (2013) 2063–2072.
[287] H. Qiao, Z. Cui, S. Yang, D. Ji, Y. Wang, Y. Yang, X. Han, Q. Fan, A. Qin, T. Wang, X.P. He, W. Bu, T. Tang, ACS nano 11 (2017) 7259–7273.
[288] C. Wang, L. Cheng, Y.M. Liu, X.J. Wang, X.X. Ma, Z.Y. Deng, Y.G. Li, Z. Liu, Advanced Functional Materials 23 (2013) 3077–3086.
[289] S.M. Tawfik, M. Sharipov, B.T. Huy, Z. Gerelkhuu, D. Biechele-Speziale, Y.-I. Lee, Journal of Industrial and Engineering Chemistry 57 (2018) 424–435.
[290] H. Li, R. Wei, G.H. Yan, J. Sun, C. Li, H. Wang, L. Shi, J.A. Capobianco, L. Sun, ACS applied materials & interfaces 10 (2018) 4910–4920.
[291] J. Zhao, H. Yang, J. Li, Y. Wang, X. Wang, Scientific reports 7 (2017) 18014.
[292] B. Liu, Y. Chen, C. Li, F. He, Z. Hou, S. Huang, H. Zhu, X. Chen, J. Lin, Advanced Functional Materials 25 (2015) 4717–4729.
[293] Y. Wang, S. Song, J. Liu, D. Liu, H. Zhang, Angewandte Chemie-International Edition 54 (2015) 536–540.
[294] Z. Yu, Y. Ge, Q. Sun, W. Pan, X. Wan, N. Li, B. Tang, Chem Sci 9 (2018) 3563–3569.
[295] F. Ai, N. Wang, X. Zhang, T. Sun, Q. Zhu, W. Kong, F. Wang, G. Zhu, Nanoscale 10 (2018) 4432–4441.
[296] K. Yan, J. Yu, B. Zhang, L. Wu,Macromolecular Chemistry and Physics 218 (2017), 1700090.
[297] X. Su, F. Zhao, Y. Wang, X. Yan, S. Jia, B. Du, Nanomedicine : nanotechnology, biology, and medicine 13 (2017) 1761–1772.
[298] K. Zhu, G. Liu, J. Hu, S. Liu, Biomacromolecules 18 (2017) 2571–2582.
[299] B.C. Dickinson, C.J. Chang, Nature Chemical Biology 7 (2011) 504.
[300] X. Wang, G. Meng, S. Zhang, X. Liu, Scientific reports 6 (2016) 29911.
[301] C. Yue, C. Zhang, G. Alfranca, Y. Yang, X. Jiang, Y. Yang, F. Pan, J.M. de la Fuente, D. Cui, Theranostics 6 (2016) 456–469.
[302] T. Zhang, H. Lin, L. Cui, N. An, R. Tong, Y. Chen, C. Yang, X. Li, J. Liu, F. Qu, European Journal of Inorganic Chemistry 2016 (2016) 1206–1213.
[303] G.Y. Lee, W.P. Qian, L. Wang, Y.A. Wang, C.A. Staley, M. Satpathy, S. Nie, H. Mao, L. Yang, ACS nano 7 (2013) 2078–2089.
[304] T. Zhang, S. Huang, H. Lin, N. An, R. Tong, Y. Chen, Y. Wang, F. Qu, New Journal of Chemistry 41 (2017) 2468–2478.
[305] X. Ai, C.J. Ho, J. Aw, A.B. Attia, J. Mu, Y. Wang, X. Wang, Y. Wang, X. Liu, H. Chen, M. Gao, X. Chen, E.K. Yeow, G. Liu, M. Olivo, B. Xing, Nature communications 7 (2016) 10432.
[306] N. Zhao, B. Wu, X. Hu, D. Xing, Biomaterials 141 (2017) 40–49.
[307] M.C. Parrott, M. Finniss, J.C. Luft, A. Pandya, A. Gullapalli, M.E. Napier, J.M. DeSimone, Journal of the American Chemical Society 134 (2012) 7978–7982.
[308] X. Zhang, P. Yang, Y. Dai, P.a. Ma, X. Li, Z. Cheng, Z. Hou, X. Kang, C. Li, J. Lin, Advanced Functional Materials 23 (2013) 4067–4078.
[309] R. Lv, P. Yang, F. He, S. Gai, G. Yang, Y. Dai, Z. Hou, J. Lin, Biomaterials 63 (2015) 115–127.
[310] M. Liras, M. González-Béjar, E. Peinado, L. Francés-Soriano, J. Pérez-Prieto, I. Quijada-Garrido, O. García, Chem. Mat. 26 (2014) 4014–4022.
[311] X. Zhu, J. Li, X. Qiu, Y. Liu, W. Feng, F. Li, Nature communications 9 (2018) 2176.
[312] L. Liu, S. Wang, B. Zhao, P. Pei, Y. Fan, X. Li, F. Zhang, Angewandte Chemie (International ed, in English) 57 (2018) 7518–7522.

Yinghui Wang received her BSc degree in chemistry from Jilin Normal University in 2006 and PhD degree in condensed matter physics from Changchun Institute of Optics, Fine Mechanics and Physics, Chinese Academy of Sciences in 2011. In the same year, she was granted the CAS Presidential Scholarship Award. Then, she worked as a postdoctoral researcher at University of Amsterdam, Netherlands. She subsequently joined the group of Prof. Hongjie Zhang at Changchun Institute of Applied Chemistry, Chinese Academy of Sciences (CAS). She is working as associate professor at Changchun Institute of Applied Chemistry, CAS. Her research interests focus on design and synthesis the multifunctional upconversion nanoparticles and their bioapplications.

Shuyan Song received his BSc degree in Chemistry in 2003 and MSc degree in Inorganic Chemistry in 2006, both from Northeast Normal University. He joined the group of Prof. Hongjie Zhang at Changchun Institute of Applied Chemistry, Chinese Academy of Sciences (CAS), where he received his PhD degree in Inorganic Chemistry in 2009. He is working as a full professor at Changchun Institute of Applied Chemistry, CAS. His research focus is primarily on the development of functional rare-earth materials for catalysis, chemical sensing and photoluminescence.

Songtao Zhang received his BSc degree from Zhengzhou University in 2016. Afterwards, he joined the group of Prof. Hongjie Zhang at Changchun Institute of Applied Chemistry, Chinese Academy of Sciences (CAS) as a PhD candidate. Working mainly on the synthesis and bioapplications of rare earth functional nanomaterials.

Hongjie Zhang received his BS (1978) from Peking University and MS (1985) from Changchun Institute of Applied Chemistry (CAS). Then, he worked as an assistant professor at the same institute from 1985–1989. He then studied at Universite de Bordeaux I (France), where he received his PhD degree in 1993. He joined Changchun Institute of Applied Chemistry (CAS), as a professor in 1994. He was elected as an academician of the Chinese Academy of Science in 2013, and a member of The World Academy of Science (TWAS) in 2015. His current research interests include synthesis and application of lanthanide functional materials.